3D Follicle Segmentation in Ultrasound Image Volumes of Ex-Situ Bovine Ovaries

A Thesis Submitted to the
College of Graduate Studies and Research
in Partial Fulfillment of the Requirements
for the degree of Master of Science
in the Division of Biomedical Engineering
University of Saskatchewan
Saskatoon, Saskatchewan

By Qian Lu

Permission To Use

In presenting this thesis in partial fulfillment of the requirements for a Postgraduate degree from the University of Saskatchewan, I agree that the Libraries of this University may make it freely available for inspection. I further agree that permission for copying of this thesis in any manner, in whole or in part, for scholarly purposes may be granted by the professors who supervised my thesis work or, in their absence, by the Head of the Department or the Dean of the college in which my thesis work was done. It is understood that any copying or publication or use of this thesis or parts thereof for financial gain shall not be allowed without my written permission. It is also understood that due recognition shall be given to me and to the University of Saskatchewan in any scholarly use which may be made of any material in my thesis.

Requests for permission to copy or to make other use of material in this thesis in whole or part should be addressed to:

Head of the Division of Biomedical Engineering
University of Saskatchewan
Saskatoon, Saskatchewan, Canada
S7N 5A9

Abstract

Conventional ultrasonographic examination of the bovine ovary is based on a sequence of two-dimensional (2D) cross-section images. Day-to-day estimation of the number, size, shape and position of the ovarian follicles is one of the most important aspects of ovarian research. Computer-assisted follicle segmentation of ovarian volume can relieve physicians from the tedious manual detection of follicles, provide objective assessment of spatial relationships between the ovarian structures and therefore has the potential to improve accuracy. Modern segmentation procedures are performed on 2D images and the three-dimensional (3D) visualization of follicles is obtained from the reconstruction of a sequence of 2D segmented follicles.

The objective of this study was to develop a semi-automatic 3D follicle segmentation method based on seeded region growing. The 3D datasets were acquired from a sequence of 2D ultrasound images and the ovarian structures were segmented from the reconstructed ovarian volume in a single step. A “seed” is placed manually in each follicle and the growth of the seed is controlled by the algorithm using a combination of average grey-level, standard deviation of the intensity, newly-developed volumetric comparison test and a termination criterion. One important contribution of this algorithm is that it overcomes the boundary leakage problem of follicles of conventional 2D segmentation procedures. The results were validated against the aspiration volume of follicles, the manually detected follicles by an expert and an existing algorithm.

We anticipate that this algorithm will enhance follicular assessment based on current ultrasound techniques in cases when large numbers of follicles (e.g. ovarian superstimulation) obviate accurate counting and size measurement.

Acknowledgements

There are many people I would like to thank. First, I thank Dr. Mark Eramian and Dr. Jaswant Singh for their supervision of my project over the past two years. Dr. Eramian encouraged me to find new ideas and made available a computer for my use. Dr. Singh has continued his instruction and financial support as well as furnishing laboratory materials. Dr. Roger Pierson and Dr. Gregg Adams, my committee members, provided their guidance. Dr. Bob Gander temporarily assisted me with financial support after my first supervisor -- Dr. Glen Watson -- retired due to poor health. Dr. Watson was a big help in improving my English.

I also thank my friends, Dr. Monte Floyd and Annette Floyd, for their proofreading of the many revisions of my thesis. They have encouraged me over the past several years, helped me through the stressful times of my study, and offered advice. Finally, I thank my family for their love, support, and trust, and my boyfriend, Andrew Yip, for his encouragement and trust.

Table of contents

List of Tables

List of Figures

List of Appendix Figures

List of Abbreviations

µm	**Micrometer**
2D	**Two dimensional**
3D	**Three dimensional**
A	**Antrum**
A-mode	**Amplitude Mode**
ANOVA	**Analysis of variance**
BL	**Basal Lamina**
B-mode	**Brightness Mode**
CL	**Corpus Luteum**
dB	**Decibel**
F	**Follicle**
FIFO	**First-in-first-out**
FSH	**Follicle-Stimulating Hormone**
GL	**Granulosa layer**
GnRH	**Gonadotropin-Releasing Hormone**
LH	**Luteinizing Hormone**
M	**Medulla**
MHz	**Megahertz**
mm	**Millimeter**
M-mode	**Motion Mode**
MRI	**Magnetic Resonance Imaging**
MTS	**Multi-resolution texture segmentation**
O	**Oocyte**
PZT	**Lead Zirconate Titanate**
S	**Stroma**
SAS	**Statistical Analysis System**
SE	**Surface epithelium**
SONAR	**Sound Navigation and Ranging**

SRG	**Seeded region growing**
TA	**Tunica albuginea**
TGC	**Time-gain compensation**
TL	**Theca layer**
X-rays	**RÖntgen ray (a type of electromagnetic radiation)**

Chapter 1

General Introduction

1.1 Thesis purpose and objectives

The purpose of this thesis is to develop a three dimensional segmentation algorithm for separating follicle volumes from other structures in ovarian ultrasound images. In the large animal research field, a complete understanding of ovarian dynamics is crucial for cattle reproduction research and management [1]. The study of the internal reproductive tract of large domestic animals and its dynamic activity became possible with the advent of real-time ultrasound imaging techniques [2]. Today, ultrasound imaging is routinely used to monitor the ovaries and dynamic changes in follicles during the estrous cycle [2-12]. Most ultrasonographic ovarian analyses of morphological and position estimation of follicles are done using two dimensional images. In order to increase the accuracy of follicle counting, size measurement and improve the visualization for assessing spatial relationships, 3D follicle analysis is desired. Current computer-based procedures to separate follicle volumes from other ovarian structures (follicle segmentation) are applied on 2D ultrasound images which are then reconstructed to obtain 3D information (2D segmentation). The goal of this research is to develop a 3D follicle segmentation method which is applied directly to a reconstructed 3D volume of the ovary obtained from a series of 2D images. The specific objectives of this study are:

(1) Develop a 3D follicle segmentation algorithm to apply on a 3D dataset constructed from a sequence of 2D images.

(2) Implement the algorithm in software and evaluate its performance.

The 3D follicle segmentation method used here is based on the seeded region growing method. The growth of the region starts from a manually-selected seed point inside the follicle and terminates based on pre-defined set of stop conditions. The hypotheses of this study are:

(1) The volume and position of follicles obtained by computer-assisted follicle segmentation will be similar to that obtained from the observer-defined follicle segmentation and aspirated follicle volume (gold standards).
(2) There will be linear relationships between computer-segmented follicle volumes, observer-defined follicle volumes and aspirated follicle volumes.
(3) There will be an agreement (perfect agreement occurs only if the points in the graph lie along the line of equality, which the slope of the line is close to one [13]) between computer-segmented follicle volumes, observer-defined follicle volumes and aspirated follicle volumes.
(4) The computer-assisted follicle segmentation results will not be sensitive to the position of the selected seed point.

We used the bovine model to develop the technique because this ultrasound model is well developed and procedures to assess the dynamics of ovarian follicles are well standardized [14]. However, the method developed in this study is applicable to all mammalian species including humans.

The details of the segmentation method will be described in Chapter Two. A general discussion of the advantages and limitations of this method in ultrasonographic ovarian analysis is provided in Chapter Three. Finally, general conclusions and suggestions for future work are presented in Chapter Four. The remainder of this chapter is devoted to: general overview of follicular development in cow (1.2); ultrasound imaging techniques in ovarian follicle research (1.3); and, some background knowledge of the computer-assisted follicle segmentation methods (1.4).

1.2 Bovine ovary

1.2.1 Ovarian anatomy

The female reproduction system consists of the ovaries, oviduct, uterus, cervix and vagina [15]. The left and right bovine ovaries lie adjacent to the tips of uterine horns in the pelvic cavity. Two crucial functions of the ovaries are: (1) production of the egg or ovum; and, (2) production of estrogen and progesterone hormones [15]. The oval-shaped bovine ovary is small in size (the major axis is about 1.5-5cm, and the average of two

minor axes is about 1-3cm). The shape and size of the ovary varies during the estrous cycle due to follicular growth and regression, ovulation, and corpus luteum growth and regression [16, 17]. Figure 1.1 illustrates the anatomy of an excised bovine ovary. The ovary is composed of an inner medulla and outer cortex. The ovarian stroma is composed of connective tissue and the ovary is surrounded by surface epithelium [15]. The dense fibrous connective tissue beneath the surface epithelium is called tunica albuginea [15]. The medulla consists of irregularly arranged fibroelastic connective tissue, lymphatics, nervous, and vascular systems [15, 17, 18]. The cortex contains ovarian follicles at various stages of development and regression. The corpus luteum (CL) is a temporary endocrine structure formed from the remainder wall of a follicle following ovulation (the release of the oocyte and antral fluid by rupture of the follicle) [17].

A fully-developed follicle is a roughly spherical structure consisting of an antrum (a fluid-filled cavity), encircled by multiple layers of granulosa cells and theca cells (the wall), the oocyte (a female germ cell) is located among the granulosa cells. Follicles in the ovaries were first described by Regnier de Graaf (1641-1673) [19]. The importance of follicles and the patterns of their growth and development remained unclear until it was discovered that the follicles in non-pregnant cattle develop and regress in a cyclical pattern known as the estrous cycle in 1928 [20]. The estrous cycle or interovulatory interval is around 19 to 23 days in cows. Cows are polyestrous animals [15]. The period of estrous cycle begins and does not stop until interrupted by pregnancy after heifers reach puberty (first ovulation) or following the postpartum anestrous period (a period of no estrous cycles after calving) [1]. In one estrous cycle, after ovulation (day 0), the remnants of the ruptured follicle wall begin to develop into a corpus luteum (CL). The CL remains functional until day 16, after which the it regresses, unless a pregnancy is established [4]. The details of follicle development and ovulation will be described in the next section.

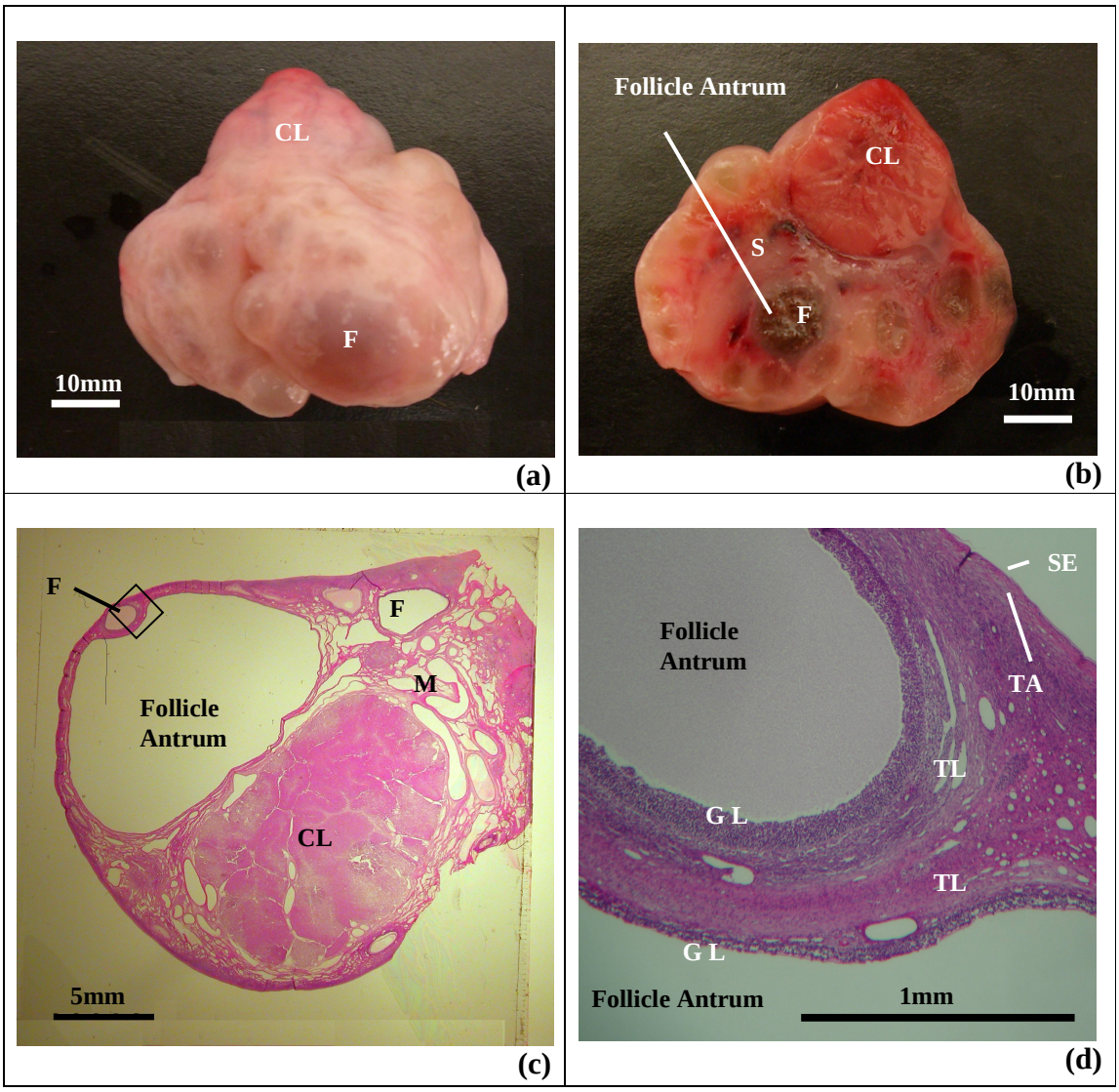

F – Follicle **CL – Corpus Luteum** **S – Stroma** **M – Medulla**
SE– Surface epithelium **TA – Tunica albuginea** **GL – Granulosa layer** **TL – Theca layer**

Figure 1.1 The structure of a bovine ovary: (a) the surface view of a bovine ovary; (b) the cut surface view of the ovary; (c) the histological slice of a bovine ovary; and, (d) the histological section of follicle enlarged from the indicated region in (c).

1.2.2 Follicle development

The bovine follicle may grow from 50µm to 15-20mm in diameter [15]. Figure 1.2 shows the different developmental stages of development of ovarian follicles. Follicles are formed during fetal life. They originate from primordial germ cells after they have migrated from the yolk sac entoderm to the genital ridge (around day 35-50 of pregnancy) and develop into an ovum, or oogonia. [20]. After the oogonia enter meiosis, they are termed as primary oocytes. Meiosis is arrested at prophase I. Primordial follicles are formed when a single layer of granulosa cells surrounds the oocyte. Approximately 150,000 primordial follicles are located in the cortex just beneath the tunica albuginea of the fetal bovine ovary [21]. Each primordial follicle is about 30-40µm and they remain quiescent in the ovary for several years before re-initiation of growth [22]. The stages of follicular growth include an increase in the size of oocyte and development of granulosa cells (primary follicle). After several layers of granulosa cells form around the enlarged oocyte (secondary follicle), many small fluid filled cavities are eventually formed among granulosa cells. The fluid-filled spaces become large and join to form a single cavity -- the follicular antrum. At this stage, the follicle is termed a tertiary follicle [18]. Upon further development, the tertiary follicle becomes a Graafian follicle, which finally leads to the process of ovulation. During ovulation, a mature Graafian follicle ruptures from the ovarian surface, follicular fluid is released, and the oocyte is transported into the oviduct [23]. In cows, usually only one follicle ovulates during an estrous cycle, the others undergo atresia at different stages of development [15]. A detailed review of ovulation is described by Hunter [23].

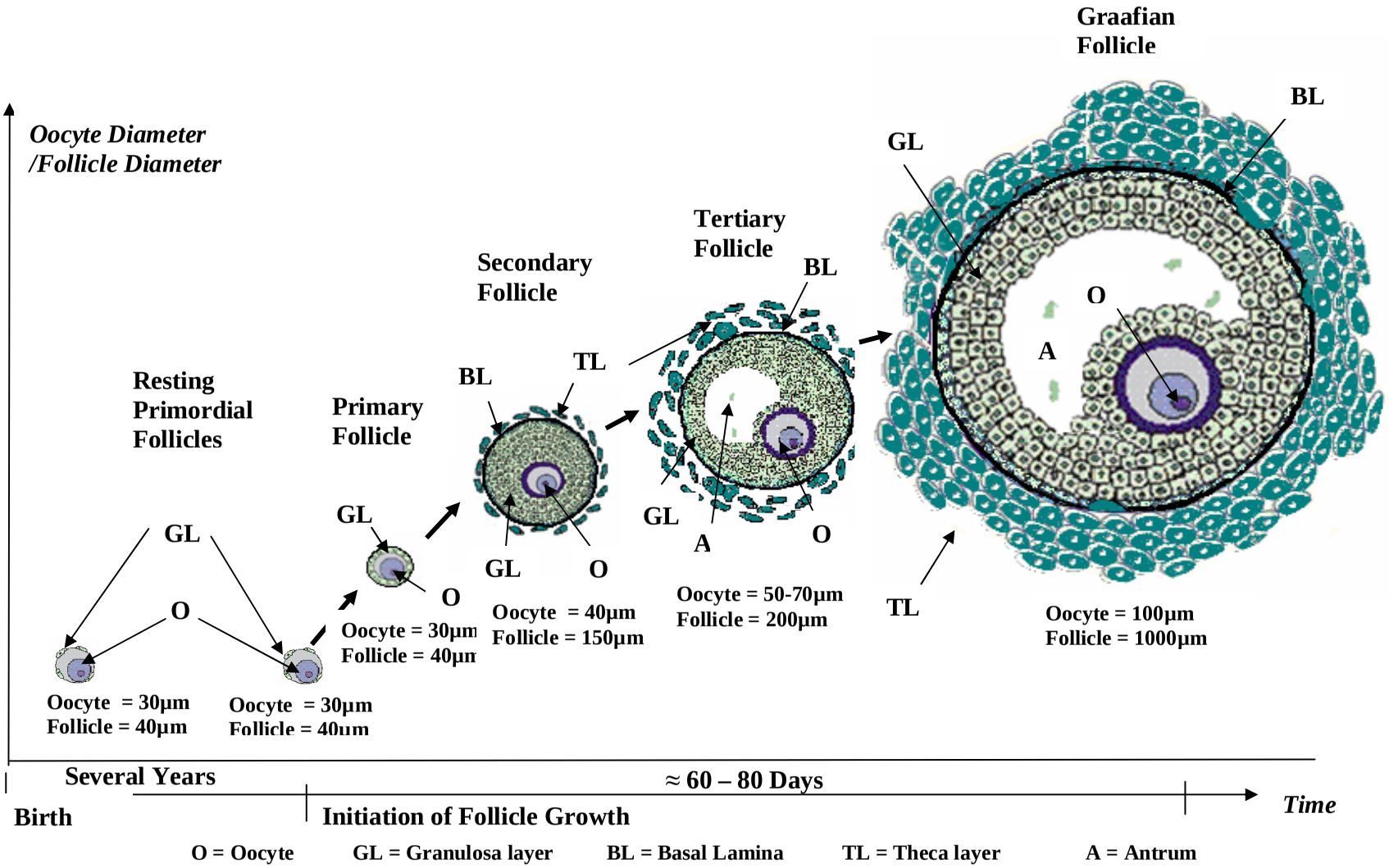

Figure 1.2 The stages of follicle development.

The growth of follicles is controlled partly by endocrine events within the ovary (intraovarian and intrafollicular) and partly by those outside the ovary [24]. The outside influence is mainly derived from the pituitary gland, located at the base of the brain [18]. The main hormones that influence follicular differentiation include FSH (follicle stimulating hormone), LH (luteinizing hormone), estradiol, and progesterone [24]. These are glycoprotein hormones controlled by the hypothalamic hormone gonadotropin-releasing hormone (GnRH) [18]. FSH stimulates the follicle's growth and function, while LH causes the follicles to rupture and the corpus luteum to develop [3, 17, 18]. The intrafollicular component is derived from granulose and theca cells, which produce the hormone estrogen [23, 24]. The amounts of the hormone estrogen increase as the size of a dominant follicle increases [23]. The corpus luteum produces progesterone [24].

Growth of bovine antral follicles ≥ 1mm occurs in waves during the estrous cycle [4, 6, 21, 25]. Rajakoski first proposed the theory of follicle waves in 1961 [26], where he determined that each follicle wave is characterized by the synchronous growth of 15-20 follicles. A review of follicle wave theories is reported by Adams [27]. Most estrous cycles have either two or three follicle waves [27]. Each wave includes a group of follicles from which one is selected as a dominant follicle while the others are deemed to be subordinate follicles. The first wave can be detected on day 0 (day of ovulation). Wave 2 is detected around day 9 to10. In cattle with three-wave cycles, wave 3 happens on day 16. In the last wave, the dominant follicle becomes the ovulatory follicle. Waves can be detected when follicles are 4 to 5 mm in size. Figure 1.3 illustrates the theory of follicle waves.

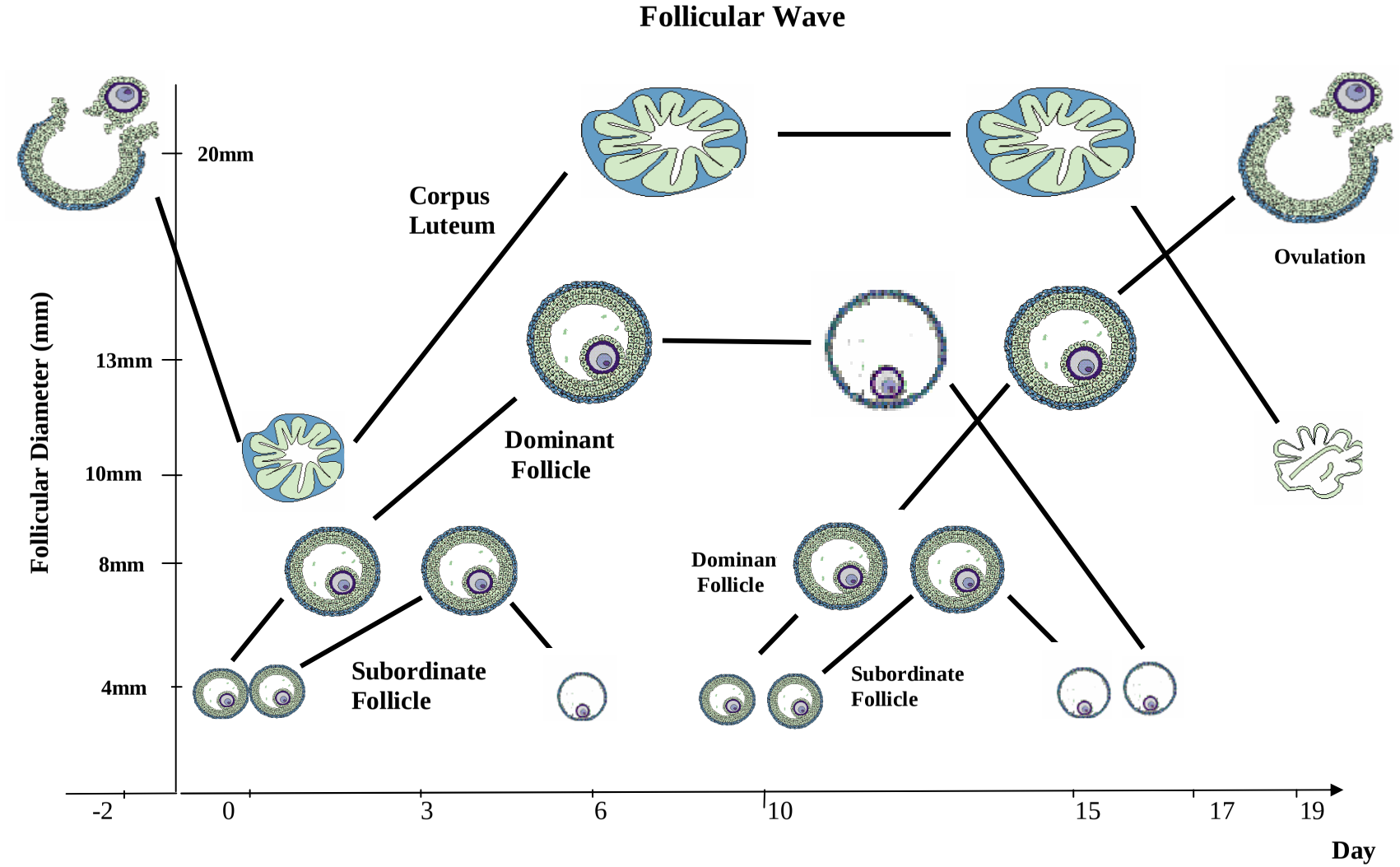

Figure 1.3 The illustration of two follicle waves in cattle.

1.3 Ovarian ultrasound

1.3.1 Overview of ultrasound imaging

In order to interpret an ultrasound image of the ovary, it is necessary to understand how acoustic wave is converted into an image, and how an ultrasound imaging system works.

Ultrasound techniques were first used for measuring distance underwater using SONAR as early as the 19th century [28]. The use of ultrasound in medicine was introduced around the 1930's and the first publication using brightness (B) – mode ultrasound imaging appeared in the 1950's [28]. There has been a rapid development of ultrasonographic imaging techniques for clinical diagnosis in recent years. A number of different ultrasound imaging techniques are now available such as 2-dimensional, 3-dimensional ultrasound, Doppler and color-flow ultrasound.

Ultrasound waves are acoustic waves with frequencies above 20K Hz. Unlike other kinds of medical imaging methods such as MRI (Magnetic Resonance Imaging) and X-rays (a form of electromagnetic radiation) imaging, ultrasound waves are mechanical waves [29], which transmit through the medium but with no permanent displacement of the medium's particles. When the sound source is turned off, the particles go back to their original position [29]. That means no foreign substances need to be introduced into the body to interact with the waves, so ultrasound is considered a non-invasive technique. For this reason ultrasound has been found to be a valuable diagnostic tool in wide range of medical disciplines, especially in the fields of obstetrics and gynecology.

Ultrasonography is the transmission of ultrasound waves into the body followed by the reception of the echoes, the signal processing, and then the display of the echoes on the screen. Figure 1.4 illustrates the system of a basic B-mode linear-array ultrasound scanner [30].

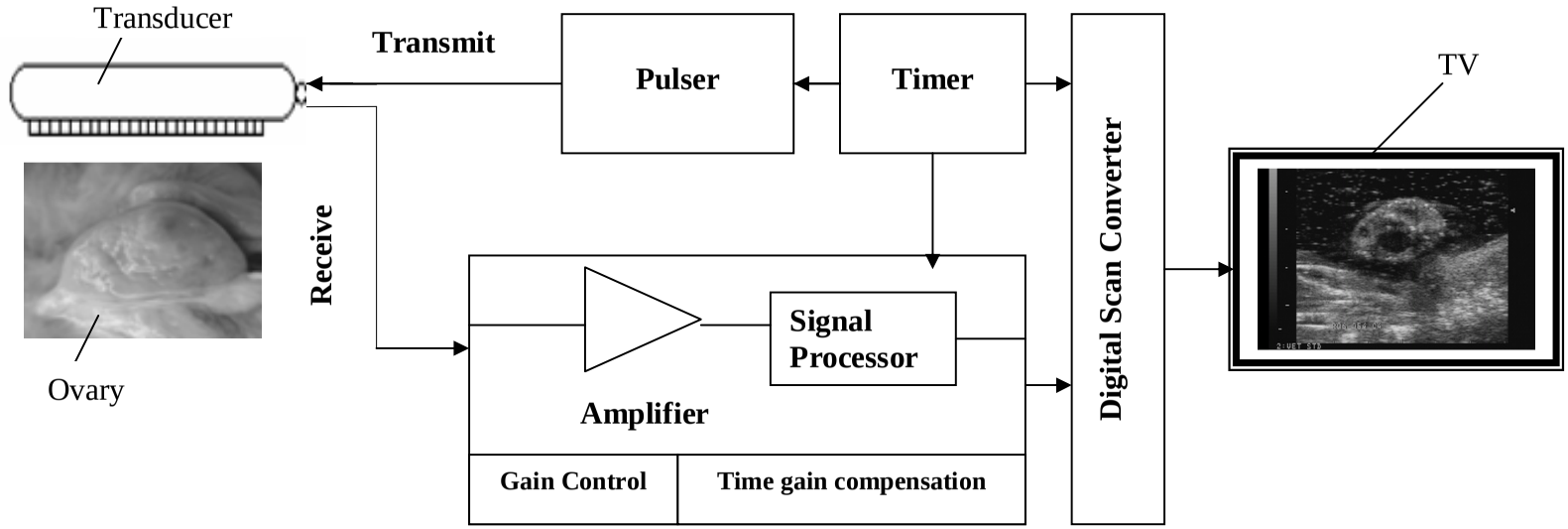

Figure 1.4 The typical ultrasonography system (Redrawn from O.J. Ginther, 1995 [30]).

The ultrasound transducer generates ultrasound waves by converting electric energy into mechanical vibration, it also receives the sound echoes reflected from body tissues and converts them back to electric signals [31]. A transducer is made of many piezoelectric elements, such as lead zirconate titanate (PZT), barium titanate [31]. Due to the different arrangement of piezoelectric elements and the different shape of the transducer, transducers are classified into three types: linear-array (side by side arrangement of the elements), convex-array (the elements are arranged into a sector-like field), and phased array (each element fires the sound beam in proper order) [30]. Low frequency transducers (e.g., 3.0-3.5MHz) are used for viewing large structures which are not close to the transducer. Higher frequency transducers (e.g. 5.0-10MHz) are used for the structures close to the transducer, or for which detailed studies are intended [12]. When sound beams are transmitted into the body, some of them are absorbed by the tissue, some of them will continue propagation into the deeper part of the body, some of them are diffracted or scattered into different directions and some are reflected at the interface of media with different acoustic impedances. The acoustic impedance Z is defined by the product of the density of a material ρ, multiplied by its speed of sound C: $Z= \rho \mathbf{C}$ [29]. The reflected echoes from different depths of the body will be received by the transducer. The pulse-echo cycle is recorded by a timer. The depth of each reflector (the tissue interface which reflects the sound waves) can be calculated from the time recorded. The received sound beams are changed into electrical signals, amplified, processed, and converted into digital signals. Each reflected beam and the location information of each echo are represented on an image display screen by dots of varying brightness (pixels). Each pixel's brightness is displayed as one of 256 grey levels (black = 0 and white = 255). White pixels represent dense tissues which reflect the major portion of incident sound energy, while black pixels represent fluid-filled structures. Ultrasound machines usually display images of 640×480 pixels on the screen.

The ultrasound console has several control knobs which are very important to control the images:

1. **Gain control:** is used to adjust the sensitivity of signal. Gain is the ratio of output of electrical power to input [30]. The gain control determines how much amplification

is accomplished in the receiver of the equipment. Generally, the gain can be varied between 30 to 90 dB [30].

2. **Time-gain compensation (TGC):** is provided to compensate for the decreased signal strengths of deeper tissues due to the greater attenuation over a long path [32]. Attenuation is dependent on the absorption and scattering of sound waves by the body tissues, thereby limiting the depth of penetration [30]. In the classic TGC model, a gain that changes similarly to the attenuation rate is applied to the echo signals over the penetration depth in the tissue [32].
3. **Modes:** Ultrasound equipment has several modes of operation. The most commonly used are A-mode, B-mode and M-mode [30]. A-mode represents a one-dimensional display. The two axes of A-mode images are amplitude and depth. B-mode is a two-dimensional display, or brightness modulation. The stronger the echo signal, the brighter the spot shown on the screen. M-mode is used to assess tissue movement over time. The M-mode is similar to an A-scan but the echo received is brightness modulated on to the screen [33]. The two axes in M-mode which show on the screen are depth and time [30]. Along the depth axis, M-mode uses B-mode principle to display the echoes.

1.3.2 Ovarian ultrasound analysis

Before ultrasonography was used for ovarian follicular monitoring and evaluation, the theory of follicle waves was just a hypothesis [26]. In 1984, Pierson and Ginther et al. used transrectal ultrasonography to support the wave theory of follicle development [11]. Now ovarian ultrasonogaphy is used to diagnose reproductive pathologies and monitor reproductive physiology for research, such as: estimating stage of the estrous cycle [4, 7, 8, 11]; detecting ovulation [5, 10, 13]; diagnosing and monitoring irregular structures [34]; monitoring hemorrhagic follicles [3]. A review of ovarian ultrasonographic analysis methods is presented by Ribadu and Nakao [35].

There are three types of *in vivo* examinations most often used in ovarian ultrasound imaging: transabdominal scan; transvaginal scan; and transrectal scan. Transabdominal ultrasound imaging means that the operator scans the body by placing the transducer in contact with the skin of the abdomen. This type of ovarian scanning in animals is particularly used for species which are too small for transrectal examination [36]. A

transvaginal or endovaginal ultrasound image is created by inserting a transducer into the vagina. This method is widely used in human examinations [37-39]. Bergfelt et al. and Brogliatti et al. used the transvaginal ultrasound-guided method to aspirate the follicles in cattle and calves as young as 10 to 16 weeks of age [40, 41]. A transrectal scan is a procedure in which an ultrasonographic probe is inserted into the rectum. For large animal studies, this technique is the preferred examination method of the reproductive tract, such as the visualization of the uterus, fetus, ovary, corpus luteum(CL), and follicles [2, 12, 30, 42, 43, 44]. Of all the *in vitro* or *ex situ* (examination of excised organs outside the living body) scanning techniques used in the animal research field, the most frequently used is water bath ultrasonography. The excised ovary is placed in a water bath and a series of ultrasonographic images of the ovary are obtained at equal interval for reconstruction of the ovarian volume [11].

1.3.3 Ultrasonographic characteristics of the ovary

The ultrasonographic appearance of the ovaries is variable depending on the stage of the estrous cycle. A normal ovary is easily distinguished from the surrounding tissue. Ultrasonographic images of the ovary are represented by low-level echo pattern. The two important and dynamic structures in the ovary are follicles and the corpus luteum.

Follicles are nonechogenic structures and appear on the ultrasonographic images as black spherical structures [30]. Sometimes if the follicles overlap with each other or are covered by artifacts (see subsection 1.3.4 for the details of artifacts), they are represented as black irregular shaped structures on the ultrasound images. In addition, follicles may take on an elliptical shape before ovulation [2]. The follicle wall is a thin and hypoechoic (a structure that reflects relatively few sound waves) area surrounding the follicle antrum. Sometimes, the follicle wall becomes discontinuous or absent because of imaging artifacts that may occur along the curved boundary of follicles. The high density and the morphological structure of the follicle wall change during different physiological phases [45]. The smallest follicles that can be detected will vary greatly depending on the design of ultrasound equipment. Normally, the minimal diameter of detected follicles is around 2mm to 3mm.

The corpus luteum is a hypoechogenic structure and the intensity of the corpus luteum varies according to physiological stage [46]. The central portion of the corpus luteum

may show as a hypoechoic structure (formed by solid material) or an anechoic (a structure in which there are no echoes being reflected) structure (due to a fluid-filled cavity) [2].

1.3.4 Artifacts of ultrasound images

The ultrasound images may contain different kinds of artifacts. The definition of artifact is “any record or image obtained in the course of applying a medical diagnostic technique which is not representative of the structures under study but is adventitious” [47]. Some of the artifacts may arise from the design of the scanner system, while others are caused by human operator error. This includes incorrect selection of the gain, TGC, and transducer and incorrect placement of the transducer. Some are inherent to the nature of ultrasound waves, such as attenuation, reflection, refraction etc., while others are due to the ultrasound tissue effects. The details of ultrasonography artifacts are described by Zagzebski [33]. A review of artifacts in diagnostic ultrasound can be found in Kirberger’s paper [47]. Among all types of artifacts specular and nonspecular reflection, shadowing, enhancement, and reverberation are common occurrences in ovarian ultrasound images [30].

Specular reflection occurs when the reflector is located at the boundary of a curved shape of a structure especially a fluid-filled object, like a follicle, (see Figure 1.5 (a), in arrows). It shows on the image as a bright, smooth surface around the boundary of the object.

Shadow usually happens beneath a very dense structure [30]. The dense structure can completely reflect or absorb the sound beams. For an ovarian ultrasound image, shadow usually occurs at the edge of the fluid-filled area of follicles, because all the sound waves are refracted from the edge of the fluid-filled area [12] (see Figure 1.5(b), in arrow 1).

If sound beams pass through the follicular fluid-filled structure, the intensity of the sound waves are not as attenuated (weakened) as they would be if they were to pass through the regular soft tissue [33]. Therefore, when the echo emerges from the deep side of the follicle, a bright area appears on the image, compared to the same structure adjacent to this area. This is referred as the enhancement artifact (see Figure 1.5 (b), in arrow 2).

Another common artifact on an ovarian ultrasound image is the reverberation artifact [30]. A strong echo is reflected by the interface and returns to the transducer. If the echo is still of significant magnitude, it will bounce back and forth between the interface and the transducer. Bright echoes are recorded on the image in this area. Usually reverberations happen because the interface is parallel to the transducer and has strongly different density in each side [33]. (see Figure 1.5 (c), in arrow).

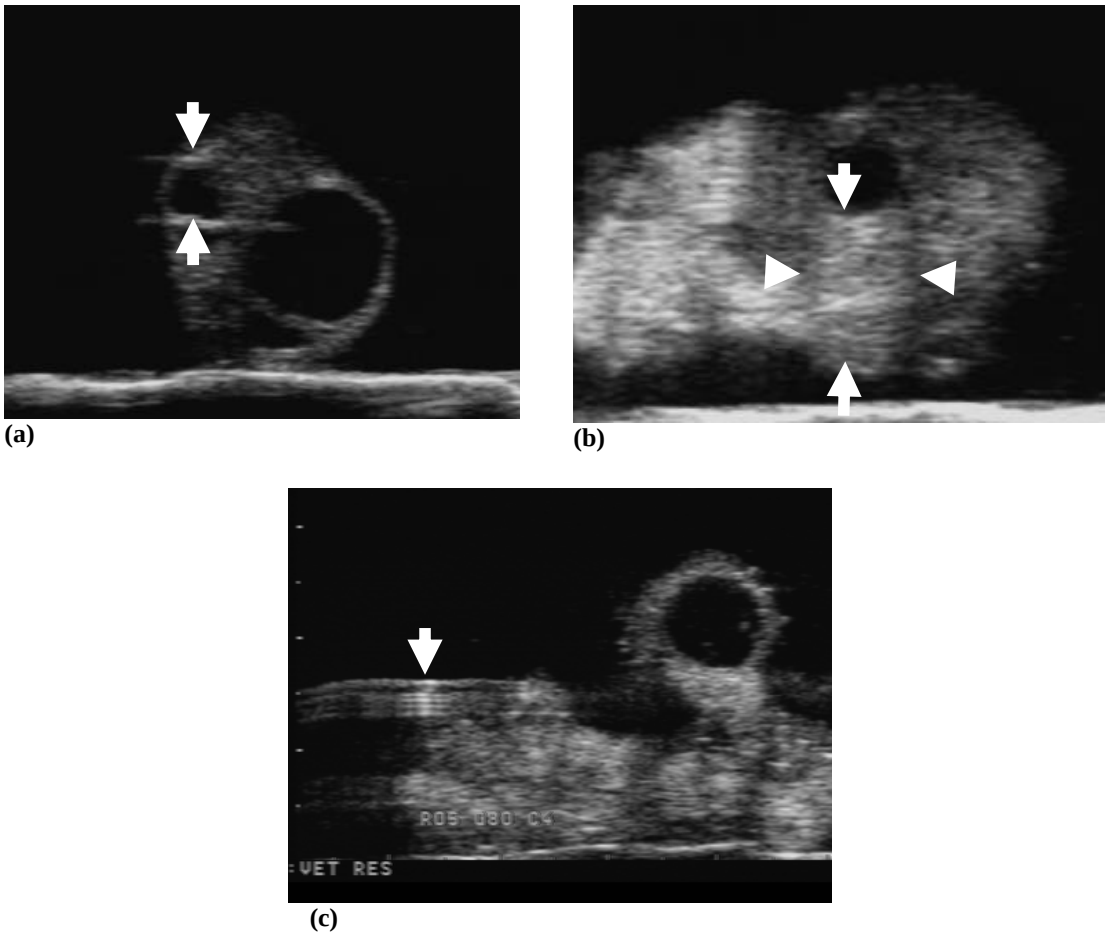

Figure 1.5 Examples of artifacts: (a) the specular artifact at the curved edge of follicle (arrows); (b) the shadow artifact at the edge of the follicle (arrow heads), and the enhancement artifact below the follicle (arrow); (c) the reverberation artifact (arrow).

1.4 Follicle segmentation literature review

1.4.1 Image segmentation

Image segmentation is the division of an image into regions which are homogeneous with respect to some criterion [48]. Homogeneity may be defined in terms of intensity, color, reflectivity, texture [48]. Segmentation is one of the most important steps of image-based medical diagnosis and analysis. Computer-based image segmentation helps the physicians not only in the visualization and inspection of anatomic structures of animals and humans, but also in patient diagnosis, surgical planning and radiotherapy planning [48].

Segmentation in medical imaging is a very difficult problem. The difficulty mainly depends on the quality of images and the complexity of the anatomic organs [48]. The ultrasound image is difficult to segment because the ultrasound images are full of artifacts which make the regions of interest heterogenous. Noise and artifacts can cause discontinuities in object boundaries; therefore a preprocessing step is usually performed prior to segmentation in order to reduce noise. The segmentation algorithm then works on the preprocessed image by separating the homogeneous objects of interest. The result of the segmentation is either a binary or labeled image followed by post-processing steps to correct mistakes in the segmentation and smoothing of object's boundary [48]. In general, segmentation methods can be divided into three groups: global knowledge (usually represented by a histogram of image), edge–based (try to find closed boundaries around regions) and region-based (try to find connected regions that are homogeneous) [48]. A survey of 3D segmentation approaches can be found in Muzzolini's paper [49].

Numerous approaches of 2D follicle segmentation have been proposed in related literatures. These include methods based on watershed segmentation [50], knowledge based segmentation [51, 52], region growing [53], cellular neural networks [54, 55], cellular automata [56], wavelet [57] and texture [58, 59]. In this study, we attempted to develop a 3D follicle segmentation method but not all of these methods can easily be extended to 3D segmentation. In the next subsection, previous works in follicle segmentation will be briefly described.

1.4.2 Follicle segmentation

1) Region growing segmentation

Region growing is an approach to image segmentation in which neighboring pixels around the initial region are examined and added to the region if they have similar pixel values, until the edge pixels are detected [48]. The initial region is determined by automatic methods or selected manually. Figure 1.6 illustrates the procedure of the region growing segmentation method.

(a) **(b)** **(c)**

Figure 1.6 The diagram of region growing segmentation method. (a) Start of region growing on a follicle ultrasound image (b) Growing process after several iterations (c) Final segmentation result (stopped along follicle boundary).

Potočnik et al. devised an automated follicle segmentation method using region growing [60]. First, the image was smoothed by using the same pre-processing as Krivanek and Sonka's method [50], which is that the original image was smoothed by using adaptive neighbourhood median filter (the performance of a median filter is that replaces the center value in the window with the median of all the pixel values in the window [48]). For the pixels darker than threshold *Th*, a large window was used (11×11 pixels) and a small window was used for the pixels brighter than *Th* (5×5 pixels). This smoothing step was repeated twice. Threshold *Th* is set to the mean grey-level value of the original image in this paper. Next, initial approximations for the follicles are determined by thresholding (threshold value *Tg* was set to mean grey-level decreased by one standard deviation of grey-levels in the smoothed image) the smoothed image, followed by separation of the merged follicles (by using watershed segmentation) determination of the similarity of pixels (if the standard deviation for the pixel in its 11×11 neighbourhood doesn't exceed threshold *Hs* and its grey-level is smaller than the

mean grey-level in the image, the pixel is marked as homogeneous), and removal of the non-follicle regions (small regions with pixels' number less than a threshold *Np*). The thresholds *Hs* and *Np* were set to half the standard deviation in the image and 50. Then, respectively, region growing is started from the resulting homogeneous regions of follicles controlled by average grey-level (the difference between the candidate pixel for merging and the mean grey-level of the current region less than α times of the standard deviation of the current region, and α is set to 2 in this paper) and a weighted gradient criterion (the difference between the weighted gradient of the candidate pixel for merging and the mean grey-level of the current region's weighted gradient less than α times of the standard deviation of the current region's weighted gradient, and α is also set to 2). This is followed by the post-processing steps to remove the non-follicle regions (remove non-compact structures and remove the regions with area smaller than 220). The final step is extracting follicles by observing the centre of gravity of each region, because follicles are always close to each other.

The recognition rate (relative number of correctly labeled image pixels) of follicles using this algorithm is around 78%. The misidentification rate (a ratio between the identified regions which are not follicles and all recognized regions in the images) was 29%. More importantly, the region growing method starts from the computer-detected central region of the follicle and stops based on the homogenous criteria. The program does not necessarily go through the whole image, which saves processing time. The only drawback of this method is that in the post-processing step, the non-spherical regions are removed, which may cause the loss of some overlapping follicles. Several methods were developed by combining this region growing method with other methods or algorithms for approaching follicle segmentation [61]. The region growing method can be easily extended to the 3D segmentation approach by changing the 2D neighborhood connection into a 3D connection.

2) Watershed based segmentation

The watershed transformation is a popular image segmentation method coming from the field of mathematical morphology [48]. The principle of the watershed transformation is quite easy to understand if we interpret a 2D image as a 3D landscape, in which the valleys of the landscape represent the low grey scale value in the image and

the mountains represent the high grey scale value. Then the water floods into each valley from each minima of the valley. When the water from two adjacent valleys would meet, a dam is built to avoid water flooding over from one to the other valley [62]. By doing this, the valleys can be successfully separated. When all the valleys are flooded by water, the process is stopped. As a result, the landscape is partitioned into regions separated by dam-line, and these lines are watershed lines (see Figure 1.7). In 1991, a fast and flexible watershed algorithm was introduced by Vincent and Soille [63]. Even though the watershed transformation has many advantages, such as being intuitive and always producing a complete closed contour of the object, it has quite a few important drawbacks [64].

a. Oversegmentation: When the image has many local minima, the result of the watershed transform contains a myriad of small regions, which makes the result hardly useful.
b. Sensitivity to noise: During the flood steps, noise can cause more small valleys and therefore change the results dramatically.
c. Poor detection of significant areas: If the boundary of interest is weak or discontinued, the watershed transform will be unable to detect the region accurately.
d. Poor detection of thin structures: When the watershed transform is applied on the gradient image, the thick edge layer makes it difficult to detect thin structure.

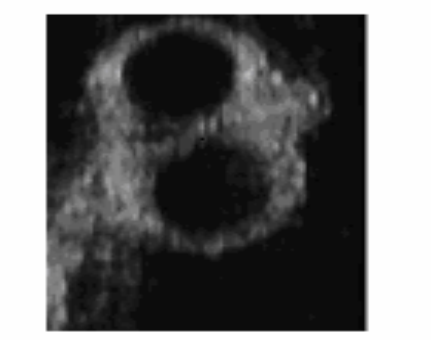

(a) The original ovarian ultrasonic image

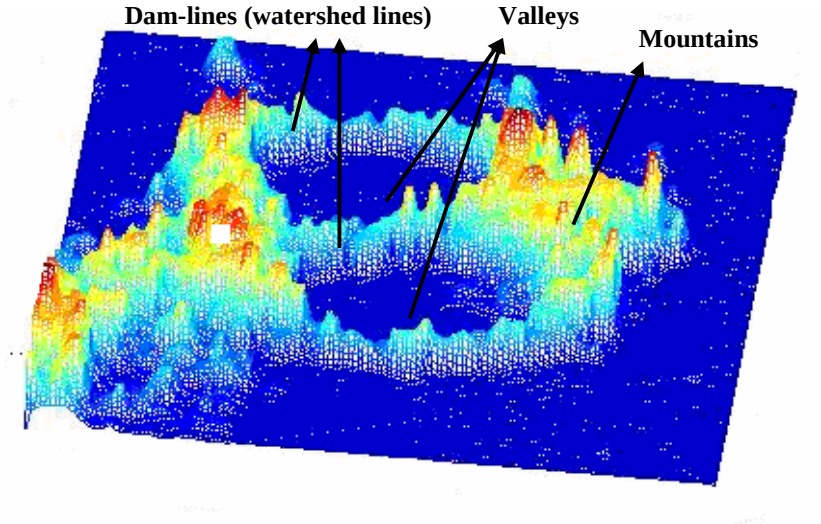

(b) The illustration of the different intensity of the original image.

Figure 1.7 The principle of the watershed segmentation.

An automatic follicle segmentation method based on watershed segmentation was reported by Krivanek and Sonka [50]. In the paper, watershed segmentation was used twice, first on the smoothed image, and second time on the binary image by thresholding from the mosaic image which is created by computing the average of the pixels of each corresponding region after watershed was first used. It was followed by a sequence of post-processing steps to separate adjacent follicles, merge the connected regions which belong to one follicle, remove the non tissue area on the image and remove the small regions and non-spherical regions.

The advantage of this method is that it is a highly automated, accurate and seems sufficient for the day-to-day follicle analysis. It also has some drawbacks. (1) Watershed segmentation was applied to smoothed images, which leads to the merging of some small adjacent follicles. (2) It will fail to estimate non-spherical follicles, because all the non-spherical regions are removed by the post-process steps. (3) The method relies on several parameters that were determined experimentally. Importantly, this method can easily extend to 3D analysis without any big modification. However, in the post-processing part, some object properties need to be computed, such as boundary length, the minor axis of the region and so on. Then the subregions are merged or split based on these properties to repair the oversegmentation and overlapping objects. These steps do not work well on 3D volumes. If a follicle connects to the background area (usually non tissue area), the follicle will fail to be recognized or suffers greatly reduced accuracy by applying this method. So it is not a good choice for 3D segmentation, especially for water bath ultrasound images.

3) Multi-resolution texture segmentation:

Multi-resolution texture segmentation (MTS) is an approach combining texture segmentation and texture classification to segment a class of the image [48]. MTS needs *a priori* information of texture characteristics of images. The procedure of an MTS approach is: first, select the best feature to determine if a region is homogeneous or not. If it is not homogeneous, split the texture block into four quarters. Repeat this step until all the regions are homogeneous. Then, merge the neighboring area by examining the similarity of a texture block [58].

This method is an efficient method for accurately segmenting the follicles. Moreover, it can also segment some other structures in the ovary, such as corpus luteum, stroma and fluid fields in the ovary, and authors were also able to achieve better results (mislabeling error is 1.16%) than previous methods [58]. The drawback of this method is that every pixel on the image needs to be detected which in turn necessitates lots of running time.

In addition, this method can be transformed to work on a 3D model of an ovary without significant modification [59]. In paper [59], the author successfully segmented corpor lutea and stroma in bovine ovaries.

Several other segmentation methods have been utilized in 2D follicle segmentation implantation. The brief description of these methods is as follows. Potočnik et al. segmented ultrasonographic follicles based on a sequence of automatic methods: a despeckling filter (homogeneous region growing mean filter [66]), Kirsch's operator (an edge detector), optimal thresholding, thinning, shape descriptions, and classification. However, the recognition rate of follicles using this method was only around 63%. The average misidentification rate is around 47%. Viher et al. utilized cellular automata [56] for follicle segmentation but lack of statistical evaluations of the results. Cigale et al. used cellular neural networks [54, 55] for follicle segmentation. The follicle recognition rate in the paper [54] was around 60%. The result in [55] is much better than in [54] which the recognition rate is 78%. Cigale et al. also used continues wavelet transform to approach follicle segmentation on real 3D ultrasound images [56]. But the heaviest problem of this method is that it is hard to detect non-spherical shape follicles. Sarty et al. determined a semi-automated method of finding the outer follicle wall border by using a knowledge-based segmentation with graph searching [51, 52]. However, this algorithm sometimes requires manual editing of an automatically defined interior boundary before finding the outer boundary, which is a clear drawback.

Some 3D follicle estimations are done by constructing a sequence of images after segmenting follicles in each single image [60, 61]. The authors [61] reported a prediction-based algorithm to improve the recognition of segmented follicles in neighboring images slices. These results then can be amalgamated to form a smooth 3D image of follicles. This method modifies the segmentation result from image to image, which is clearly time-consuming. It can also introduce some errors when measuring the volume of follicles because this method considered only the neighboring slices not the whole volume [61].

Chapter 2

3D Follicle Segmentation in Ultrasound Image Volumes of Ex-Situ Bovine Ovaries

2.1 Introduction

Diagnostic ultrasonography is an effective tool to evaluate the development of ovarian follicles during various stages of the estrous cycle because it is a non-invasive, rapid and low-cost imaging modality. The analysis of ovarian follicles can enhance the ability to manipulate and manage reproductive performance [15]. At present, ovarian structures are examined by interpreting a series of two dimensional (2D), cross-sectional ultrasound images by scanning the ovary aligned with it longitudinal axis. A physician needs to measure the size and shape of the follicle many times over a number of days to determine the structures of a follicle within an ovary, which is tedious and time-consuming. Computer-assisted follicle image analyses can segment follicles from their surrounding tissues automatically or semi-automatically, making physicians' jobs much easier. Current methods of computer-assisted follicle segmentation are performed using 2D images [50-60], while researchers are interested to know the morphology and the spatial relationships of follicles during the whole estrous cycle. Three-dimensional (3D) follicle images can provide those information better than 2D follicle images can do and thus been used to provide more information about the volume, shape and position of follicles [67-70]. Furthermore, volume estimation based on 3D ultrasound images has been developed to increase accuracy and precision [59]. Thus, there is an increasing need for more accurate 3D ovarian follicle segmentation technologies.

The task of 3D follicle segmentation is challenging. One of the primary reasons is because of the weak follicle boundary information on the images. There are currently only a few 3D follicle segmentation algorithms described in the literature [59]. Some

approaches to 3D follicle segmentation are based on a series of cross-section images [61].

The main objective of this study is to develop an accurate 3D follicle segmentation method that can be applied to 3D ovarian volumes previously constructed from a series of 2D cross-section images. An algorithm based on 3D volumes was designed, implemented, and validated using standard techniques.

The 3D follicle segmentation method used here is based on the seeded region growing method, which in this study the growth of the region starts from a selected seed point inside the follicle that is to be segmented. The hypotheses of this study are:

(1) The volume and position of follicles obtained by computer-assisted follicle segmentation will be similar to that obtained from the observer-defined follicle segmentation and aspirated follicle volumes (gold standards).

(2) There will be linear relationships between computer-segmented follicle volumes, observer-defined follicle volumes and aspirated follicle volumes.

(3) There will be an agreement between computer-segmented follicle volumes, observer-defined follicle volumes and aspirated follicle volumes.

(4) The computer-assisted follicle segmentation results will not be sensitive to the position of the selected seed point.

The background knowledge of seeded region growing method and evaluation methods were described in Section 2.2. The region-growing based 3D segmentation algorithm which was designed is detailed in Section 2.3. Section 2.4 presents the results of the developed segmentation algorithm on images of bovine ovaries and a discussion of the results can be found in Section 2.5. Finally, the conclusion and some suggestions for future work are presented in Section 2.6.

2.2 Background knowledge

2.2.1 3D seeded region growing (SRG) algorithm

Seeded region growing is an efficient method for segmenting medical images [71-73]. The advantages of the SRG algorithm include speed and applicability to a wide range of data types [71, 73]. The general SRG method is discussed in Justic's paper [71] and is

summarized as follows: First, seeds are generated manually by selecting subregions known to be within each object that is to be segmented. The seeds' pixel addresses belonging to the i-th region are put into a seed set A_i. The input to the SRG algorithm are the sets of seed pixels (regions) A_1, A_2, …, A_n. The output image is a label image. Each pixel of the grown regions receives a label from 1 to n, corresponding to the region set to which it was assigned. The growing can either start from each seed region individually or start from different regions at the same time. In an iterative process, the connected neighbors (generally, 4 or 8 neighboring pixels for 2D region growing, 6, 18 or 26 neighboring pixels for 3D region growing) of one of these seed pixels S_j, $S_j \in A_i$, are considered to see whether or not they can be added into set A_i as determined by one or more homogeneity criteria. These criteria coerce the pixels forming the region to have similar grey level values, texture, color, etc. If the neighbor pixel satisfies the criteria, it will be added into set A_i. Each neighbor which is added into set A_i will become a new seed point and its neighbors then become new pixels to be considered for addition to the region. This is the main loop of the algorithm. The growing of this region terminates when no more pixels can be added into set A_i without violating the homogeneity criteria.

One of the most common problems of follicle segmentation by using SRG algorithm is boundary leaking. Ultrasonographic images may contain several types of artifacts such as shadowing (caused by blockage of the sound beam beneath a dense structure), beam width artifact (caused by reflection/refraction of the sound beams on the side of a curved boundary of a structure) etc., which may make the edge information of follicles weak and discontinuous (see Chapter 1.3.4 Artifacts of ovarian ultrasound images for details). These unclear or uncompleted boundaries allow seed regions to grow well beyond the actual boundary of the structure if the image outside the structure is homogeneous with the seed region according to the criteria. Several methods have been reported to correct boundary leakage. For example, a watershed segmentation is used after region growing to "close off" leaked regions [74].

2.2.2 Evaluation methods

After a follicle segmentation algorithm is implemented, the efficiency and correctness of the segmentation must be evaluated. But, evaluating the segmentation results on medical images is a very difficult task. The main reasons of which include lack of a

"gold standard" (for 2D single image segmentation, manually detected segmentation by medical experts is the only standard available), and lack of standardized statistical protocols. [75]. The most commonly used mathematic methods for evaluating the follicle segmentation results in the literature mentioned above are simple linear regression analyses and the evaluation procedure reported by Potočnik (evaluate the quality of the segmentation result by measuring with two ratios r_1 and r_2 ,where r_1 is the ratio between the areas of the intersection and the original object, and r_2 is the ratio between the areas of the intersection and the segmented region) [75]. In addition, Hausdorff distance, root mean squared distance, average absolute distance and the Dice coefficient are commonly used in follicle segmentation evaluation [50, 52, 60, 65]. In general, Potočnik's method and the Dice coefficient are used to determine the follicle recognition rate [60, 65]. Linear regression is usually used to evaluate the correlation of computer assisted segmented follicular areas and/or volumes with a manual expert segmentation [52, 60]. The Hausdorff distance, root mean squared distance and average absolute distance are used to evaluate the accuracy of follicles' boundaries and the position of follicles [50, 51, 60, 61]. The details of these methods are as follows:

Linear regression is used to evaluate the linear relationship between two variables. In follicle segmentation evaluation, the two variables are computer-isolated follicles $X, X = \{X_1, X_2, ..., X_n\}$ and the operator's detection results $Y, Y = \{Y_1, Y_2, ..., Y_m\}$. Here, $X_1, X_2, ..., X_n$ and $Y_1, Y_2, ..., Y_m$ are the parameter values that are going to be compared. They can be sets of region area, volume, boundaries, etc. The regression equation is: $Y = a + bX$. Here a is the intercept of Y, b is the gradient or slope of the line. a and b can be obtained from:

$$b = \frac{n\sum X_i Y_i - (\sum X_i)(\sum Y_i)}{n\sum X_i^2 - (\sum X_i)^2} \tag{2.1}$$

and

$$a = \frac{\sum Y_i - b\sum X_i}{n} \tag{2.2}$$

where, n is the number of follicles to evaluate.

The value of slope b and intercept a can be used to evaluate the correlation of the segmentation results. A high correlation is determined if b and a do not differ significantly from one and zero, respectively.

In Potočnik's evaluation method, two ratios r_1 and r_2 were measured [75]. If r_1 is equal to or greater than a given threshold D_1, and at the same time, r_2 is equal to or greater than a given threshold D_2, the region is marked as correctly recognized [75].

The Hausdorff distance is defined as the maximum of the smallest distance between two points on two curves (boundaries) A and B [76]. a_i is one point in curve A and b_j is one point in curve B. $d(b_j, A)$ is the smallest distance from every point in B to curve A:

$$d(b_j, A) = \min_i \| b_j - a_i \| \tag{2.3}$$

As the same, $d(a_i, B)$ is the smallest distance from every point A to curve B:

$$d(a_i, B) = \min_j \| a_i - b_j \| \tag{2.4}$$

The maximum Hausdorff distance is defined as [76]:

$$D(A, B) = \max\left[\max_i [d(a_i, B)], \max_j [d(b_j, A)] \right] \tag{2.5}$$

For evaluating the segmentation result, $D(A, B)$ means that all the pixels belonging to A are not farther than $D(A, B)$ from some pixels of B. Therefore, the lower value of $D(A, B)$ means the higher correlation.

The root mean squared distance is a measure of the average squared error between two curves (boundaries) $E = \{e_1, e_2, ..., e_m\}$ and $F = \{f_1, f_2, ..., f_n\}$ [77]. The same as the first step of computing the Hausdorff distance, $d(e_j, F)$ is the smallest distance from every point in region E to region F, and $d(f_j, E)$ is the smallest distance from every point in region F to region E. The root mean squared distance is defined as [77]:

$$RMSD(E, F) = \sqrt{\frac{1}{m+n}\left(\sum_{i=1}^{m} d^2(e_i, F) + \sum_{j=1}^{n} d^2(f_j, E) \right)} \tag{2.6}$$

As with Hausdorff distance, a highly correlated boundary is indicated by a low root mean squared distance value.

The average absolute distance is defined as [60]:

$$AAD(G,K)=\frac{1}{2}\left(\frac{1}{m}\sum_{i=1}^{m}d(g_i,K)+\frac{1}{n}\sum_{j=1}^{n}d(k_j,G)\right) \tag{2.7}$$

where, $G=\{g_1,g_2,...,g_m\}$ and $K=\{k_1,k_2,...,k_n\}$ are two boundaries. $d(g_j,K)$ is the smallest distance from every point in boundary G to boundary K, and $d(k_j,G)$ is the smallest distance from every point in boundary K to boundary G. The lower value of the average absolute distance means the higher correlation.

The Dice coefficient is defined as follows [78]: let a set $H=\{h_1,h_2,...,h_m\}$ and set $I=\{i_1,i_2,...,i_n\}$ be sets of region pixels from the automatically segmented and manually segmented regions, respectively. Elements h_i and i_j represent coordinates of the pixels inside set H and set I. The Dice coefficient is calculated by:

$$Dice\ coefficient=\frac{2\times|H\cap I|}{|H|+|I|} \tag{2.8}$$

The Dice coefficient evaluates the degree of overlap for region H and region I. The result is a value smaller than one. A high correction rate is indicated if the Dice coefficient is close to one.

In this study, linear regression and the Dice coefficient are the methods used here to evaluate the correlation of computer assisted segmented follicle with the manually detected segmentation and the recognition rate.

2.3 Materials and methods

2.3.1 Data acquisition

The 3D data sets used herein are acquired from a sequence of 2D images. The series of ultrasonographic images is obtained from *ex-situ* scanning of ovaries in a water bath. The water bath imaging consists of putting a dissected ovary in a vat of liquid and then scanning along the longitudinal axis of the ovary under the liquid (see Figure 2.1) in half millimeter increments (around 8-9 pixels/mm). Two serials of datasets were used in this study – the training dataset and the test dataset. The acquisition of the training dataset is the same as in Singh's paper [79]: The dissected ovaries were placed in ice-cold

phosphate buffered saline (0.1 m phosphate buffer, 0.9% (w/v) sodium chloride, PH 7.2-7.4) and transported to the laboratory within 45 minutes of ovariectomy. Then the ovaries were placed in a degassed phosphate buffered saline bath and imaged using a broad-band (5-9MHz), convex-array, ultrasound transducer (ATL Mark 9 HDI ultrasound machine). The test dataset was obtained in a similar manner, but the liquid used in the bath was water, and it was put aside for at least 24 hours before the experiment to reduce reverberation artifacts due to air bubbles. The imaging was carried out by a single operator using an Aloka SSD-900 B-scan ultrasound console equipped with a 7.5 MHz linear transducer (UST-5821-7.5, Aloka, Japan). The control for overall gain was set between 70 and 80. However, a single gain setting was used for the acquisition of all images of a given ovary. In both of the training dataset and the test dataset, the time gain compensation (TGC) slopes, which can compensate for the decreasing strengths of sound beams by passing through deeper tissues, were set to the minimum levels.

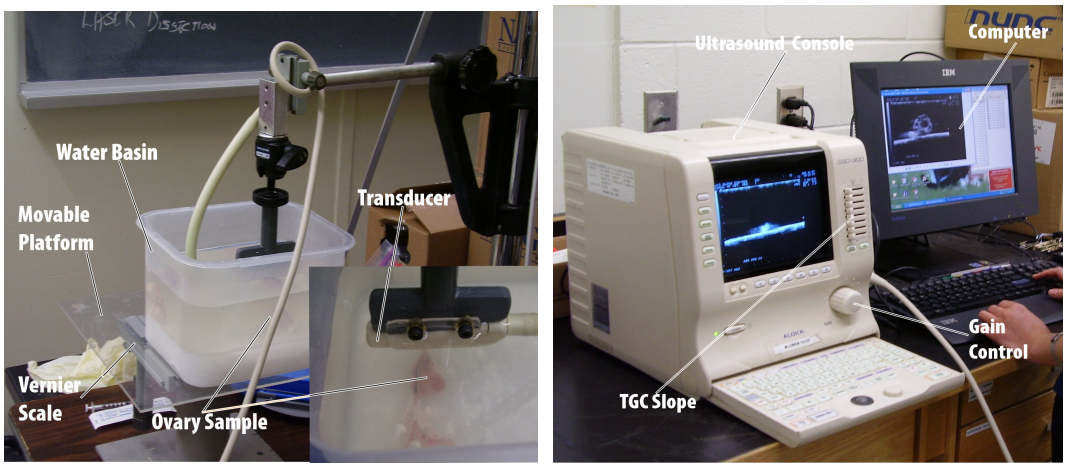

Figure 2.1 Illustration set-up for the acquisition of 3D ultrasonographic dataset from an exised bovine ovary using water bath. The ovary sample is put in the bottom of the water basin and fixed by needles. The basin is settled on a movable platform with a vernier scale. Segmental ultrasonographic images were recorded at 0.5 millimeter intervals by moving the platform. A computer was connected to the ultrasound console for digitizing the images.

To obtain a 3D dataset, the sequence of parallel image slices of an ovary is amalgamated to construct a 3D volume which forms the input to our segmentation. This

volume has some special properties: First, the distance between each slice is 0.5mm while the x and y axis resolution is 8~9 pixels/mm, which means the unit length along z-axis of the volume is 4~5 times larger than in x and y axes. This makes a spherical follicle look more like an ellipsoid in this 3D data volume. Actually, this is a disk-shaped (oblate spheroid) ellipsoid which has the same equatorial radii (the length of x and y axes), and is 4~5 times bigger than the polar radius (the length of z axes). Second, the way we generate the 3D data exacerbates the boundary leaking problem. The reasons are: (1) If there is boundary leakage on the adjacent slices at the same location on each image, this will become a major leaked region on the 3D volume surface; (2) the *ex-situ* imaging will make edge information even worse than *in vivo* imaging (where the outer region will be different shade of gray than the follicle antrum). The ovary sample is surrounded by water in this experiment, therefore, if a follicle is located close to the surface of the ovary on the ultrasonographic image, there may be sections of follicle wall that are not imaged successfully resulting in a lack of boundary between the follicle's interior and the background, an example of this phenomenon can be seen in Figure 2.2 (a). If the general 3D seeded region growing algorithm is used on this kind of data, one slice of the result will look like Figure 2.2 (b).

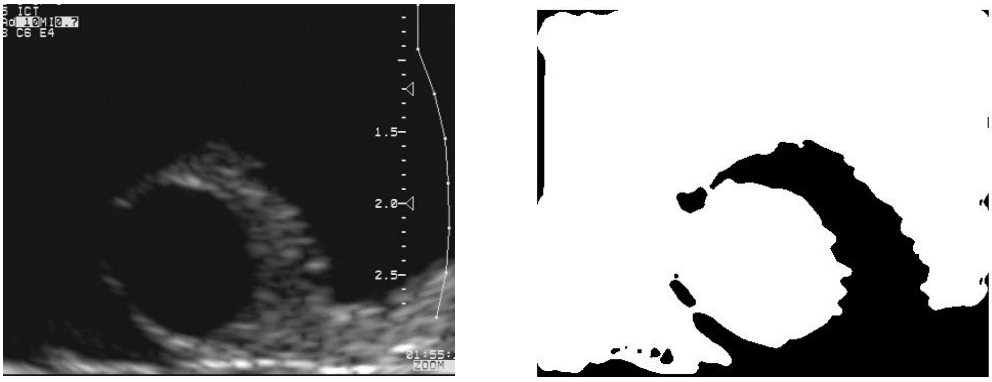

(a) **(b)**

Figure 2.2 Example of the boundary leakage image (a) and its SRG algorithm result (b).

2.3.2 3D SRG based follicle segmentation algorithm

The algorithm developed herein upgrades the general SRG algorithm [71] to overcome the problems caused by the characteristics of ovarian ultrasonography (noise, artifacts,

etc) and the constructed 3D volume. The algorithm begins by pre-processing the data to reduce noise. Then, a new seeded region growing algorithm is used to get the rough segmentation. Finally, a post-processing step is performed to obtain volumes with smooth surfaces. The algorithm is implemented in MATLAB, with the 3D SRG part written in C using mex files to interface with MATLAB.

1) Pre-processing: Ultrasound images are characterized by speckle noise. Therefore, the first step of this algorithm is speckle noise reduction and image smoothing. Smoothing was achieved using an adaptive neighborhood median filter [60]. A large kernel was used (11×11 pixels) for pixels darker than threshold T, and a small kernel is used (5×5 pixels) for the pixels brighter than threshold T. Here, T is a preset value. In contrast to [60], the threshold T we selected was 60% of the mean grey-level value in the original image. The reason is that since there was a large dark area on the water bath based ultrasonographic image, the intensity of the interior region of the follicles were consistently below 60% of the mean intensity of the whole image.

2) The developed SRG algorithm: In this study, the region growing begins from one manually selected seed point for each object (follicle) and the seed point must be selected close to the centre of the object. The reason is that the seed point will be treated as the true centroid of the follicle, and will be compared with the centroid of the grown region to determine whether the growing process should terminate. The algorithm begins from each seed point individually.

In each iteration of the algorithm, instead of growing each immediate neighborhood of the seeded region (6, 18 or 26 neighbors), we used a special size of the neighborhood of 11×11×3 pixels, because of the ellipsoid shaped follicle volume in this dataset. To achieve this growing procedure, a first-in-first-out (FIFO) queue is used. A queue is a type of data structure in which the elements are kept in order and principal operations are removing elements from the front of the queue and adding elements to the rear of the queue. The detail of the growing procedure in this study is as follows: first, the boundary pixels' addresses in one slice of the current region (see Figure 2.3 (a)) were put into a queue. A marker (a special value) was put to the end of the queue. Each element removed from the queue was considered as to whether or not its two dimensional neighbors (8 neighbors in this study) could pass the homogeneity tests. If yes, the

neighbors were put to the rear of the queue. Then the next element in the queue was tested and removed from the queue. When the current element being tested is the marker, a new marker was put to the end of the queue. Actually, markers can be treated as the number of circles of this region growing process. If the markers show up 5 times, that means the growing has been done 5 circles out of the current region (see Figure 2.3 (b)). This stage of growing terminated after 5 circles of growing were performed. This process was repeated in each slice of the original growing region (see Figure 2.3 (c)). After that, the result region will be grown using a 3D neighborhood (6 neighbors is used in this study) (see Figure 2.3 (d)). Due to this, the region is growing as the same ellipsoid shape as the entire object.

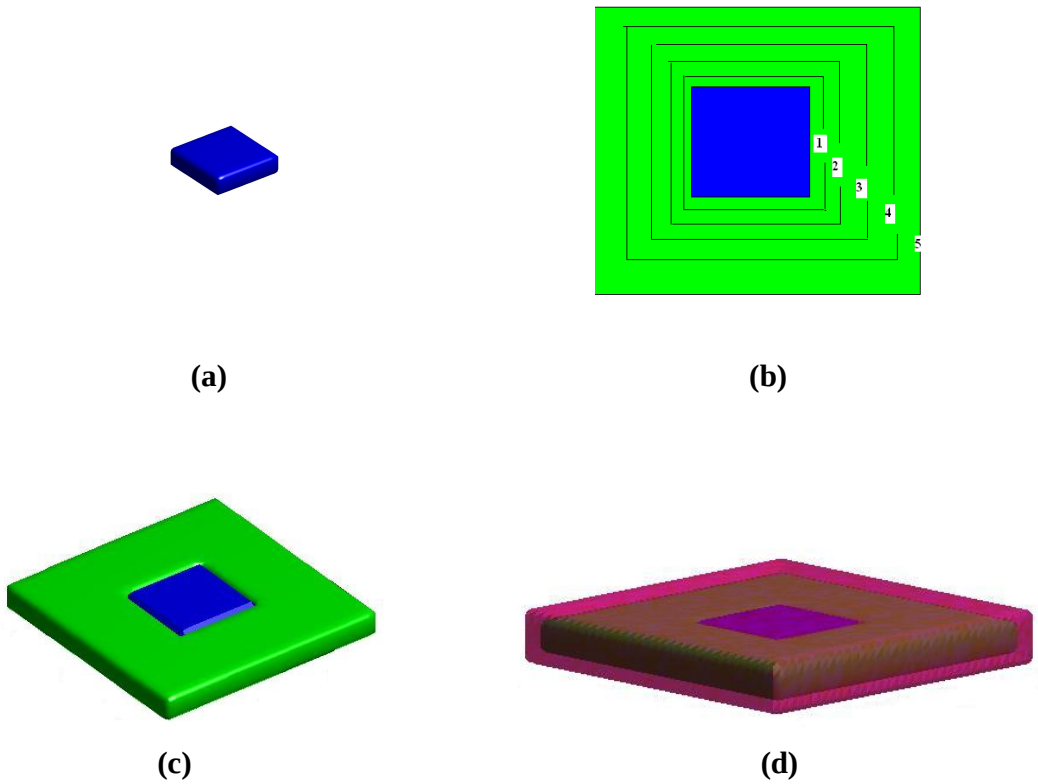

Figure 2.3 Illustration of the growing procedure of the $11\times11\times3$ pixels' neighborhood (a) is the current region, (b) is the illustration of the growing process in one slice (c) is the grown result after growing in each 2D slice, and (d) is the grown result after.

The homogeneity tests used in our SRG are a sequence of criteria based on [53] and on Haralick's region growing algorithm [78]. A formal description of the homogeneity tests is as follows: let the current homogeneous region, be denoted $R_0 = \{r_1, r_2, , , r_n\}$ where $r_1, r_2, , , r_n$ are the pixels belonging to R_0. Let the mean intensity of pixels in R_0 be $M(R_0)$, and let the standard deviation of pixel intensities in R_0 be $\sigma(R_0)$. Then, the first criterion of homogeneity tests is:

$$\left| I(x) - M(R_0) \right| \leq m \tag{2.9}$$

where x is a potential pixel candidate adjacent to R_0, $I(x)$ is the intensity of x and m is a preset threshold. In this study, m is set to 0.7$\times$the mean value of the 3D ovary volume currently being segmented. This criterion requires that the intensity of the candidate pixel has intensity similar to the mean intensity of the current region.

The second criterion is to calculate the change in standard deviation supposing that x is added to R_0:

$$\left| \sigma(R_1) - \sigma(R_0) \right| \leq \alpha \tag{2.10}$$

Where, R_1 is the region resulting from adding x to R_0 and α is another preset threshold. The selection of α depends on the image quality: if the quality is poor (huge boundary leaking occurs and/or lots of speckle noises), α = 2 times of the standard deviation of the whole ovary volume; if the quality is good enough (no or little boundary leaking occurs and/or little noise), α = the standard deviation of the whole volume. The threshold value of α is manually selected and it is ovary based, it will keep the same for all the follicles of one ovary. $\sigma(R_1)$ is the standard deviation of the region R_1 which can be computed incrementally from $\sigma(R_0)$:

$$\sigma^2(R_1) = \sigma^2(R_0) + [I(x) - M(R_1)]^2 + N(R_0)[M(R_1) - M(R_0)]^2 \tag{2.11}$$

$N(R_0)$ is the number of the pixels in R_0 and $M(R_1)$ is the updated mean value after adding x into region R_0 which can also be obtained incrementally from:

$$M(R_1) = \frac{M(R_0) \times N(R_0) + I(x)}{N(R_0) + 1} \tag{2.12}$$

In addition to the intensity-based homogeneity criteria, a shape-based criterion was used to overcome the boundary leaking problem. This criterion is only used in the 3D growing process (3D neighborhood). Because of the compact structure of spherically shaped follicles, a compactness test is usually added to the segmentation algorithms to extract the follicles from other non-follicle objects [53] or to fix the identified follicle regions [50]. The classical measure of compactness is the ratio between the square of the boundary perimeter (the cube of area of enclosing surface in 3D) to the area (the square of volume in 3D), as defined in [53]. Due to the non-spherical shape of the follicles in this constructed 3D volume, a volume comparison test C_v was used instead of the classical compactness test. C_v is defined as the ratio between the real volume of the current grown region and the volume of its "best–fit" ellipsoid volume, where the equatorial radii of the "best-fit" ellipsoid region equals the largest distance between the boundary pixels and the seed point we selected; the polar radius of this approximate ellipsoid equals one of the equatorial radius divided by 5 (because in the dataset used in this study, follicles are ellipsoid shaped with the polar radius 5 times shorter than equatorial radius). This criterion is determined as:

$$C_v \le C \tag{2.13}$$

In this study, the threshold C is set to 1.5. If the region R_1 passes this criterion as well, it can be permanently added into the list of this region set, and pixel x receives the follicle label value $L(R)$. Then the region R_0 will be updated to R_1. Otherwise, if it passes the homogeneity tests and fails the compactness test, x cannot receive the label value, but is nonetheless put into the list. After checking its neighborhood χ, x will be tested again as a non-labeled neighbor of χ. Because during the growing procedure, the region may be non-compact due to the noise and artifacts, but will become compact later after adding more pixels into the region.

A fourth criterion was used to solve the boundary leaking problem. As the region expands (growing), the surface area of the growing region should become increasingly larger unless most of the surface pixels already touch the edge of the object (follicle wall) and stop growing. If the program still has not stopped, it is possible that boundary leakage has happened. So a percentage value P is set here. If $1-P\%$ of surface pixels

stopped growing, the whole program stops. For different image quality, the threshold value P is different, usually a small value (or zero) for the follicles which have the completed boundaries or have little boundary leakage, and a large value for the follicles which have great boundary leakage problems. The P value of each follicle being segmented is automatically selected by using an iterative search algorithm. After each time running the whole SRG program for a follicle, the centroid of the grown region is calculated. If the distance between this centroid point and the pre-selected seed point is bigger than a threshold T_d, then boundary leakage may have occurred. Then $P = P + 1$, and the SRG program is repeated for that follicle until the centroid point is close enough to the seed point. T_d in this study is set to 20.

The flowchart of 3D SRG based follicle segmentation is summarized in Figure 2.4.

3*) Post-processing:* All of the follicles segmented individually are added into a new volume which has the same size as the original ovary volume with zero grey value, according to their address index. The holes inside the follicles are filled. Finally, the resulting regions are smoothed and visualized in 3D by using the MATLAB building in 3D smoothing and 3D visualization tools.

2.3.3 Validation method

Unlike other follicle segmentation research, we not only compared the segmentation result with the human observer-defined results, but also with follicle aspiration volumes. Immediately following image acquisition, follicle aspiration volumes were measured. In this study, 5ml syringes (Monoject™; Tyco Health Care Group, Mansfield, Massachusetts) fitted with $1.2mm \times 38.1mm$ needles (Monoject™; Tyco Health Care Group, Mansfield, Massachusetts) were used for aspirating the fluid in follicles with diameter (the diameter is measured in the slice in which the follicle shows the largest) bigger than 5mm in diameter; 3/10 ml insulin syringes (Monoject™; Tyco Health Care Group, Mansfield, Massachusetts) fitted with 29 ga, ½ inch ($0.33mm \times 13mm$) needles (Monoject™; Tyco Health Care Group, Mansfield, Massachusetts) were used for the follicles with diameter smaller than 5mm. Then the volume of fluid from each follicle was carefully measured.

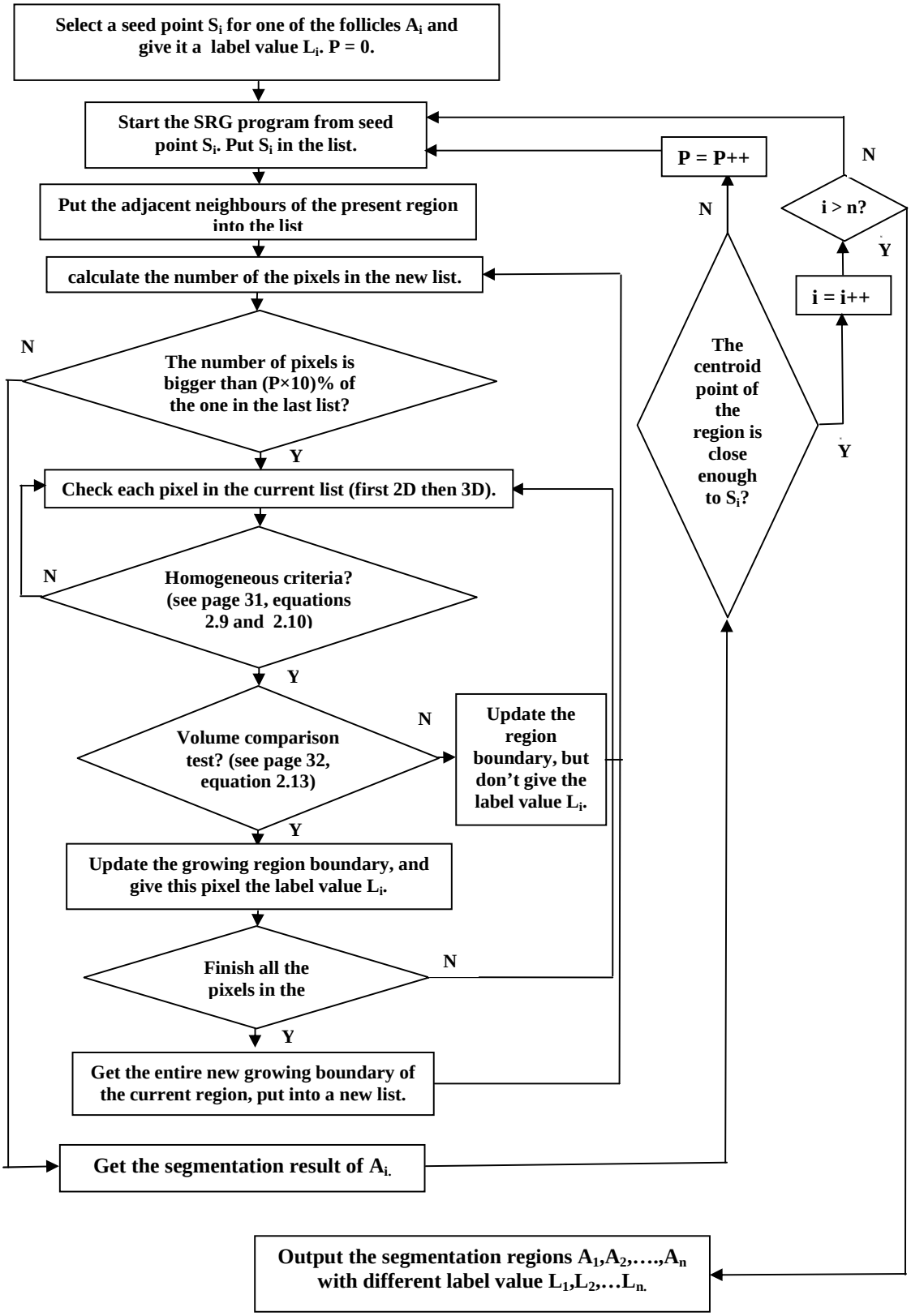

Figure 2.4 The flowchart of the follicle SRG algorithm.

The computer based follicle volume (the SRG segmented follicle volume and the human observer-defined follicle volume) was calculated by simply counting the number of voxels belonging to the detected follicle. The physical dimensions of each voxel are $\frac{1}{8}mm \times \frac{1}{8}mm \times \frac{1}{2}mm = \frac{1}{128}mm^3$ (1 pixel in each slice equal to $\frac{1}{8}mm$, while the interval between each slice is $\frac{1}{2}mm$).

We assumed that the relationship among the computer segmented follicle volume, the manually detected volume and the aspiration volume can be summarized as a straight-line graph. Linear regression was used for comparing among those three results.

The Dice coefficient was used to evaluate the position error between the computer-based segmentation and the human observed result.

Pearson's correlation coefficient can be used to calculate the similarity between two variables. If two variables $X = \{X_{1,}, X_2, ...X_n\}$ are $Y = \{Y_{1,}, Y_2, ...Y_n\}$ and, with means $\overline{X}$ and $\overline{Y}$, and standard deviations S_x and S_y. The Pearson correlation is [80]:

$$r = \frac{\sum_{i-1}^{n}(X_i - \overline{X})(Y_i - \overline{Y})}{(n-1)S_x S_y} \tag{2.14}$$

The coefficient r is a number between -1 and +1. A positive value implies a positive correlation, while a negative value implies a negative or inverse correlation. Value 1 means perfect positive correlation, while value -1 means perfect negative correlation.

In this study, Pearson's correlation coefficient was calculated to evaluate the difference between each two results among the aspiration results, the human observer-defined results, and the computer segmented results.

2.4 Results

In this section, the results of our current algorithm are presented. All datasets are obtained from the water bath experiments. Usually, in the ultrasound images of ovaries, follicles with a diameter greater than 2mm can be perceived clearly. In this study, only the follicles of 2.5mm or more in diameter were segmented. Ovarian ultrasound images

are in 256 shades of grey. For pre-processing, 350×414 sub-images were extracted from 640×480 original images. The program running time is different for each follicle depending on the follicle size and the boundary situation. It is usually approximately several seconds to 30 minutes for each follicle.

First, typical results are presented. In Figure 2.5, a sequence of original image slices through one ovary is demonstrated. The images shown here are 20 out of 65 images from the entire image sequence and determined by their slice numbers.

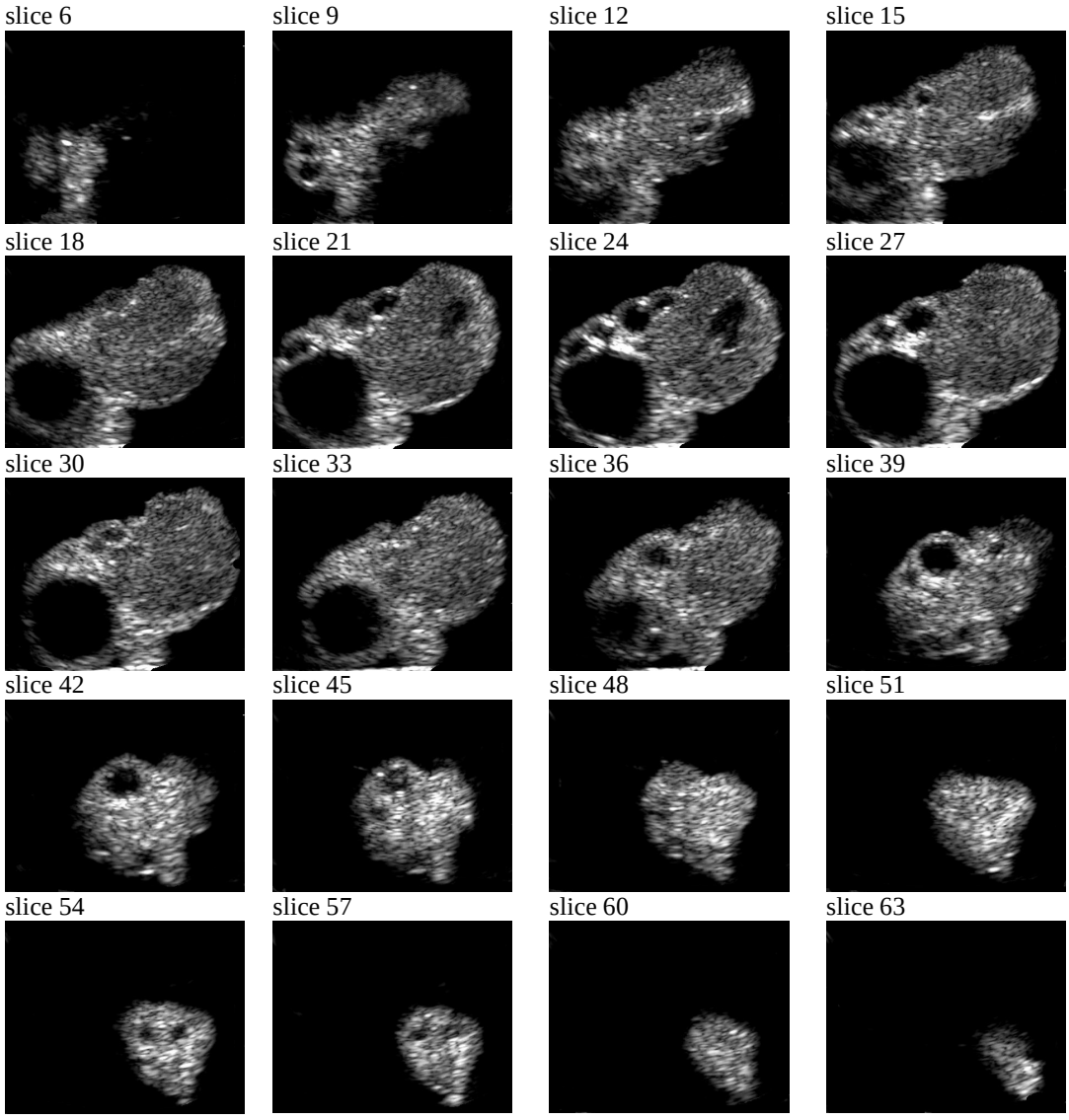

Figure 2.5 Original image sequence of cow ovary (ovary number 68 from training dataset) ultrasonographic images (20 slices out of 65 slices).

Then the entire image sequence is constructed into a 3D ovarian volume, see Figure 2.6.

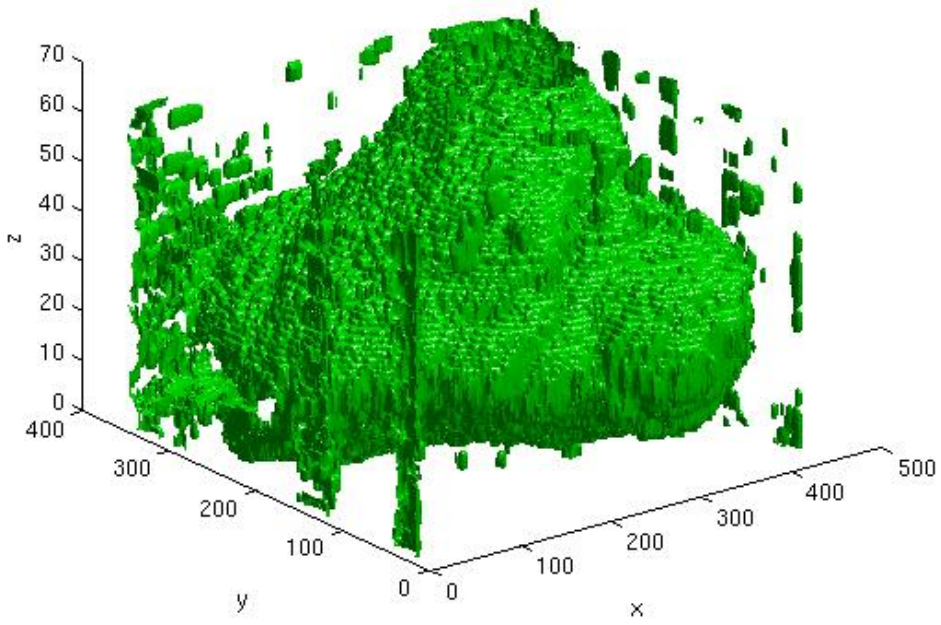

Figure 2.6 3D reconstruction result of the cow ovary (number 68 from training dataset). The coordinate (x,y) comes from 2D slices, and coordinate z is from the sequence of images.

Our follicle SRG algorithm is applied to this 3D dataset. The results are presented slice by slice in Figure 2.7. The segmented follicles are superimposed (outline in white) on the original image, and aligned in the same way as showed in the original images. From the Figure 2.7, we can see that boundary leakage occurred on the largest follicle in the image at the bottom left on slices from 27 to slice 48. The obtained results can be visualized in 3D, as in Figure 2.8.

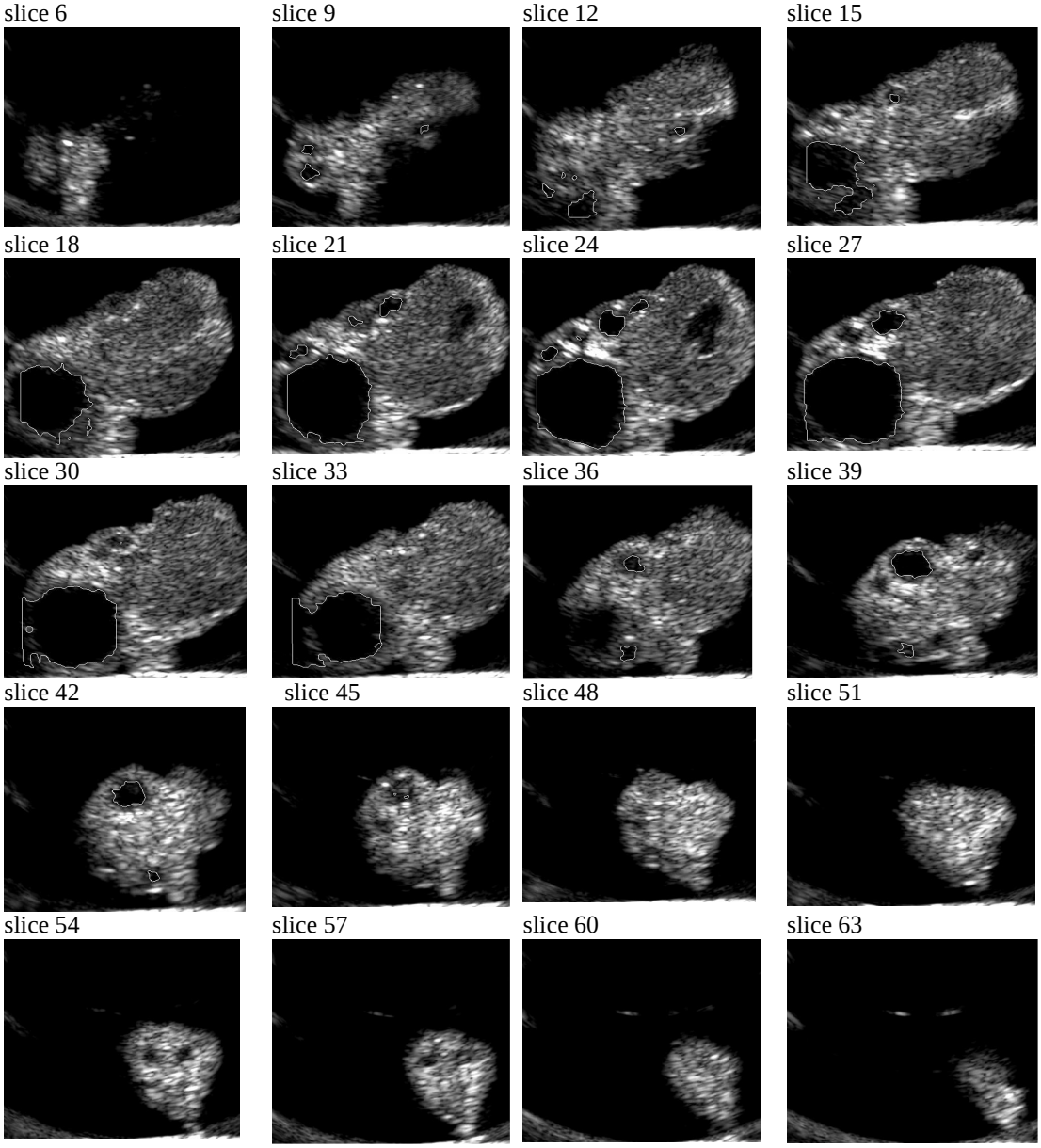

Figure 2.7 Sequence of the images from the SRG segmentation result, aligned in the same way as inFigure 2.5 (ovary number 68 from the training dataset).

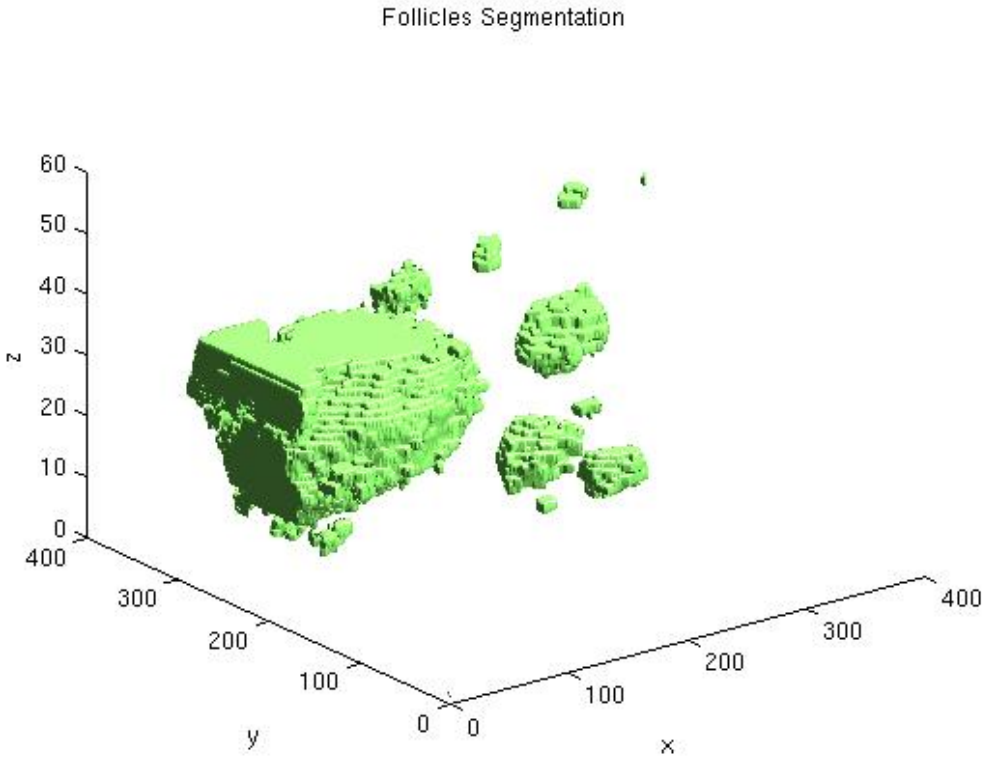

Figure 2.8 3D vision of the follicle segmentation result (ovary number 68 from the training dataset). The coordinate (x,y) comes from 2D slices, and coordinate z comes from the sequence of images.

In Figure 2.9, the results are compared with manually determined follicles by an expert, and also aligned in the same way as shown in the original images. Finally, Figure 2.10 shows the 3D volume of the manually determined segmentation result.

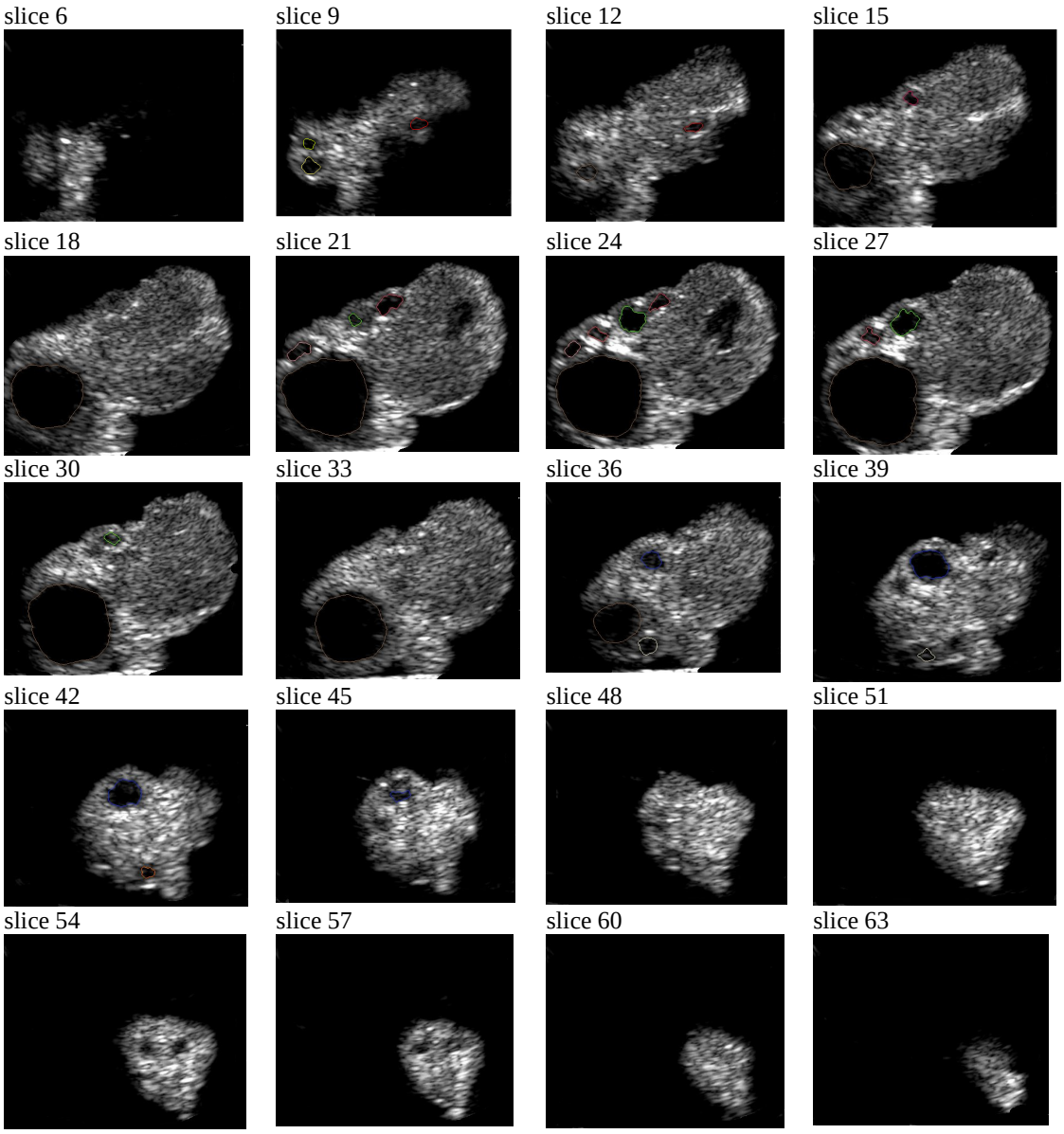

Figure 2.9 Sequence images of manually determined follicles, aligned in the same way as in Figure 2.5 (ovary number 68 from the training dataset).

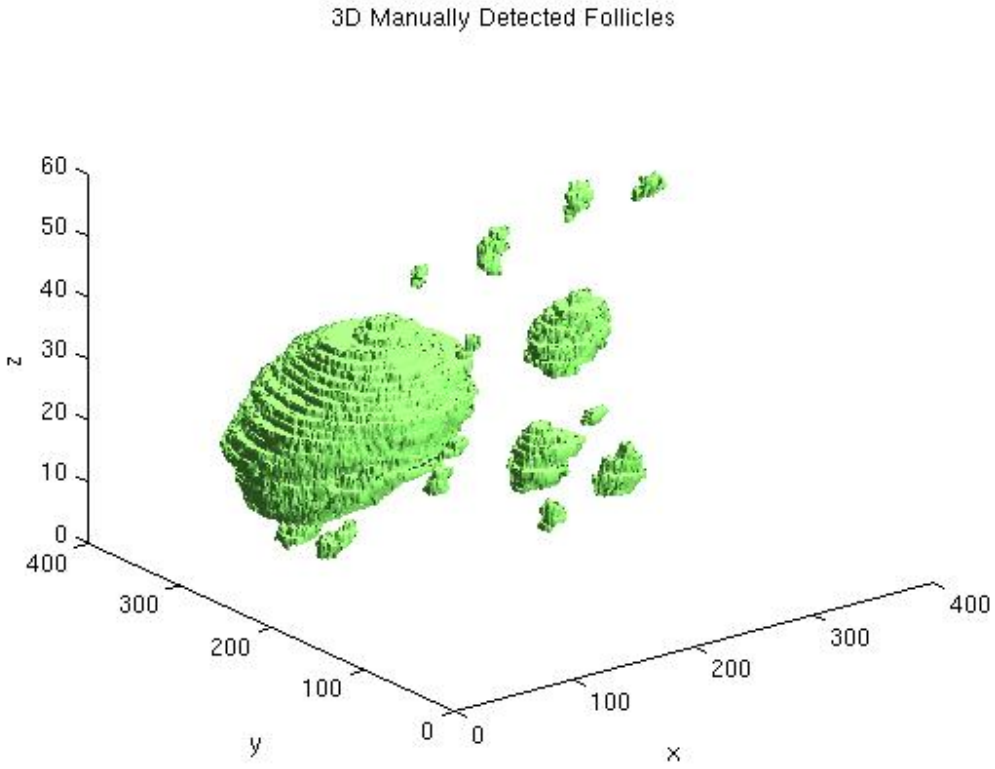

Figure 2.10 3D vision of the manually determined follicles (ovary number 68 from the training dataset). The coordinate (x,y) comes from 2D slices, and coordinate z comes from the sequence of images.

Next, the best segmentation result is presented in Figure 2.11a, and its observer-defined result is shown in Figure 2.11b

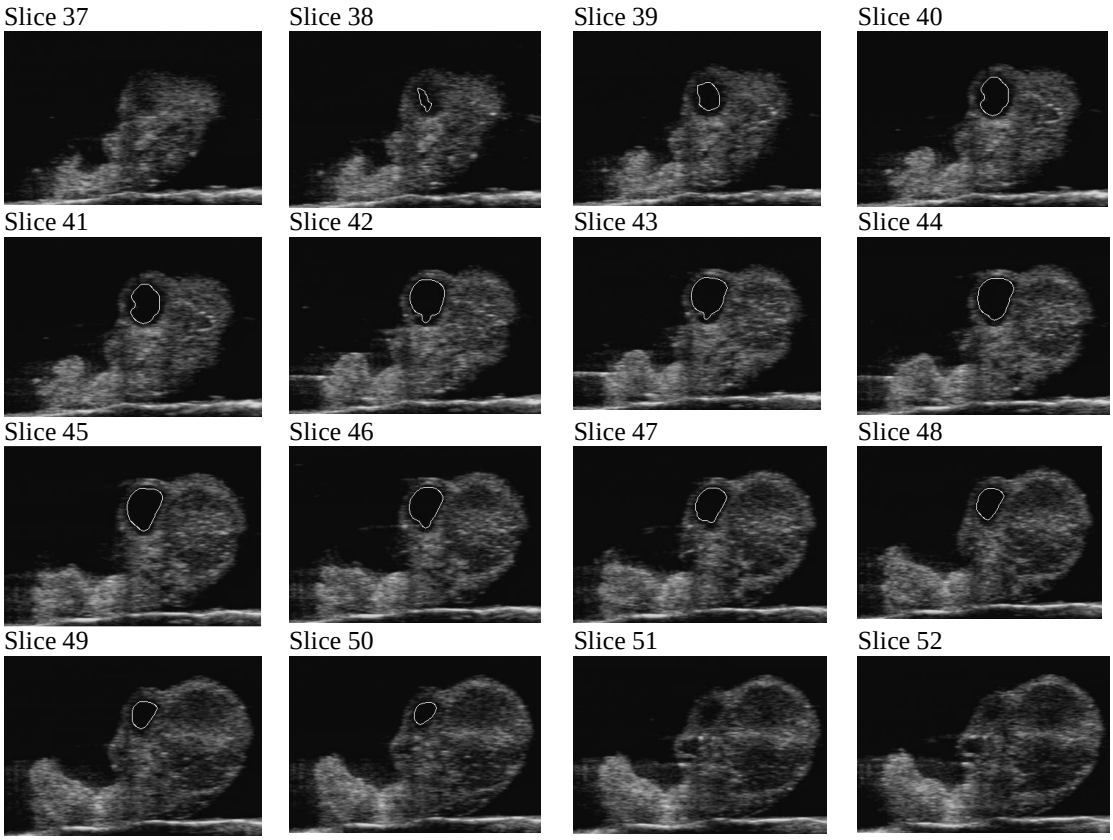

Figure 2.11a The computer-segmented boundary of the best follicle segmentation result.

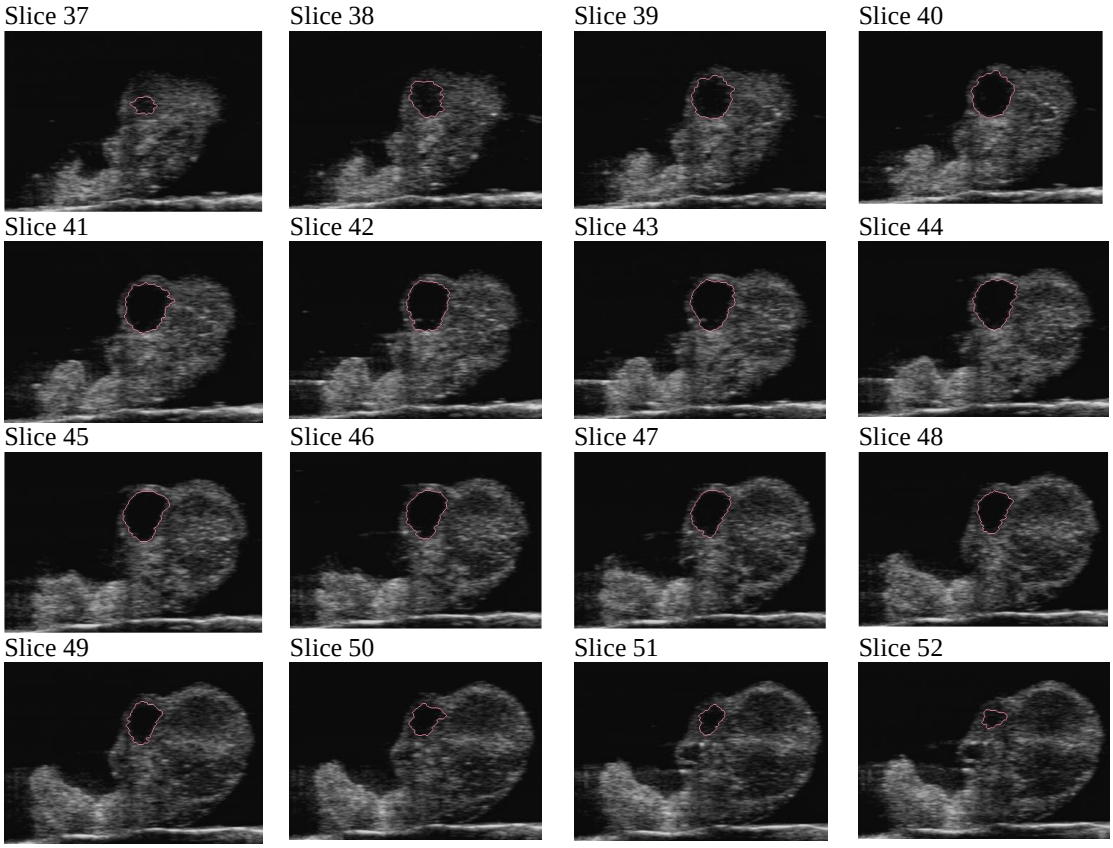

Figure 2.11bThe observer-defined boundary of the best segmentation result. In this case, the Dice coefficient of this follicle is 72.8%; the volume of the computer segmented result is 0.376 ml; the aspiration volume is 0.227 ml; and the volume of the manually detected result is 0.6571 ml.

The worst segmentation result is shown in Figure 2.12.

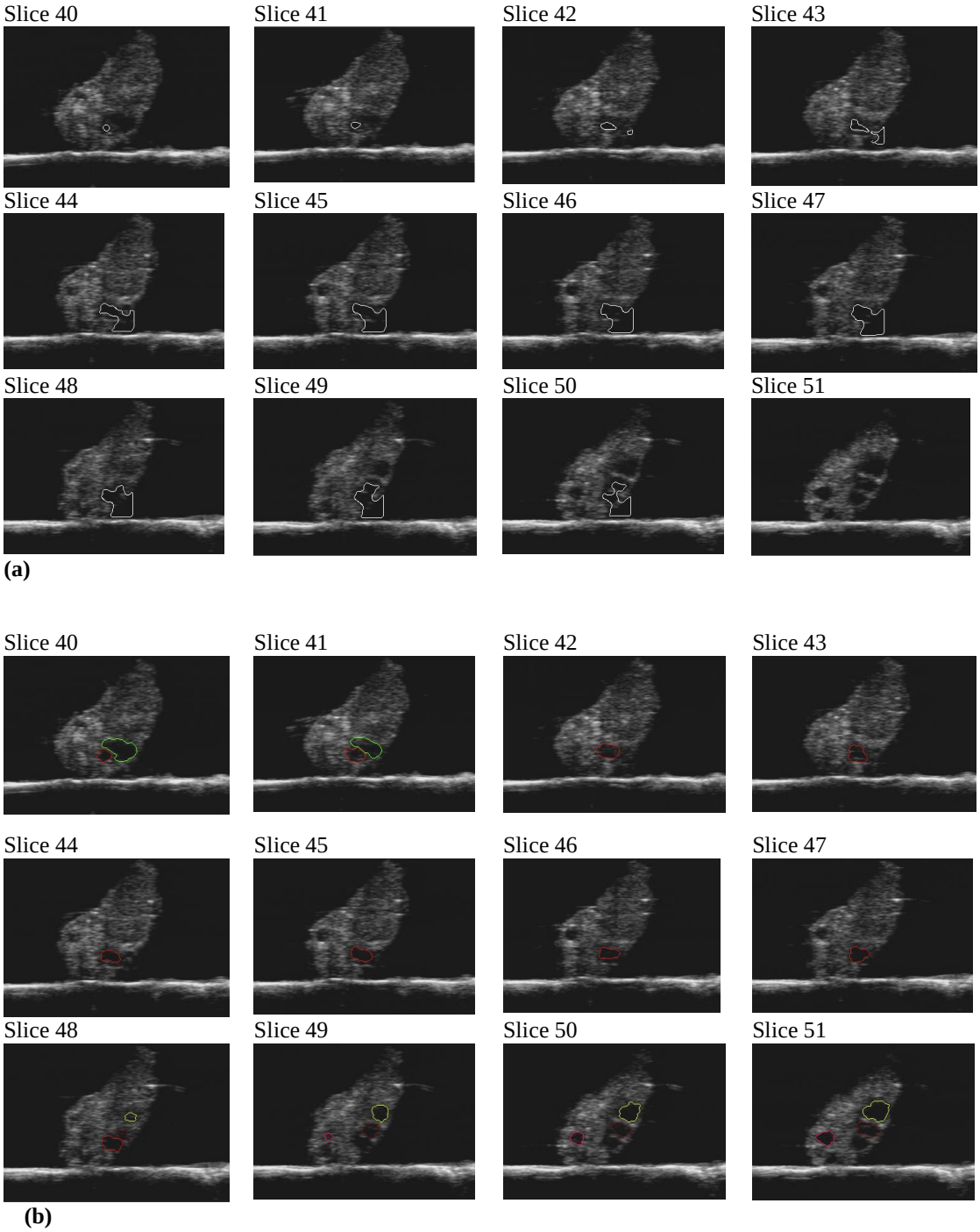

Figure 2.12 An example of a poorly segmented follicle (a) is its computer-segmented boundary and (b) is the observer-defined boundary. In this case, the Dice coefficient of this follicle is only 29.34%; the volume of the computer segmented result is 0.2124 ml; the aspiration volume is 0.060 ml; and the volume of the manually detected result is 0.0914 ml.

All together, 16 ovaries were used as test dataset. In total, 138 follicles in the ovaries dataset were analyzed. Since the follicles were segmented individually, we evaluated all the follicles together without considering the differences of each ovary. The statistical analyses were conducted using the Statistical Analysis System (SAS Institute; Cary, NC, USA).

The linear regression statistical comparisons of the follicles' volumes are given in Figure 2.13, Figure 2.14 and Figure 2.15. In Figure 2.13, we obtained the statistical comparison between our SRG follicle segmentation results and the aspiration results. Figure 2.14 shows the statistical comparison between the SRG follicle segmentation result and the manually determined segmentation result. Figure 2.15 shows the statistical comparison between aspiration result and the manually determined segmentation result. The statistical analysis support one of the hypotheses that there will be linear relationships between the computer-segmented follicle volumes, aspirated follicle volumes and observer-defined follicle volumes (respectively, $y = 0.857x + 0.005$, $R^2 = 0.946$, $P < 0.0001$, see Figure 2.13; $y = 1.512 – 0.025$, $R^2 = 0.936$, $P < 0.0001$, see Figure 2.14; $y = 0.544x + 0.030$, $R^2 = 0.931$, $P < 0.0001$, see Figure 2.15). There was no perfect agreement between the aspiration result and the SRG segmentation result (slope = 0.857, see Figure 2.13), no agreement between the manually defined result and the SRG segmentation result (slope = 1.512, see Figure 2.14), and no agreement between the aspiration result and the manually defined result (slope = 0.544, see Figure 2.15). These results did not support the hypothesis that there will be an agreement between each two results among the SRG follicle segmentation results, the aspiration results and the manually determined results.

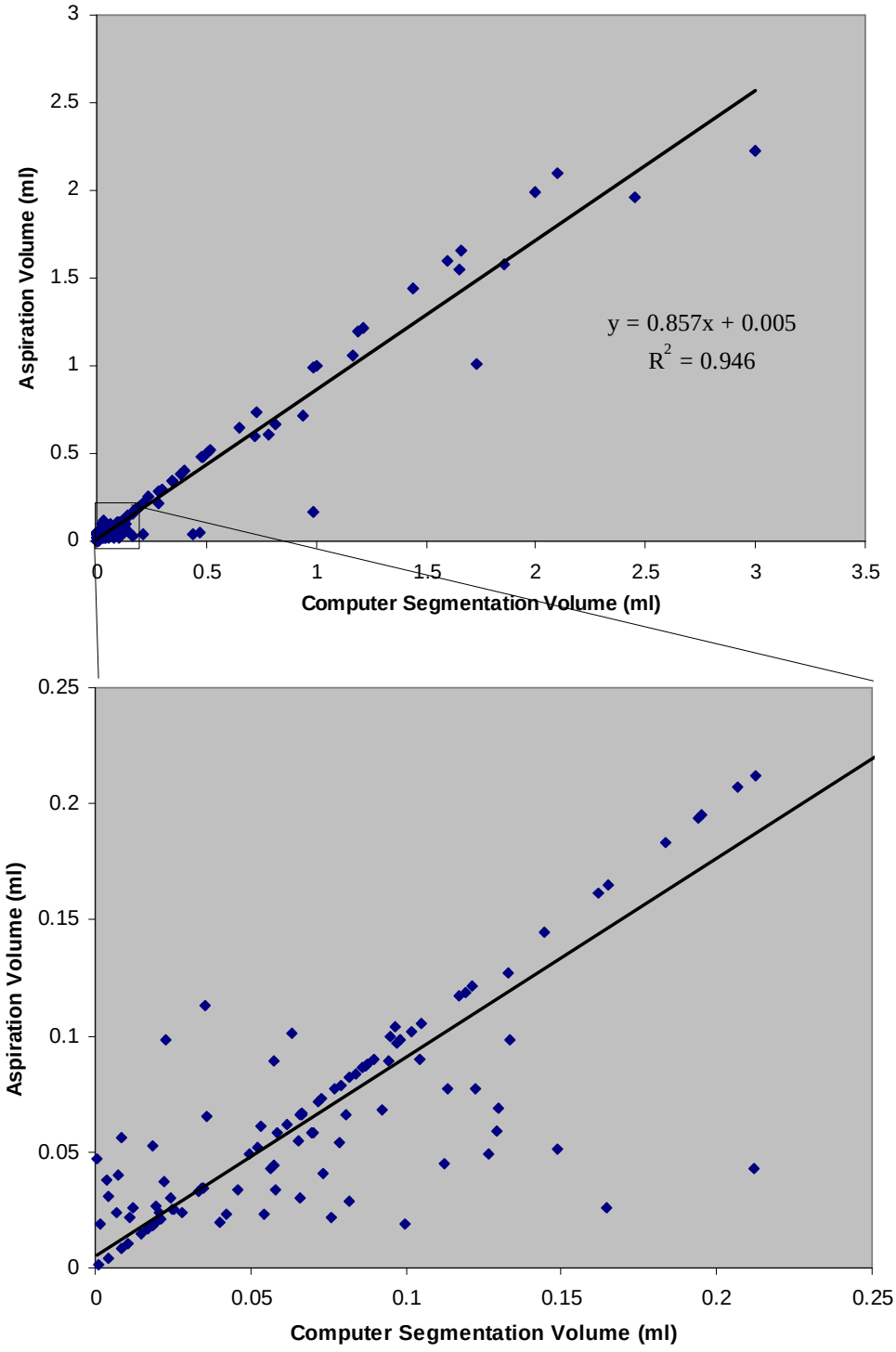

Figure 2.13 Comparison of the computer segmentation and follicle aspiration volume ($y = 0.857x + 0.005$, $R^2 = 0.946$, $P < 0.0001$).

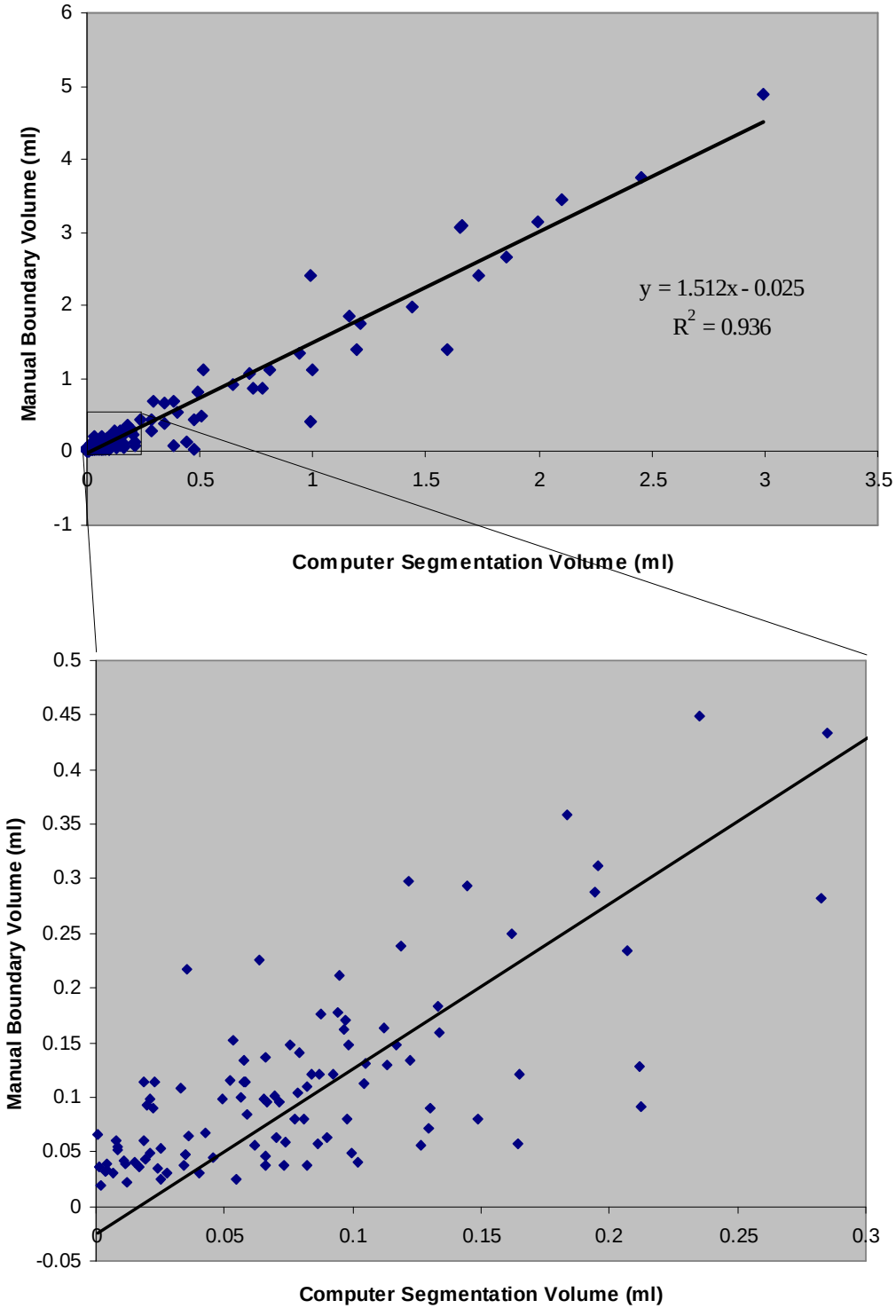

Figure 2.14 Comparison of the computer segmentation and observer-defined volume ($y = 1.512x - 0.025$, $R^2 = 0.936$, $P<0.0001$).

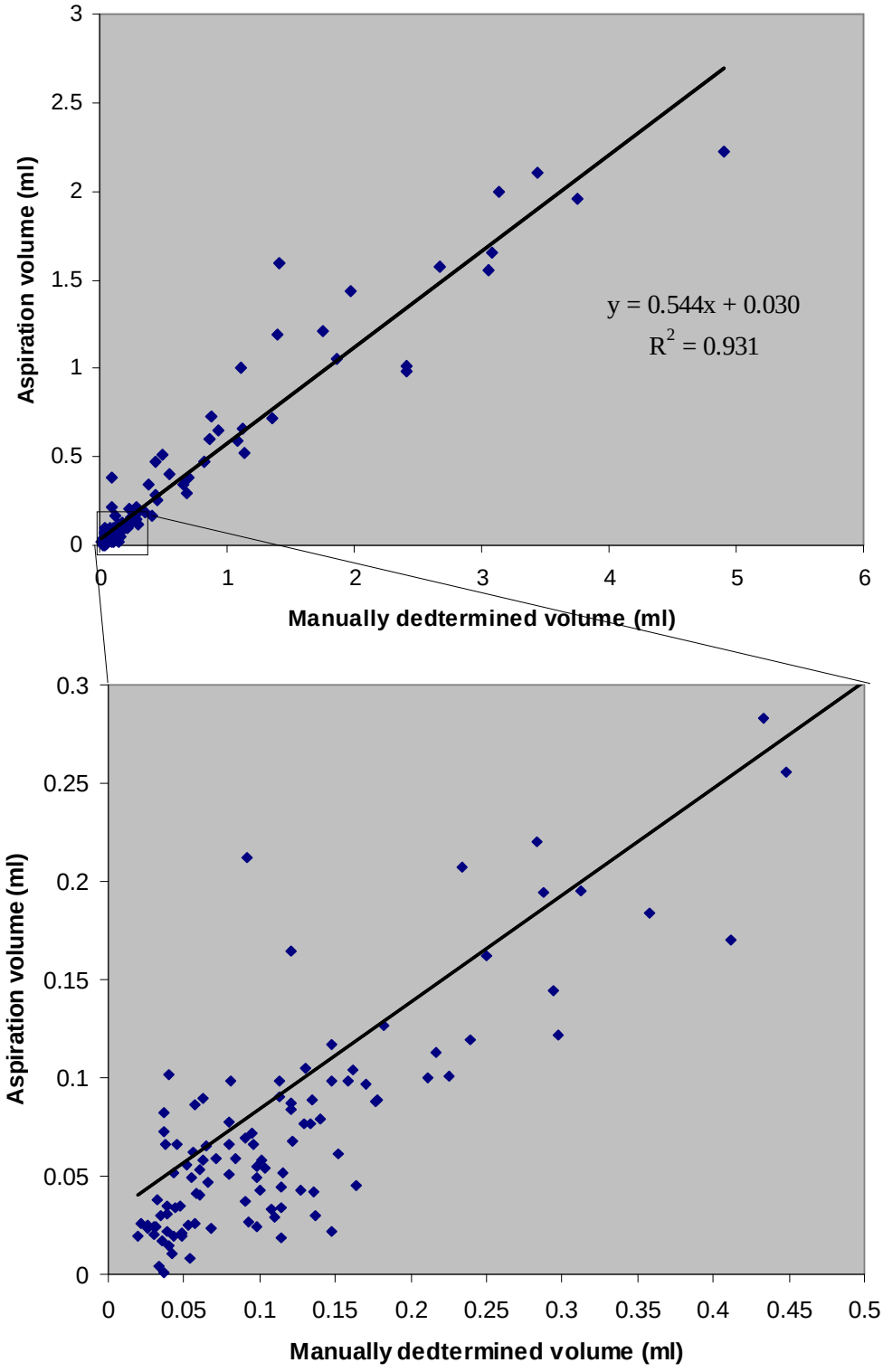

Figure 2.15 Comparison of the aspiration volume and observer-defined volume (y = 0.544x + 0.030, R^2 = 0.931, P <0.0001).

In addition to the overall analysis of the follicles among the SRG segmentation results, the aspiration result and the manually determined segmentation result, the evaluation among follicles in different size categories was also considered in this study. Ten categories were defined here: 3mm diameter or less, 3 to 4, 4 to 5, 5 to 6, ….., 11mm or greater. Table 2.1 shows the difference of the aspiration result and the manually determined result (Mean ± Standard Error) among the categories by analysis of variance (ANOVA) followed by the Tukey Post-hoc test (a multiple pairwise comparisons procedure). The letter superscripts (a,b,c,d…) are used in the table indicate a difference. The results with different superscripts within the same column were significantly different at a significant level of 0.05 by using Tukey Post-hoc test. As the diameter increases, the aspiration volume and the manually determined follicular volume increase. Analysis with ANOVA indicated a statistically significant difference between follicle categories in both the aspiration volume and the manually determined volume (overall ANOVA, $P<0.0001$). By Tukey Post-hoc test, aspiration volumes of small size follicles (diameter of follicles $\leq$ 6mm, the first 4 groups of size categories) were not significantly different between groups. For the follicles in diameter from 6 to 8 mm, the aspiration volumes were not significantly different. Follicles in diameter from 8 to 10 mm also had same volume. In manually determined follicle volume, the Tukey Post-hoc test revealed follicles in diameter from 4 to 8mm were not significantly different and follicles from 8 to 10mm had same volume.

Table 2.1 Mean aspiration volume and manually determined volume of the follicles within a follicle size category.

Diameter categories	Number of follicles	Aspiration volume	Manual volume
≤ 3mm	54	0.046 ± 0.005^{a}	0.065 ± 0.005^{a}
3~4mm	36	0.084 ± 0.011^{a}	0.118 ± 0.009^{b}
4~5mm	12	0.149 ± 0.033^{a}	0.234 ± 0.029^{c}
5~6mm	9	0.268 ± 0.060^{a}	0.410 ± 0.076^{c}
6~7mm	7	0.516 ± 0.104^{b}	0.764 ± 0.080^{c}
7~8mm	4	0.553 ± 0.034^{b}	0.929 ± 0.123^{c}
8~9mm	4	1.17 ± 0.253^{c}	1.39 ± 0.017^{d}
9~10mm	3	1.22 ± 0.124^{c}	2.05 ± 0.195^{d}
10~11mm	7	1.56 ± 0.160^{d}	2.81 ± 0.203^{e}
>11mm	2	2.09 ± 0.135^{e}	4.33 ± 0.574^{f}
Overall ANOVA P-value		< 0.0001	< 0.0001

* Different superscripts (a,b,c,…) indicate difference in follicle category at $P<0.05$ using Tukey Post-hoc comparison. Means are presented ± standard error along with the total number of follicles evaluated in each size category.

As a result, in the future analyses, we can combine several non-significantly different groups into one group to evaluate the accuracy of our algorithm. Considering that the first three groups have 70% of the total number of follicles, we separated the138 follicles into 2 groups: one group of follicles with diameters no more than 5mm; the other with diameters bigger than 5mm. Then, the simple linear regression for these two groups was computed. Figure 2.16, Figure 2.17 and Figure 2.18 shows the linear regression results between each two results among the computer assisted follicle segmentation result, the manually detected follicle volume and the aspiration volume of the small size ($\leq$ 5mm) follicles. Figure 2.19, Figure 2.20 and Figure 2.21 shows the linear regressions of the large size (> 5mm) follicles. The statistics results of the small size follicles show that there were statistically significant linear relationships between the aspiration result and the SRG segmentation result ($y = 0.520x + 0.026$, $R^2 = 0.463$, $P < 0.0001$, see Figure 2.16), between the manually defined result and the SRG segmentation result ($y = 0.421x + 0.067$, $R^2 = 0.249$, $P < 0.0001$, see Figure 2.17), and between the aspiration result and the manually determined result ($y = 0.627x + 0.007$, $R^2 = 0.480$, $P < 0.0001$, see Figure 2.18). In the group of large size follicles, there were significant linear relationships between the aspiration result and the SRG segmentation result ($y = 0.832x + 0.0520$, $R^2 = 0.907$, $P < 0.0001$, see Figure 2.19), between the manually defined result and the SRG segmentation result ($y = 1.549x – 0.055$, $R^2 = 0.901$, $P < 0.0001$, see Figure 2.20), and between the aspiration result and the manually determined result ($y = 0.501x + 0.134$, $R^2 = 0.876$, $P < 0.0001$, see Figure 2.21). Moreover, if we compared the statistics results between the two groups of the small size follicles and the large size follicles, we found that there were better correlations between the SRG segmentation volumes, the aspiration volumes and the manually determined volumes in the large size follicles than that in the small size follicles ($R^2 = 0.463$ in Figure 2.16 vs. $R^2 = 0.907$ in Figure 2.19; $R^2 = 0.249$ in Figure 2.17 vs. $R^2 = 0.901$ in Figure 2.20; $R^2 = 0.480$ in Figure 2.18 vs. $R^2 = 0.876$ in Figure 2.21). From the slopes of the regression lines, there was no agreement between each two volumes among the SRG segmentation result, the manually detected follicle volume, the aspiration volume.

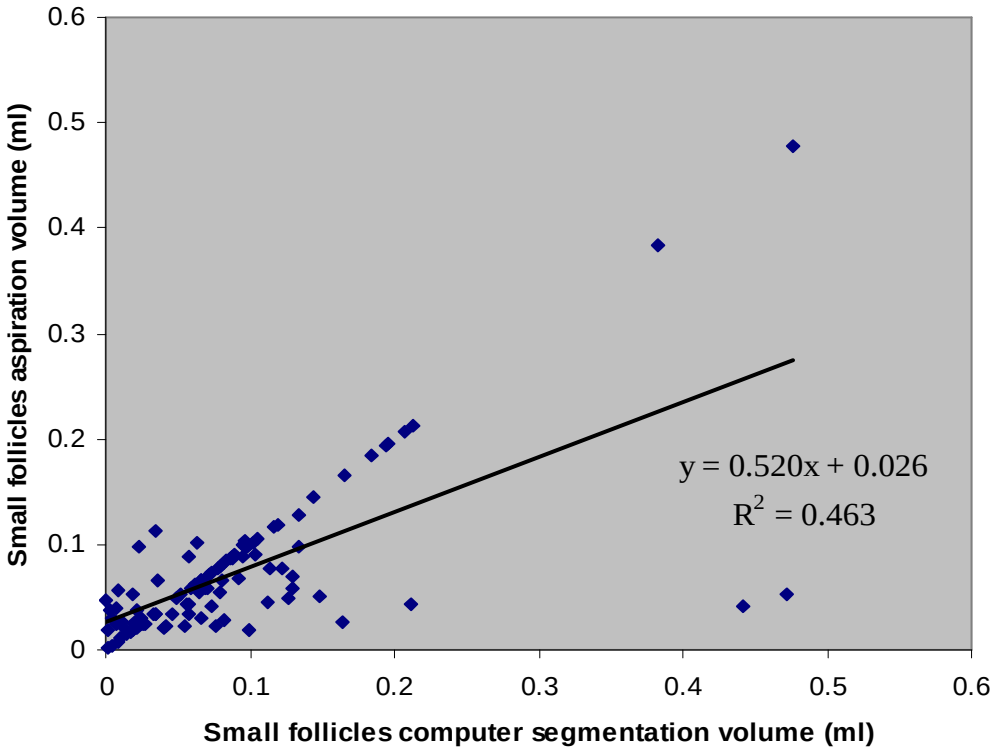

Figure 2.16 Comparison of the SRG segmentation volume and follicle aspiration volume of small size (≤ 5mm) follicles (y = 0.520x + 0.026, R^2 = 0.463, P < 0.0001).

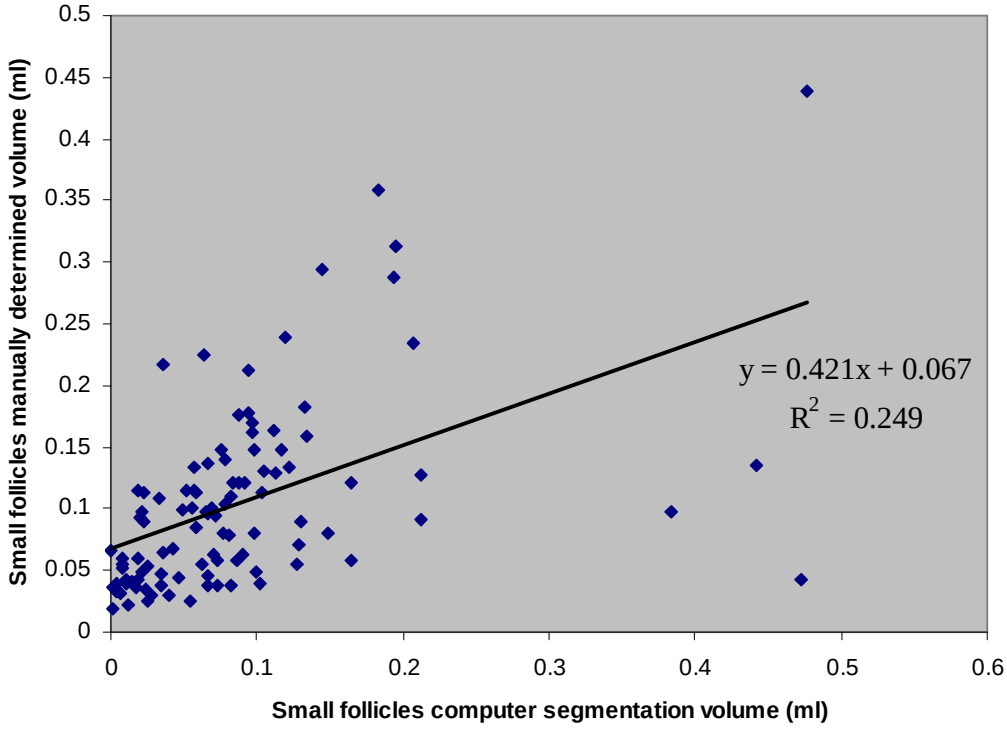

Figure 2.17 Comparison of the SRG segmentation volume and observer-defined volume of small size (≤ 5mm) follicles (y = 0.421 + 0.067, R^2 = 0.249 P < 0.0001).

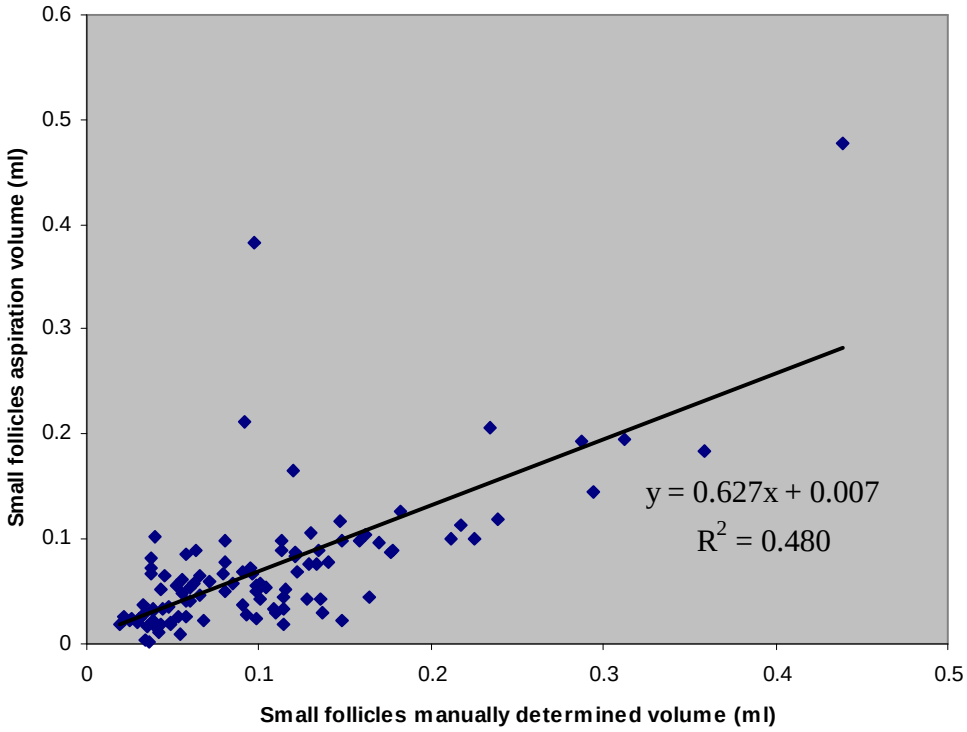

Figure 2.18 Comparison of the aspiration volume and observer-defined volume of small size (≤ 5mm) follicles ($y = 0.627x + 0.007$, $R^2 = 0.480$, $P < 0.0001$).

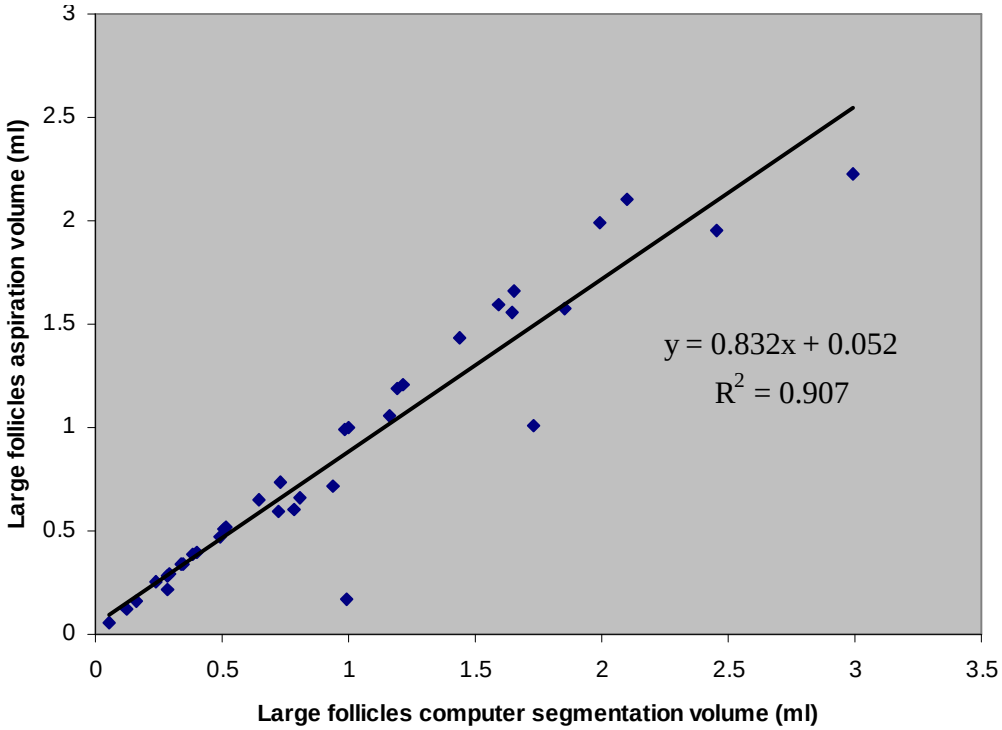

Figure 2.19 Comparison of the SRG segmentation volume and follicle aspiration volume of large size (> 5mm) follicles ($y = 0.832x + 0.052$, $R^2 = 0.907$, $P < 0.0001$).

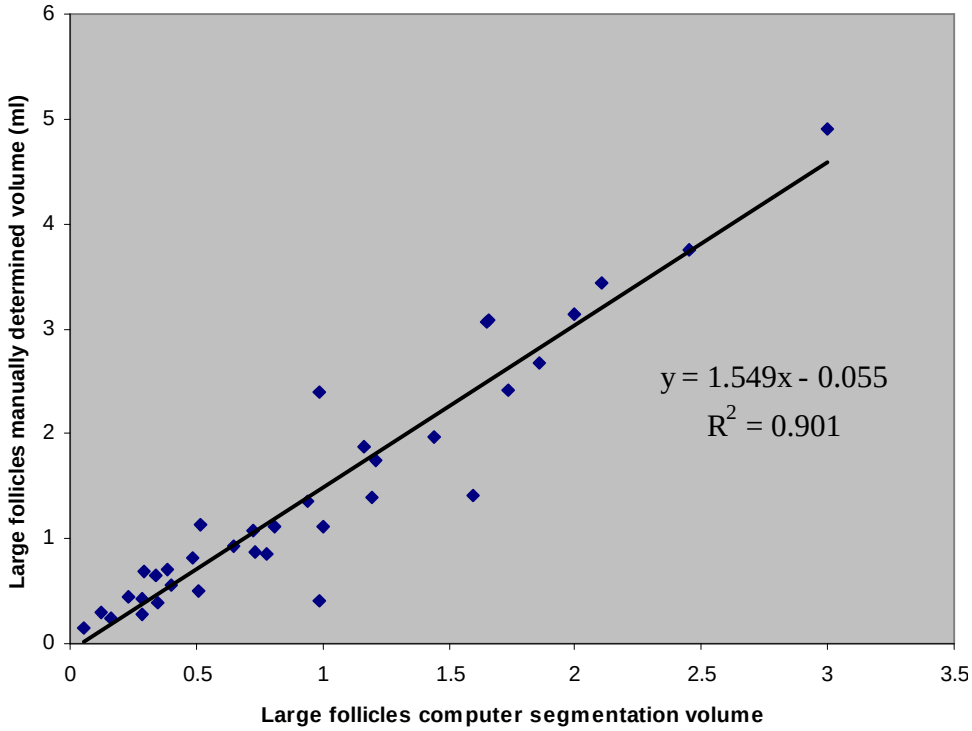

Figure 2.20 Comparison of the SRG segmentation volume and observer-defined volume of large size (> 5mm) follicles (y =1.549 - 0.055, R^2 = 0.901, P < 0.0001).

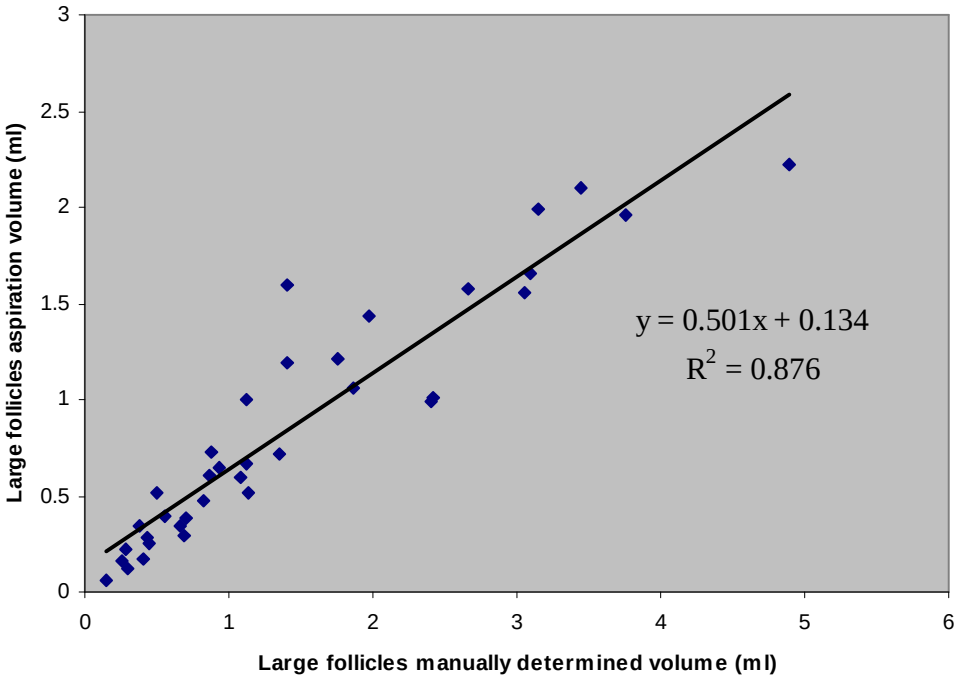

Figure 2.21 Comparison of the aspiration volume and observer-defined volume of large size (> 5mm) follicles (y = 0.501x + 0.134, R^2 = 0.876, P < 0.0001).

For testing the sensitivity of the seed point selected for each follicle, two more seed points were generated by using the 3D Gaussian random function with the standard deviation equal to the one third of the radium of each follicle, as long as the generated seed points were located inside the follicle. All the 16 ovaries were tested two more times by using the new generated seed points. The SAS PROC MIXED model (a SAS institute's program that allows researchers to model the covariance structure of the data, SAS institute, 1999) analysis with unstructured structure (covariance structures represent the correlations among the repeated measurements. The 'unstructured' structure makes no assumption regarding correlation [81]) was used to determine the effects of follicle diameter categories, the segmentation results by using three sets of different seed points, and the interaction of follicle categories and the segmentation results by using three sets of seed points. The segmented results were evaluated among each randomly selected seed point and the operator manually selected seed point within different size categories (Table 2.2). The superscripts (a,b,c,d…) have the same meaning as in Table 2.1. Superscripts (x,y..) indicate the difference in the same row at $P<0.05$. There were no significant differences between the segmented follicular volumes among the three sets of seed points (row comparison, $P \geq 0.05$), except for the follicle in diameter categories 5~6mm, 6~7mm and 8~9mm and >11mm which were sensitive to the seed point position. In the mean computer segmented follicle volumes of three sets of seed points, there was no significant difference among the diameter categories ≤ 3mm, 3~4mm, and 4~5mm (column comparison, $P \geq 0.05$), and no significant difference among the diameter categories 5~6mm, 6~7mm, and 7~8mm and between the categories 9~10mm and 10~11mm (column comparison, $P \geq 0.05$). Overall, from Table 2.2, we can see the segmentation results are sensitive to the selected seed points. This did not support the hypothesis that the follicle segmentation results from the computer will not be sensitive to the position of the selected seed point.

Table 2.2 Mean computer segmented follicle volume within different size categories among the original manually selected seed points, the randomly selected seed points (group 1 and 2).

Diameter categories	Operator selected seed point	Randomly selected seed points		Mean value by using three sets of seed points
		1	2	
≤ 3mm	0.065 ± 0.010 ^{X}	0.077 ± 0.013 ^{X}	0.079 ± 0.020 ^{X}	0.074 ± 0.009 ^{a}
3~4mm	0.099 ± 0.016 ^{X}	0.112 ± 0.026 ^{X}	0.086 ± 0.015 ^{X}	0.099 ± 0.011 ^{a}
4~5mm	0.149 ± 0.033 ^{X}	0.141 ± 0.030 ^{X}	0.119 ± 0.023 ^{X}	0.136 ± 0.016 ^{a}
5~6mm	0.365 ± 0.097 ^{X}	0.234 ± 0.061 ^{Y}	0.502 ± 0.236 ^{Z}	0.367 ± 0.087 ^{b}
6~7mm	0.538 ± 0.111 ^{X}	0.404 ± 0.114 ^{Y}	0.547 ± 0.112 ^{Y}	0.496 ± 0.063 ^{b}
7~8mm	0.610 ± 0.065 ^{X}	0.636 ± 0.061 ^{X}	0.634 ± 0.063 ^{X}	0.627 ± 0.034 ^{b}
8~9mm	1.24 ± 0.191 ^{X}	1.01 ± 0.119 ^{Y}	0.934 ± 0.109 ^{Y}	1.06 ± 0.086 ^{c}
9~10mm	1.46 ± 0.151 ^{X}	1.52 ± 0.056 ^{X}	1.52 ± 0.114 ^{X}	1.50 ± 0.058 ^{d}
10~11mm	1.63 ± 0.157 ^{X}	1.53 ± 0.300 ^{X}	1.69 ± 0.184 ^{X}	1.62 ± 0.123 ^{d}
>11mm	2.72 ± 0.271 ^{X}	2.84 ± 0.046 ^{X}	3.32 ± 0.267 ^{Y}	2.96 ± 0.152 ^{e}
Repeated Measure ANOVA Analysis (Pro Mixed)	Follicle category P< 0.0001 Three sets of seed points P = 0.0132 Follicle category * Three sets of seed points P = 0.0001			

* Different superscripts (X, Y, Z,…) indicate selection mode differences (row comparison) at $P < 0.05$.
* * Different superscripts (a, b, c, d,…) indicate difference in follicle category (column comparison) at $P< 0.05$

The simple linear regression was used again to compare the mean computer segmentation volume of three sets of seed points with both the manually detected follicle volume and the aspiration volume. Figure 2.22 shows the statistical comparison between aspiration result and the mean computer segmented follicle volume of three sets of seed points. Figure 2.23 shows the linear regression result between the mean computer segmented follicle volume of three sets of seed points and the manually determined segmentation result. The statistical results show that there were significant linear relationships between the aspiration result and the mean computer segmented follicle volume ($y = 0.816x + 0.017$, $R^2 = 0.902$, $P < 0.0001$, see Figure 2.22); and between the manually defined result and the mean computer segmented follicle volume ($y = 1.458x – 0.010$, $R^2 = 0.915$, $P < 0.0001$, see Figure 2.23). The slopes of the regression lines show there was no perfect agreement between the aspiration follicle volume and the mean value of computer segmented follicle results by using three sets of seed points; or between the manually detected follicle result and the mean value of computer segmented follicle volume.

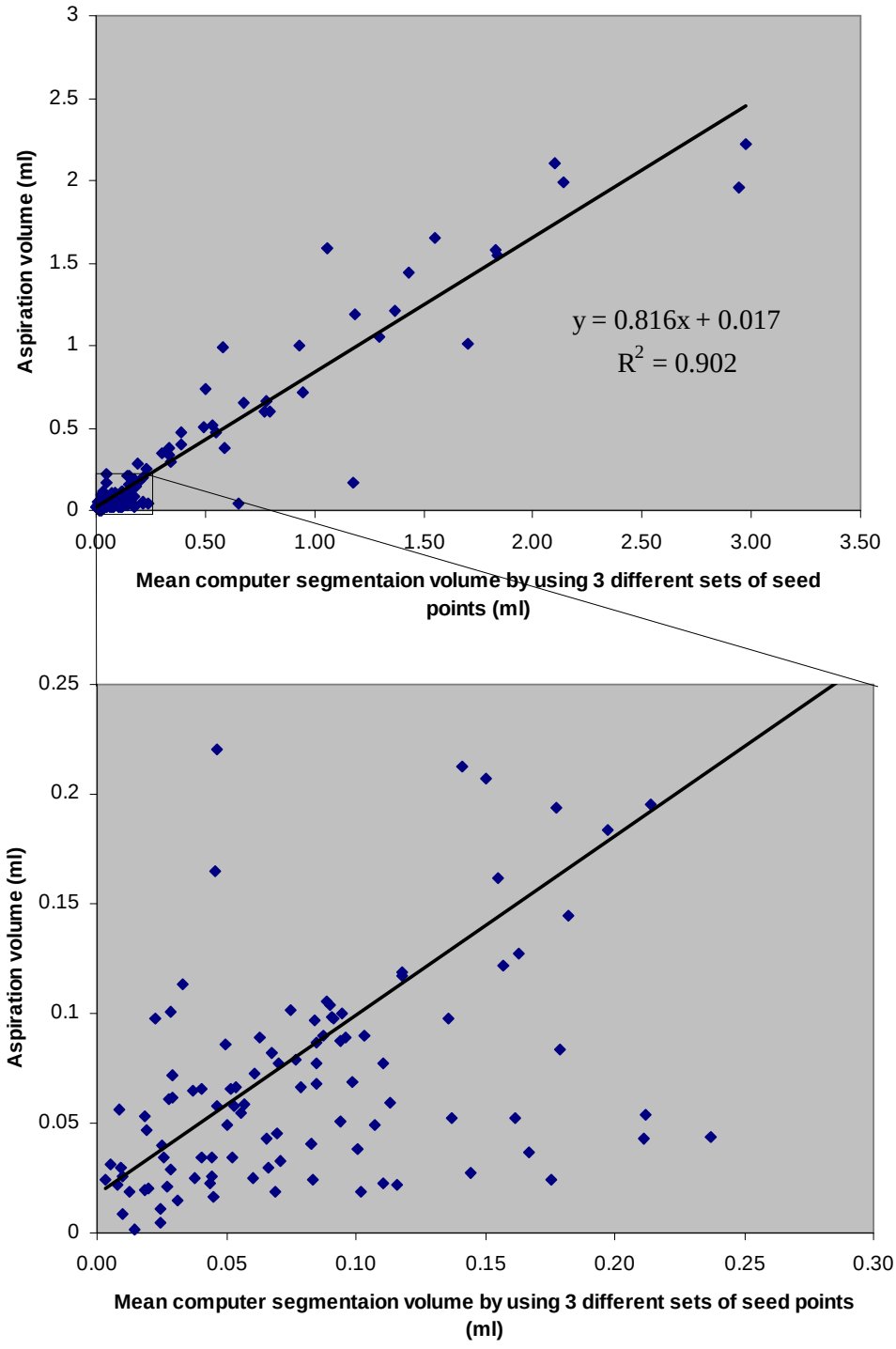

Figure 2.22 Comparison of the mean value of computer segmentation volume of three sets of seed points and follicle aspiration volume (y = 0.816x+0.017, R^2 = 0.902, P < 0.0001).

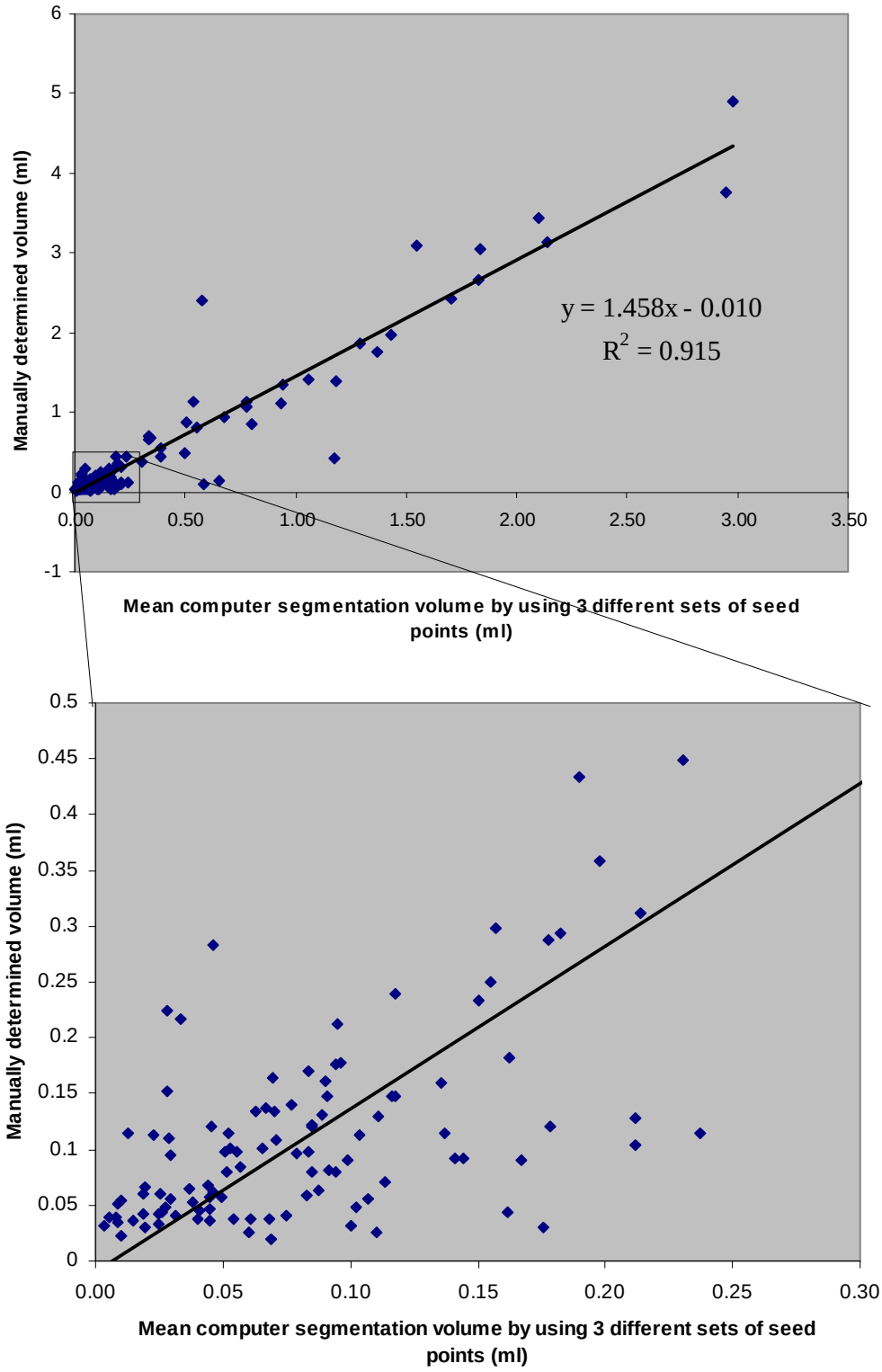

Figure 2.23 Comparison of the mean value of computer segmentation volume of three sets of seed points and manually defined follicle volume ($y = 1.458\ x - 0.010$, $R^2 = 0.915$, $P < 0.0001$).

Meanwhile, the Pearson correlation coefficient and P value were used to compare the difference between each of the two values among aspiration volume, manually determined volume, and the computer segmented volume, see Table 2.3. According to Table 2.3, the overall aspiration volume, manually determined volume, and the mean computer segmented volumes were significantly and positively correlated to each other (aspiration volume vs. manual volume: r =0.965, P=0.0001; aspiration volume vs. mean computer volume: r=0.950, P=0.0001; manual volume vs. mean computer volume: r=0.961, P=0.0001). In different size categories, those three volumes were positively correlated to each other, except for the diameter category of 9~10mm (aspiration volume vs. manual volume: r=-0.629, P=0.5669; aspiration volume vs. computer volume: r = -0.755, P=0.4553). And in the category of follicle diameter >11mm, there was perfect positive correlations between each other (r =1). When follicles were classified into two categories, both the small size follicles (≤ 5mm) and the large size follicles (> 5mm) have significant correlations among aspiration volume, manually detected volume and mean value of computer segmented follicle volumes by using three sets of seed points ($P<0.05$); except in small size follicles' group, there was a tendency towards significant correlation between aspiration volume and mean value of computer segmented results (P=0.0657).

Table 2.3 Pearson Correlation coefficient (P value) for comparison of aspiration volume, manual volume and mean computer volume (the operator selected seed points, the randomly selected seed points group 1 and 2).

Diameter categories	Number of follicles	Aspiration volume VS. Manual volume	Aspiration volume VS. mean computer volume	Manual volume VS. mean computer volume
Overall (including all categories)	138	0.965 (P<0.0001)	0.950 (P<0.0001)	0.961 (P<0.0001)
≤3mm	54	0.315 (P<0.0203)	0.157 (P<0.2567)	0.413 (P<0.0019)
3~4mm	36	0.383 (P<0.0213)	0.731 (P<0.0001)	0.202 (P<0.2369)
4~5mm	12	0.872 (P<0.0002)	0.924 (P<0.0001)	0.793 (P<0.0021)
5~6mm	9	0.947 (P<0.0001)	0.327 (P<0.3908)	0.520 (P<0.1516)
6~7mm	7	0.947 (P<0.0012)	0.888 (P<0.0076)	0.906 (P<0.0049)
7~8mm	4	0.575 (P<0.3105)	0.898 (P<0.0387)	0.646 (P<0.2387)
8~9mm	4	0.954 (P<0.1935)	0.517 (P<0.6539)	0.750 (P<0.4604)
9~10mm	3	-0.629 (P<0.5669)	-0.755 (P<0.4553)	0.985 (P<0.1116)
10~11mm	7	0.895 (P<0.0065)	0.896 (P<0.0063)	0.690 (P<0.0860)
>11mm	2	1	1	1
Small Follicles (≤5mm)	102	0.478 (P<0.0000)	0.183 (P<0.0657)	0.416 (P<0.0000)
Large Follicles (>5mm)	36	0.986 (P<0.0000)	0.942 (P<0.0000)	0.934 (P<0.0000)

We also calculated the correction of follicle segmentation with both of the aspiration results and the manually determined result in different size categories. The definitions of the corrections are as follow:

$$\text{Aspiration correction} = 1 - \frac{|\ SRG\,volume - aspiration\,volume\ |}{aspiration\,volume} \tag{2.15}$$

$$\text{Manual correction} = 1 - \frac{|\ SRG\,volume - manually\,defined\,volume\ |}{manually\,defined\,volume} \tag{2.16}$$

Table 2.4 and Table 2.5 show the aspiration correction and the manual correction of the follicles in different size categories.

In Table 2.4, there was no significant difference among the correction values by using three sets of seed points (P = 0.8791). There was no significant difference among different size categories of follicles (P = 0.2316).

In Table 2.5, there was no significant difference among the correction values by using three sets of seed points (P = 0.9400). There was no significant difference among different size categories of follicles (P = 0.2917).

For the analyses of position accuracy, the Dice coefficients of the follicles were used to evaluate the probability of overlap for the computer segmented region and the manually determined region. The average Dice coefficients between the computer segmented results by using the operator selected seed points and the manually detected result was 58.43%. Table 2.6 shows the Dice coefficients of the follicles in different size categories by using three sets of seed points. In Table 2.6 there was no significant difference among the Dice coefficients by using three sets of seed points (P = 0.7245). The mean value of Dice coefficients by using three sets of seed points was no significantly different among different size categories (column comparison, $P \geq 0.05$).

Table 2.4 Aspiration correction within different follicle categories among the three groups of seed points.

Diameter categories	Operator selected seed point	Randomly selected seed points		Mean value of corrections by using three sets of seed points
		1	2	
≤ 3mm	-0.219 ± 0.224	-0.899 ± 0.474	-0.790 ± 0.544	-0.636 ± 0.251
3~4mm	0.067 ± 0.271	-0.276 ± 0.460	0.126 ± 0.220	-0.027 ± 0.191
4~5mm	0.592 ± 0.093	0.545 ± 0.104	0.679 ± 0.093	0.606 ± 0.055
5~6mm	0.289 ± 0.514	0.716 ± 0.084	-0.710 ± 1.36	0.099 ± 0.481
6~7mm	0.765 ± 0.073	0.676 ± 0.116	0.689 ± 0.058	0.710 ± 0.048
7~8mm	0.835 ± 0.060	0.793 ± 0.062	0.801 ± 0.051	0.810 ± 0.031
8~9mm	0.360 ± 0.320	0.696 ± 0.074	0.794 ± 0.052	0.617 ± 0.116
9~10mm	0.503 ± 0.119	0.432 ± 0.048	0.439 ± 0.089	0.458 ± 0.047
10~11mm	0.850 ± 0.027	0.658 ± 0.108	0.735 ± 0.047	0.748 ± 0.042
>11mm	0.700 ± 0.046	0.637 ± 0.066	0.398 ± 0.231	0.578 ± 0.086
Repeated Measure ANOVA Analysis (Pro Mixed)	Follicle category P = 0.2316 Three sets of seed points P = 0.8791 Follicle category * Three sets of seed points P = 0.9976			

Table 2.5 Manual correction within different follicle size categories among the three groups of seed points.

Diameter categories	Operator selected seed point	Randomly selected seed points		Mean value of corrections by using three sets of seed points
		1	2	
≤ 3mm	0.345 ± 0.062	-0.288 ± 0.346	0.033 ± 0.260	0.030 ± 0.146
3~4mm	0.239 ± 0.274	0.249 ± 0.229	0.365 ± 0.099	0.284 ± 0.122
4~5mm	0.570 ± 0.064	0.576 ± 0.078	0.511 ± 0.063	0.553 ± 0.039
5~6mm	0.553 ± 0.138	0.539 ± 0.086	0.128 ± 0.474	0.407 ± 0.165
6~7mm	0.665 ± 0.077	0.514 ± 0.106	0.678 ± 0.083	0.619 ± 0.052
7~8mm	0.683 ± 0.084	0.717 ± 0.082	0.716 ± 0.074	0.705 ± 0.043
8~9mm	0.805 ± 0.056	0.728 ± 0.086	0.673 ± 0.078	0.736 ± 0.042
9~10mm	0.712 ± 0.011	0.753 ± 0.052	0.746 ± 0.029	0.737 ± 0.019
10~11mm	0.578 ± 0.035	0.536 ± 0.098	0.604 ± 0.060	0.573 ± 0.038
>11mm	0.633 ± 0.021	0.667 ± 0.078	0.790 ± 0.167	0.697 ± 0.056
Repeated Measure ANOVA Analysis (Pro Mixed)	Follicle category P = 0.2917 Three sets of seed points P = 0.9400 Follicle category * Three sets of seed points P = 0.9984			

Table 2.6 Dice coefficient within different follicle size categories among the three groups of seed points.

Diameter categories	Operator selected seed point	Randomly selected seed points		Mean value of Dice coefficients by using three sets of seed points
		1	2	
≤ 3mm	0.497 ± 0.028	0.478 ± 0.032	0.473 ± 0.031	0.482 ± 0.018 [a]
3~4mm	0.566 ± 0.032	0.566 ± 0.035	0.575 ± 0.033	0.569 ± 0.019 [a]
4~5mm	0.651 ± 0.049	0.580 ± 0.069	0.582 ± 0.068	0.604 ± 0.036 [a]
5~6mm	0.604 ± 0.056	0.624 ± 0.069	0.545 ± 0.089	0.591 ± 0.041 [a]
6~7mm	0.716 ± 0.033	0.586 ± 0.101	0.716 ± 0.031	0.673 ± 0.038 [a]
7~8mm	0.754 ± 0.041	0.780 ± 0.042	0.783 ± 0.039	0.772 ± 0.022 [a]
8~9mm	0.781 ± 0.062	0.799 ± 0.054	0.782 ± 0.057	0.787 ± 0.029 [a]
9~10mm	0.803 ± 0.007	0.812 ± 0.051	0.823 ± 0.030	0.813 ± 0.017 [a]
10~11mm	0.721 ± 0.029	0.648 ± 0.110	0.713 ± 0.044	0.694 ± 0.039 [a]
>11mm	0.806 ± 0.031	0.779 ± 0.038	0.801 ± 0.010	0.795 ± 0.014 [a]
Repeated Measure ANOVA Analysis (Pro Mixed)	Follicle category P <0.0001 Three sets of seed points P = 0.7245 Follicle category * Three sets of seed points P = 0.9911			

* Different superscripts (a, b, c, d, …) indicate difference in follicle category (column comparison) at P< 0.05.

The overall Dice coefficient is defined as follows:

$$Overall\ Dice\ coefficient = \frac{4 \times |M \cap C \cap R_1 \cap R_2|}{|M| + |C| + |R_1| + |R_2|} \quad (2.17)$$

where, M is the manually determined follicle region, C is the computer segmented region by using the seed points selected by the operator, R_1 is the computer segmented region by using the first group of randomly selected seed points, R_2 is the computer segmented region by using the second group of randomly selected seed points.

The overall Dice coefficient in different size categories are shown in Table 2.7. The superscripts (a,b.c..) have the same meaning as in Table 2.1. The differences among size categories were compared with ANOVA followed by Tukey Post-hoc. Analysis with ANOVA indicated a statistically significant difference between follicle categories (overall ANOVA, P<0.0001). Differences of overall Dice coefficient among follicles size categories were significant (Tukey Post-hoc, P<0.05).

Table 2.7 The overall Dice coefficient within different follicle size categories.

Diameter categories	Number of follicles	Overall Dice coefficient
≤ 3mm	54	0.315 ± 0.034^{a}
3~4mm	36	0.500 ± 0.043^{b}
4~5mm	12	0.524 ± 0.097^{c}
5~6mm	9	0.457 ± 0.101^{d}
6~7mm	7	0.530 ± 0.139^{e}
7~8mm	4	0.797 ± 0.035^{f}
8~9mm	4	0.743 ± 0.084^{g}
9~10mm	3	0.811 ± 0.022^{h}
10~11mm	7	0.674 ± 0.118^{i}
>11mm	2	0.772 ± 0.017^{j}
Overall ANOVA P-value		< 0.0001

*Different superscripts indicate difference at P<0.05 using Tukey Post-hoc comparison.

2.5 Discussion

This experiment is an evaluation of the performance of a 3D SRG follicle segmentation algorithm. It can be used on *in vivo* images too. In Figure 2.16, the result of performing the same program on a transrectal image sequence is given. The parameters are selected as follows: the threshold of the adaptive neighborhood median filter is: T = 0.6 × the mean value of the ovary volume; the mean intensity threshold for the first criterion is: m = 0.7×the mean voxel of the 3D ovary dataset; the standard deviation threshold for the second criterion is: α = the standard deviation of pixel intensity over the whole volume; threshold of the volume comparison test is: C = 1.3; and the threshold used to test whether the boundary leakage may occur is set to T_d = 20.

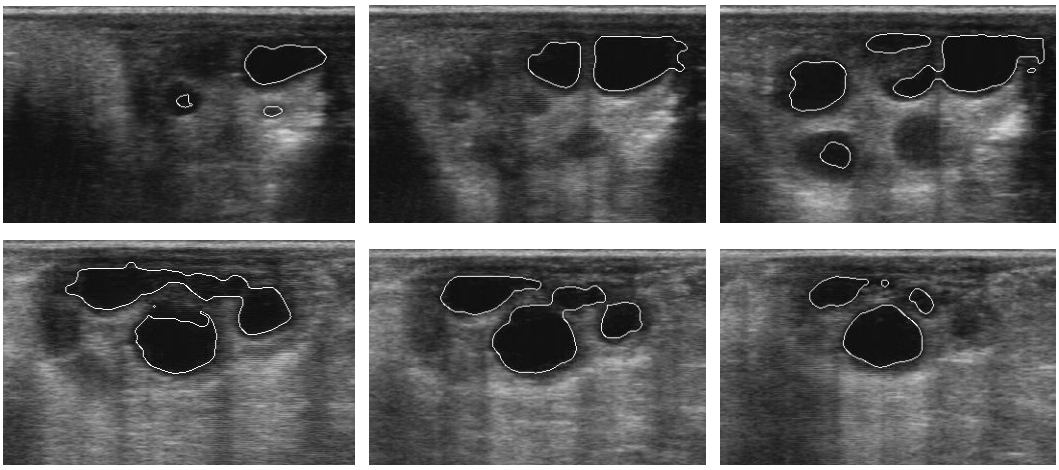

Figure 2.24 Follicle SRG segmentation result of an *in vivo* ultrasonographic dataset.

From the statistical evaluation results (see 2.4 Results for detail) we found our SRG algorithm is not an excellent algorithm. Comparing the position accuracy of our method with other existing 2D follicle detection methods, we see that our algorithm was worse than the algorithm described in Reference [50, 51, 60], see Table 2.8. The Hausdorff distance obtained in our study is about 30 times bigger than those in Reference [50, 51]. The main reason is that in our study, huge boundary leakage problem happened not only on each single slice (x and y directions) but may also extend to the connected slices (z direction), sometimes even extend to the edge of the images. The Root mean square distance and average absolute distance of this study are about twice the values in Reference [50, 51, 60]. However, in our case, different from those papers, the algorithm

was performed on 3D datasets based on a sequence of water bath images (with huge boundary leakage problem and lots of dark areas on the images).

Table 2.8 Comparison of Hausdorff distance, root mean squared distance and average absolute distance of our SRG algorithm with the results in algorithm described in [50, 51, 60]. Empty entries in the table indicate that a metric was not computed in the validation methodology for a particular algorithm.

	Hausdorff distance	Root mean squared distance	Average absolute distance
Our SRG algorithm	39.9 ± 5.61	1.87 ± 1.36	0.84 ± 0.82
Krivanek's method [50]	1.47± 0.83	0.59 ± 0.28	
Sarty's method [51]	1.64 ± 1.92	0.63 ± 0.36	
Potočnik's method [60]			0.8 ± 0.15

Since both of our SRG algorithm and the method in Potočnik's paper [60] (see Chapter 1.4.2 follicle segmentation for detail) are based on region growing algorithm, it is more reasonable to compare these two methods by using the same dataset due to the different data acquisition in those two methods. Therefore we performed Potočnik's algorithm [60] on each 2D image slice in the test dataset of this study, then the segmented follicles were amalgamated to construct 3D volumes and compared with the 3D follicle volumes obtained by using our SRG algorithm. In contrast to Potočnik's paper [60], the selection of threshold *Th* of the image smoothing step was set to 80% of the mean grey-level of the image instead of the mean grey-level of the image, because there were larger dark areas (caused by the waterbath imaging) on the images of this dataset than on the images used in Potočnik's paper [60]. The threshold *Tg* was set to 70% of the mean grey-level of the smoothed image instead of the mean grey-level decreased by one standard deviation of grey-levels in the smoothed image. Because the mean grey-level is very low and standard deviation is very high in water bath images, if we kept use the same method as in paper [60] to get the *Tg*, the value of *Tg* will become very small or even negative which is totally invalid. The threshold *Hs* was set to ¼ of the standard deviation

of the image instead of half of it also because of the high standard deviation value in the images of our dataset. The parameters in the region growing step were the same as in Potočnik's paper [60]. In the post processing step, the regions with area smaller than 50 were removed instead of 220 in Potočnik's paper [60], because the follicle in one slice could be very small even though it is big in 3D. The regions with area around 220 could be follicles with diameter of 2mm in one single slice, but the regions with area around 50 emerge because of speckle noise. Compared with using the same parameters in paper [60], the follicle segmentation results are much better by using the parameters we selected here (better recognition rate and the boundary of the segmented follicles are more close to the real follicle boundaries).

Potočnik's method is a good method for recognizing follicles on 2D single images, but when performing on our water bath based images, lots of dark area around the ovary was misidentified as follicle area; lots of small follicles were not recognized, and huge boundary leakage happened on many follicles. In the worst case, the follicle region did not stop growing until touch the edge of the image. Moreover, the huge dark area on the images caused the program to require a long running time. The longest running time was about 1.5 hours for one slice of the images. Figure 2.25 shows the simple linear regression between the segmented follicle volumes and their related manually detected follicle volumes. The result shows that there was statistically significant linear relationship between them ($y = 0.145x + 0.378$, $R^2 = 0.150$, $P < 0.001$). But there was no agreement between them (the slope of the linear regression line is 0.145). If comparing with our SRG segmentation result, we found our SRG algorithm has better agreement between the computer segmented follicle volumes and the manually detected follicle volumes (the slope of the linear regression line is 1.512). For comparing the position accuracy, Table 2.9 compared the Hausdorff distance, root mean squared distance and Dice coefficient of our SRG segmentation results with those obtained by using Potočnik's method. From Table 2.9, we found our method obtained better Hausdorff distance, root mean squared distance and Dice coefficient compared with Potočnik's method applied to our data set.

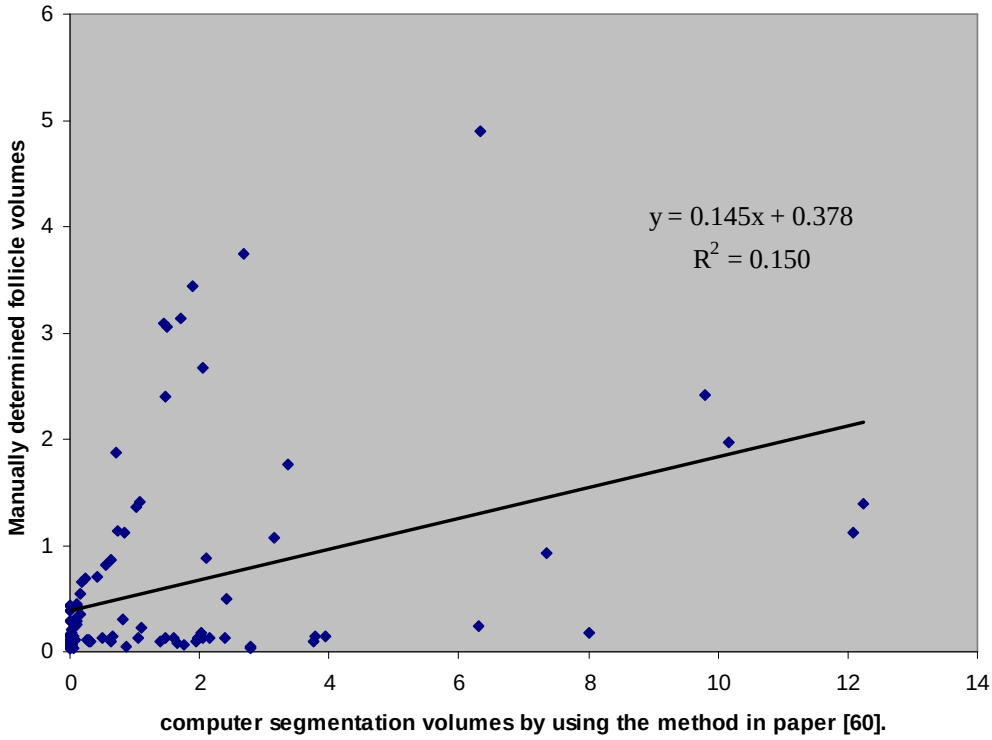

Figure 2.25 Comparison of the follicle segmentation volume by using the method in paper [60] on our data set with the manually detected follicle volume ($y = 0.145x + 0.378$, $R^2 = 0.150$, $P < 0.001$)

Table 2.9 Comparison of Hausdorff distance, root mean squared distance and Dice coefficient of our SRG algorithm with the distances obtained by using Potočnik's method [60] on our data set.

	Hausdorff distance	Root mean squared distance	Mean Dice Coefficient
Our SRG algorithm	39.9 ± 5.61	1.87 ± 1.36	58.43%
Segmentation result by using Potočnik's method [60]	42.5 ± 8.90	8.58 ± 5.55	27.63%

In General, the SRG segmentation method we developed has significant advantages as well as some drawbacks.

One of the most attractive advantages is that the method performs quite well on the images which have significant boundary leaking problems or very weak edges information. The second advantage is that it is simple. The algorithm does not have any complicated theory or mathematic computation associated with it. The third advantage is that the algorithm operates quickly on follicles where boundary leaking is not a problem; the algorithm doesn't need to go through every pixel in the image. The speed of segmentation depends on the size of the follicle. But for the follicles for which boundary leakage occurs, the speed of the algorithm is relative to the condition of the boundary. A follicle which has less boundary leakage will result in less operation time compared with one which has a greater boundary leakage problem. The fourth advantage is that judicious selection of seed points will help to separate overlapping follicles (two follicles adjacent to each other separated by a very weak boundary), because the shape-based criterion and the special growing neighborhood used in the algorithm can keep the growing region in ellipsoid shape and therefore keep it from growing into the adjacent follicle.

On the other hand, the algorithm has three weaknesses. The first and perhaps most important weakness is that for the follicles which have great boundary leakage problems, it is not a fully repeatable segmentation for one follicle; the result depends on the selected seed point. Different seed points in one follicle cannot get totally same result (see Table 2.2). Sometimes, choosing a different seed point will improve the segmentation result. Second, this algorithm relies on several parameters that were determined experimentally, however, some can be selected automatically, such as the threshold of the program stop criterion P, although this comes at great computational expense. The mean value threshold and standard deviation threshold can be determined from the mean value and the standard deviation of pixel intensities over the whole volume. However, the standard deviation threshold still needs to be determined manually in order to use two times the standard deviation of the whole ovary volume or one time of the standard deviation of the whole volume. Finally, the algorithm can be performed in the ultrasound images sequence with different thickness of intervals

between each slice and also can work on a truly 3D (isotropic) dataset, but the 3D region growing neighborhood has to be modified the size so that it is symmetric.

2.6 Conclusions and future work

The research in this paper represents a new SRG algorithm applied to a constructed 3D ultrasonographic dataset. A new growing neighborhood is created here for matching a special ellipsoid shaped object in each iteration of the SRG algorithm. Growing the initial homogeneity region is controlled with two criteria: mean grey-level and standard deviation. A similar 3D compactness test is used as a third criterion. A global stopping criterion solves the boundary leakage problem in poor quality images. Quantitative comparison among the SRG segmentation results, the aspiration results, and the manually determined results indicate there were significant linear relationships between the computer segmentation volumes, the aspiration volumes, and the manually detected volumes. This supported the second hypothesis that there will be linear relationships between the computer-segmented follicle volumes, observer-defined follicle volumes and aspirated follicle volumes. We separated the total segmented follicles into 2 groups – the big size follicles (follicles with diameters > 5mm), and the small size follicles (follicles with diameters $\leq$ 5mm). After the evaluation by using the same validation methods, we found that there were significant relationships between the SRG segmented follicle volumes, the aspiration volumes and the manually detected follicle volumes in both of the groups of the small size follicles and the big size follicles. The third hypothesis that there will be an agreement between computer-segmented follicle volumes, observer-defined follicle volumes, and aspirated follicle volumes was rejected because the slopes of every regression lines were not close enough to 1. The average overlap correction rate between the computer segmented results and the manually detected result is 58.43%. This did not support the first hypothesis that the volume and position of follicles obtained by computer-assisted follicle segmentation will be similar to that obtained from the observer-defined follicle segmentation and aspirated follicle volumes (gold standards). The segmentation results are sensitive to the selected seed points ($P<0.05$), but the overlap correction rates are not sensitive to the selected seed points. This did not support the last hypothesis of this study that the follicle

segmentation results from the computer will not be sensitive to the position of the selected seed point.

Clearly, this algorithm is a semi-automatic method. Changing it to a totally automatic method will become the basis of a future project where the seed points are arrived at by an automatic method. For the follicles which have boundary leaking problem, the SRG program needs to run several times with increased stop control value P. This is clearly time-consuming. Sometime, the whole program will run around 20~30 minute for one follicle due to this. A step which can make the program doesn't need to go back to the seed point and run all over again is desired. The algorithm used an ellipsoid shaped growing neighborhood. This increases the computational complexity of the method. A better 3D construction method which can fill the distance between each slice of the sequence of ovarian ultrasound images to make the constructed volume close to the ground truth volume is desired. Moreover, the pre-processing step used in this algorithm was aimed at reducing the speckle noise in images. A sequence of other pre-processing methods could be added to this algorithm to improve smoothing of the images, potentially leading to better results.

Chapter 3

General Discussion

The study described in this thesis can make an analysis of follicles not only in the horizontal and vertical planes but also in the frontal plane based on a sequence of ultrasonographic ovarian images. This method makes the computer-based measurement of volume available without using a 3D ultrasound imaging system. In this chapter, we will discuss the efficiency of this study and its limitations.

3.1 Diameter measurement versus volume measurement

In most current studies, follicles status is established based on the estimation of follicle diameter, whereas the desired follicular measurement is the true volume of the follicle [82-85]. The diameter of each follicle is measured in two or three axes [82, 84]. In two axes, the two diameters across the follicle are measured in the slice in which the follicle appears the largest [82]. The third diameter is measured at approximately right angles to the other two diameters [84]. The volume of the follicle then can be predicted by using the mean value of these diameters for spherical follicles or the longest and shortest diameters for ellipsoidal follicles [84]. This method works better for approximately spherical follicles than for those of other shapes [84]. However, in clinical research, there are many follicles having ellipsoidal or irregular shape, especially during superstimulated cycles, where there can be several follicles pressing against each other [84]. 2D diameter based volume measurement is usually a poor approximation in such cases.

Although based on 2D images, the volume measurement method in this thesis does not need to consider the shape of the follicle. The volume is calculated by simply counting the number of voxels belonging to the computer segmented follicle. The physical

dimensions of each voxel are $\frac{1}{8}mm \times \frac{1}{8}mm \times \frac{1}{2}mm = \frac{1}{128}mm^3$ (1 pixel in each slice equal to $\frac{1}{8}mm$, while the interval between each slice is $\frac{1}{2}mm$, see Chapter 2 2.3.1 Data acquisition for detail). The accuracy of the measurement of follicle volume depends on the segmentation and the ultrasound scanning method. The noise inside the follicle, the follicle boundary's condition, the seed's position selected by the operator and the selection of the threshold value all affect the segmentation result. Moreover, accurate imaging of the organ, including accurately scanning each slice and moving the organ equidistantly and accurately, can affect the result of volume measurement.

3.2 2D ultrasound measurements versus 3D ultrasound measurements

Recently, 3D ultrasound has become more and more commonly used in follicle analysis. The most important reason for applying 3D ultrasound in the analysis of follicles is that it can give accurate information about the number of follicles, size, positions and response to hormonal stimulation [86].

The size information of a follicle consists of the measurement of the follicle volume. Some studies have demonstrated that volume measured by using 3D freehand ultrasound is more correct than the calculation based on the conventional 2D diameter based measurement (see Section 3.1 Diameter measurement versus volume measurement in this Chapter) if the aspirated follicle volume is treated as a gold standard [87, 88]. However, it has not been proven that will contribute to the ovarian follicular research [89]. The volume measurement in this thesis is different from both of these methods just described. Further study should evaluate the accuracy and efficiency between the 3D ultrasound volume measurement and volume measurement introduced in this thesis to see whether or not the method described in this thesis can substitute for the 3D ultrasound measurement.

3.3 The limitations of this research

Another important requirement in clinical research is counting the number of follicles in the ovary. However, the method presented in this thesis will fail to provide this

information automatically because manually selecting the seed points in turn necessitates counting the number of follicles manually. This is a clear drawback of this method.

Chapter 4

General Conclusions

4.1 Summary

In Chapter 1 the main goal of the thesis and the relative background knowledge were presented. Section 1.1 described the purpose, objectives and hypotheses of this thesis and an overview of ovary anatomy and follicle development was provided in Section 1.2, followed by a review of ovarian ultrasound (Section 1.3). This includes: a review of ultrasound imaging system (Section 1.3.1), an overview of ovarian ultrasound analysis methods (Section 1.3.2), a description of ovarian and follicular characters on the ultrasound images (Section 1.3.3), and a discussion of artifacts commonly occurring on ovarian ultrasound images (Section 1.3.4). Finally, background knowledge and literatures about the computer-based follicle segmentation methods were discussed (Section 1.4).

Chapter 2 provided a detailed description of the algorithm in this study – the 3D seeded region growing based follicle segmentation algorithm. In this chapter, a special introductory focus on the 2D and 3D follicle segmentation methods was given (Section 2.1). Then background knowledge of the 3D seeded region growing algorithm, as well as the advantages and disadvantages of using this method to approach follicle segmentation was described (Section 2.2.1) followed by a description of validation methods for evaluating the follicle segmentation results (Section 2.2.2). This was followed by the description of the data acquisition method (Section 2.3.1), the detail of the algorithm procedure (Section 2.3.2), and the evaluation methods for evaluating the results of follicular volume segmentation (Section 2.3.3). Then, the results of the algorithm and the evaluation were presented (Section 2.4) followed by a discussion about this algorithm and its results was presented (Section 2.5). At the end, a conclusion and some suggestions of future work about the algorithm were described (Section 2.6).

Chapter 3 discussed the volume measurement method based on the segmentation results of this study, compared it both with the 2D diameter based volume calculation (Section 3.1) and the volume measurement based on 3D ultrasonography techniques (Section 3.2). Then, the limitations of the method generated in this thesis were described (Section 3.3).

4.2 Contributions

The first contribution of this thesis is the development of an algorithm for segmenting volumetric ultrasound data. The algorithm approached a region-based segmentation method by determining the homogeneous grey-level of the object regions in combination with a shape-based criterion. The emphasis of the segmentation algorithm is on developing a shape-based criterion to terminate the region growing program correctly.

The second contribution of this thesis is the developed validation method for evaluating the follicular segmentation results. The validation method compares the results among the computer segmentation volume, the manually detection volume, and the aspiration volume, instead of only considering the computer segmented result with either the manually detection result or the aspiration result. In the most recent study of computer assisted follicle segmentation, the results were either compared against the manual detection result (2D single image segmentation) or compared with the aspiration volume (3D image segmentation). Both of these two evaluation methods have their weakness. The comparison with manual detection results for 2D images is hard to assess the accuracy of the 3D volume, and the comparison with aspiration volume is hard to assess the shape and location of the follicles. This study uniquely evaluated the results with both of these two methods, and therefore, enhances the accuracy of the assessment. Moreover, we also provided an evaluation between the aspiration volume and the manual detection volume to study the effect of follicle volume measurement methods.

The third contribution of this thesis is the addition of a program termination criterion for the region-growing program. The algorithm records the outer boundary pixels of the present growing region. If a certain percentage of the outer boundary pixels terminate to grow, the whole program stops. Moreover, the percentage is variable and determined by the program automatically.

The fourth contribution of this thesis is its development of an irregular growing neighborhood for the region growing algorithm. An ellipsoid shaped neighborhood (11×11×3 pixels) was used in this thesis instead of the regular 6, 18, or 26 pixels' neighborhood.

Finally, after testing 138 follicles in 16 ovaries, the evaluation result shows: (1) There were significantly linear relationships between the computer segmentation volumes, the aspiration volumes, and the manually determined volumes. (2) We separated the total segmented follicles into 2 groups – the large size follicles (follicles with diameters >5mm), and the small size follicles (follicles with diameters ≤5mm). After the evaluation by using the same methods, we found that there were significant relationship between the SRG segmented follicle volume, the aspiration volumes, and the manually detected follicle volumes in both the groups of the small size follicles and the large size follicles (3) There was no agreement between each two results among the among the SRG segmentation results, the aspiration results and the manually detected follicle results (the slopes of the regression lines are not close to 1). (4) The segmentation results (both the size and position results) are sensitive to the selected seed points ($P<0.05$). (5) The average overlap correction rate between the computer segmented results and the manually detected result is 58.43%.

For testing the hypotheses in this study, we found the first hypothesis that the volume and position of follicles obtained by computer-assisted follicle segmentation will be similar to that obtained from the observer-defined follicle segmentation and aspirated follicle volumes is not supported. The second hypothesis that there will be statistical linear relationships between computer-segmented follicle volumes, observer-defined follicle volumes and aspirated follicle volumes is supported. The third hypothesis that there will be an agreement between computer-segmented follicle volumes, observer-defined follicle volumes, and aspirated follicle volumes is rejected. The last hypothesis that the follicle segmentation results from the computer will not be sensitive to the position of the selected seed point is rejected.

4.3 Future work

Although this method developed the 3D follicle segmentation techniques, there are still further studies and development that are required. First, in this study, we succeeded in segmenting the follicles, measuring their volumes, and comparing the result volumes with both the aspiration volume and the manually detected follicular volume. However, whether this result can satisfy the clinical requirements is still unclear. Second, the algorithm developed in this thesis is obviously a semi-automatic method. To develop this method to a totally automatic segmentation method (automatically select seed points for each follicle) is desired; such a method can count the number of follicles in the ovary automatically.

References

1. T. Sutton. *Introduction to animal reproduction*. Vermilion, AB, Canada: E.I. Sutton Consulting, pp. 336, 2000.

2. O.J. Ginther. *Ultrasonic imaging and reproductive events in the mare.* Cross Plains, WI, USA: Equiservices, pp. 378, 1986.

3. G.P. Adams, R.L. Matteri, J.P. Kastelic, J.C.H. Ko, and O.J. Ginther. *Association between surges of follicle-stimulating hormone and the emergence of follicular waves in heifers*. Reproduction and Fertility 94: 177-188, 1992.

4. O.J. Ginther, J.P. Kastelic, and L. Knopf. *Composition and characteristics of follicular waves during the bovine estrous cycle*. Animal Reproduction Science 20: 187-200, 1989.

5. D.H. Townson and O.J. Ginther. *Duration and pattern of follicular evacuation during ovulation in the mare*. Animal Reproduction Science 15: 131-138, 1987.

6. R.A. Pierson and O.J. Ginther. *Ovarian follicular populations during early pregnancy in heifers*. Theriogenology 26: 649-659, 1986.

7. R.A. Pierson and O.J. Ginther. *Follicular populations during the estrous cycle in heifers I: Influence of day.* Animal Reproduction Science 14: 165-176, 1987.

8. R.A. Pierson and O.J. Ginther. *Follicular populations during the estrous cycle in heifer III: Time of selection of ovulatory follicle.* Animal Reproduction Science 16: 81-95, 1988.

9. R.A. Pierson and O.J. Ginther. *Reliability of diagnostic ultrasonography for identification and measurement of follicles and detecting the corpus luteum in heifers*. Theriogenology 28: 929-936, 1987.

10. R.A. Pierson and O.J. Ginther. *Ultrasonography of the bovine ovary*. Theriogenology 21: 495-504, 1984.

11. R.A. Pierson, O.J. Ginther, and J.P. Kastelic. *Basic principles and techniques for transrectal ultrasonography in cattle and horses.* WCVM June conference, pp. 1-9, 1992.

12. D.H. Townson and O.J. Ginther. *Ultrasonic characterization of follicular evacuation during ovulation and fate of the discharged follicular fluid in mares*. Animal Reproduction Science 20: 131-141, 1989.

13. J.M. Bland, D.G. Altman. *Statistical methods for assessing agreement between two methods of clinical measurement.* Lancet 1: 307-310, 1986.

14. G.P. Adams, R.A. Pierson. *Bovine model for study of ovarian follicular dynamics in humans*. Theriogenology 43: 113-120, 1995.

15. P.J.H. Ball, A.R. Peters. *Reproduction in cattle.* Oxford, UK: Blackwell publishing, pp. 242, 2004.

16. K.M. Dyce, W.O. Sack, C.J.G. Wensing. *Textbook of veterinary anatomy.* Philadelphia: Saunders, pp. 840, 2002.

17. B. Hafez and E.S.E. Hafez. *Anatomy of female reproduction*. in *Reproduction in farm animals.* pp. 13-29. Edits E.S.E. Hafex and B. Hafez. London, UK: Academic Press, 1998.

18. B.J. Van Voorhis. *Follicular development*. in *Encyclopedia of reproduction, volume 2.* pp. 376-389. Edits E. Knobil, J.D. Neill. London, UK: Academic Press, 1998.

19. H.D. Jocelyn, B.P. Setchell. *Regnier de Graaf's new treatise concerning the generative organs of women.* Journal of Reproduction and Fertility Supplements 17: 77-209, 1972.

20. E.M. Eddy, J.M. Clark, D. Gong, B.A. Fenderson. *Origin and migration of primordial germ cells in mammals*. Molecular Reproduction and Development 4: 333-362, 1981.

21. R.S. Jaiswal, J. Singh, G.P. Adams. *Developmental pattern of small antral follicles in the bovine ovary*. Biology of Reproduction 71: 1244-1251, 2004.

22. R.S. Jaiswal. *Developmental pattern of the small (1-3mm) follicles in cattle.* [PhD. Thesis], Department of Veterinary Biomedical Sciences, University of Saskatchewan, pp. 90, 2003.

23. R.H.F. Hunter. *Physiology of the graafian follicle and ovulation*. New York, Cambridge Univeristy Press, pp. 263-294, 2003.

24. S.S. Guraya. *Biology of ovarian follicles in mammals*. Berlin, German: Springer-Verlag, pp. 320, 1985.

25. R.A. Pierson and O.J. Ginther. *Ultrasonic imaging of the ovaries and uterus in cattle*. Theriogenology 29: 21-37, 1988.

26. E. Rajakoski. *The ovarian follicular system in sexually mature heifers with special reference to seasonal, cyclical, end left-right variations*. Acta Endocrinol Suppl (Copenh) 34 (Suppl 52): 1-68, 1960.

27. G.P. Adams. *Comparative patterns of follicle development and selection in ruminants*. Journal of Reproduction and Fertility Supplement 54: 17-32, 1999.

28. J. Woo. *A short history of the development of ultrasound in obstetrics and gynecology*. In http://www.ob-ultrasound.net/history1.html,

29. P.N.T. Wells. *Biomedical ultrasonics.* London, UK: Academic Press, pp. 635, 1977.

30. O.J. Ginther. *Ultrasonic imaging and animal reproduction: Fundamental Book 1*. Cross Plains, WI: Equiservices, pp. 225, 1995.

31. D.A. Christensen. *Ultrasonic Bioinstrumentation.* New York: John Wiley and Sons, pp.235, 1988.

32. R. L. Powis, W.J. Powis. *A thinker's guide to ultrasonic imaging.* USA: Urban and Schwarzenberg, pp. 417, 1984.

33. J.A. Zagzebski. *Essentials Of ultrasound physics.* St. Louis, MO: Mosby, pp. 220, 1983.

34. R. Douthwaite, H. Dobson. *Comparison of different methods of diagnosis of cystic ovarian disease in cattle and an assessment of its treatment with a progesterone-releasing intravaginal device*. The Veterinary Record 147: 355-359, 2000.

35. A.Y. Ribadu and T. Nakao. *Bovine reproductive ultrasonography: a review*. Journal of Reproduction and Development 45: 13-28, 1999.

36. O. Botero, F. Martinat-Botte, F. Bariteau. *Use of ultrasound scanning in swine for detection of pregnancy and some pathological conditions*. Theriogenology 28: 267, 1986.

37. G.J. Scheffer, F.J. Broekmans, M. Dorland, J.D. Habbema, C.W. Looman, E.R. te Velde. *Antral follicle counts by transvaginal ultrasonography are related to age in women with proven natural fertility*. Fertility and Sterility 72: 845-51, 1999.

38. D.C. Schoot, H.J. Coelingh Bennink, B.M. Mannaerts, S.W. Lamberts, P. Bouchard, B.C. Fauser. *Human recombinant follicle-stimulating hormone induces growth of preovulatory follicles without concomitant increase in androgen and estrogen biosynthesis in a woman with isolated gonadotropin deficiency*. Journal of Clinical Endocrinology and Metabolism 74: 1471-3, 1992.

39. W. Feichtinger, P. Kemeter. *Transvaginal sector scan sonography for needle guided transvaginal follicle aspiration and other applications in gynecologic routine and research.* Fertility and Sterility 45: 722-725, 1986.

40. D.R. Bergfelt, G.M. Brogliatti, G.P. Adams. *Gamete recovery and follicular transfer (Graft) using transvaginal ultrasonography in cattle*. Theriogenology 50: 15-25, 1998.

41. G.M. Brogliatti, C.D. Swan, G.P. Adams. *Transvaginal ultrasound-guided oocyte collection in calves 10 to 16 weeks of age.* Theriogenology 43: 177-177(1), 1995.

42. E. Palmer, G. Duchamp, J. Bezard,M. Magistrini, A. King, D. Bousquet, K. Betteridge. *Recovery of follicular fluid and oocytes of mares by non-surgical puncture of the preovulatory follicle*. Theriogenology 25: 178, 1986.

43. H. Callesen, T. Greve, F. Christense. *Ultrasonically guided aspiration of bovine follicular oocytes*. Theriogenology 27: 217, 1987.

44. J.J. Reeves N.W. Rantanen, M. Hauser. *Transrectal real-time ultrasound scanning of the cow reproductive tract*. Theriogenology 21: 485-494, 1984.

45. J. Singh, and G.P. Adams. *Histomorphometry of dominant and subordinate bovine ovarian follicles*. The Anatomical Record 258: 58-70, 2000.

46. J. Singh, R.A. Pierson, G.P. Adams. *Ultrasound image attributes of the bovine corpus luteum: structural and functional correlates*. Journal of Reproduction and Fertility Supplements 109: 35-44, 1997.

47. Robert M Kirberger. *Imaging artifacts in diagnostic ultrasound - a review*. Veterinary Radiology and Ultrasound 36: 297-306, 1995.

48. M. Sonka, V. Hlavac, R. Royle. *Image processing, analysis and machine vision.* London, UK: International Thomson Computer Press, pp.800, 1993.

49. R.E. Muzzolini, Y,H. Yang, R.A. Pierson. *Three dimensional segmentation of volume data*. Image processing,1994, IEEE International Conference 3: 488-492, 1994.

50. A. Krivanek, M. Sonka. *Ovarian ultrasound image analysis: follicle segmentation*. IEEE Transactions on Medical Imaging 17: 935-44, 1998.

51. G.E. Sarty, W. Liang, M. Sonka, R.A. Pierson. *Semiautomated segmentation of ovarian follicular ultrasound images using a knowledge-based algorithm*. Ultrasound in Medicine and Biology 24: 27-42, 1998.

52. G.E. Sarty, M. Sonka, W. Liang, R.A. Pierson. *Development of an automatic follicle isolation tool for ovarian ultrasonographic images*. Medical Imaging 1997: Image Processing, Kenneth M. Hanson; 3034: 1997.

53. B. Potocnik, D. Zazula. *Automated ovarian follicle segmentation using region growing.* In First International Workshop on Image and Signal Processing and Analysis, Pula, Croatia, 157-162; 2000.

54. B. Cigale, D. Zazula. *Segmentation of ovarian ultrasound images using cellular neural networks*. International Journal of Pattern Recognition and Artificial Intelligence 18: 563-581, 2004.

55. B. Cigale, M. Lenič, D. Zazula. *Segmentation of ovarian ultrasound images using cellular neural networks trained by support vector machines.* Knowledge-based Intelligent Information and Engineering Systems: 515-522, 2006.

56. B. Viher, A. Dobnikar, D. Zazula. Cellular automata and follicle recognition problem and possibilities of using cellular automata for image recognition purposes. International Journal of Medical Informatics 49: 231-41, 1998.

57. B. Cigale, D. Zazula. Segmentation of 3D ovarian ultrasound volumes using continuous wavelet transform. in Medicon 2007, IFMBE Proceedings 16. pp. 1017-1020. Edits T. Jarm, P. Kramar, A. Županič. Heidelberg, Germany: Springer-Verlag, 2007.

58. R. Muzzolini, Y.H. Yang, R.A. Pierson. *Multi-resolution texture segmentation with application to diagnostic ultrasound images*. IEEE Transactions on Medical Imaging 12: 108-124, 1993.

59. R. Muzzolini. *A volumetric approach to segmentation and texture characterization of ultrasound images.* [PhD. Thesis]. Department of Computer Science, University of Saskatchewan, pp. 230, 1996.

60. B. Potocnik, D. Zazula. *Automated analysis of a sequence of ovarian ultrasound images. Part I: segmentation of single 2D images*. Image and Vision Computing 20: 217-225, 2001.

61. B. Potocnik, D. Zazula. Automated analysis of a sequence of ovarian ultrasound images. Part II: prediction-based object recognition from a sequence of images. Image and Vision Computing 20: 01/03/2002, 2002.

62. S. Beucher, C. Lantuejoul. *Use of watersheds in contour detection*. Proc. Int. Workshop Image Processing 17-21, 1979.

63. L. Vincent , P. Soille. *Watersheds in digital spaces: an efficient algorithm based on immersion simulations* IEEE Transactions on Pattern Analysis and Machine Intelligence 13: 583-598, 1991.

64. V. Grau, A.U.J. Mewes, M. Alaniz, R. Kikinis, S.K. Warfield. *Improved watershed transform for medial image segmentation using prior information*. IEEE Transactions on Medical Imaging 23: 447-458, 2004.

65. B. Potocnik, D. Zazula, D. Korze. *Automated computer-assisted detection of follicles in ultrasound images of ovary*. Journal of Medical Systems 21: 445-57, 1997.

66. J.I. Koo, S.B. Park, *Speckle reduction with edge preservation in medical ultrasonic images using a homogeneous region growing mean filter (HRGMF).* Ultrasonic Imaging 13:211-237, 1991.

67. B.M. ter Haar Romeny B.Titulaer, S.Kalitzin, G.Scheffer, F.Broekmans, and E. te Velde. *Computer assisted human follicle analysis for fertility prospects with 3D ultrasound*. Lecture Notes Computer Science 1613: 56-69, 1999.

68. J. Kimura, Y. Hirano, S. Takemoto, Y. Nambo, T. Ishinazaka, R. Himeno, T. Mishima, S. Tsumagari, H. Yokota. *Three-dimensional reconstruction of the equine ovary*. Anatomia, Histologia, Embryologia. 34: 48-51, 2005.

69. P.A. Brathwaite, K.B. Chandran, D.D. McPherson, E. Dove. *Lumen detection in human IVUS images using region-growing*. Computers in Cardiology. pp. 37-40, 1996.

70. O.H. Gijia, T. Hausken, A. Berstad, S. Ødegaard. *Measurements of organ volume by ultrasonography*. Proceedings of the Institution of Mechanical Engineers, Part H: Journal of Engineering in Medicine 213: 247-295, 1999.

71. R.K. Justic, E.M. Stokely, J.S. Strobel, R.E. Ideker, W.M. Smith. *Medical image segmentation using 3D seeded region growing*. Medical Imaging 1997: Image Processing, Kenneth M. Hanson; 3034: 900-910, 1997.

72. T. Heimann, M. Thom, T. Kunert, H.P. Meinzer. *New methods for leak detection and contour correction in seeded region growing segmentation*. 20th ISPRS Congress, Istanbul 2004, International Archives of Photogrammetry and Remote Sensing XXXV, Part B: 317-322, 2004.

73. H.L.J. Chen, F.F. Samavati, M.C. Sousa, J.R. Mitchell. *Sketch-based volumetric seeded region growing*. EUROGRAPHICS Workshop on Stetch-base Interfaces and Modeling 123-129, 2006.

74. V. Chalana, Y. Kim. *A methodology for evaluation of boundary detection algorithms on medical images*. IEEE Transactions on Medical Imaging 16: 642-652, 1997.

75. B. Potocnik, D. Zazula. *Assessing the efficiency of the image segmentation algorithms*. Elektrotechnical Review 68: 97-104, 2001.

76. C.J. van Rijsbergen. *Information retrieva*l. London: Butterworths: Kluwer Academic Publishers. pp. 352, 1979

77. H.L. Lamecker, M.S. SeebaB, H.C. Hege, P. Deuflhard. *A 3D statistical shape model of the pelvic bone for segmentation*. in *Medical imaging 2004: image processing, proceedings of SPIE*. PP. 1341-1351. Edits M. Sonka. 2004.

78. R.M. Haralick, L.G. Shapiro. *Image segmentation techniques*. Computer Vision, Graphics, and Image Processing 29: 100-132, 1985.

79. J. Singh, R.A. Pierson, G.P. Adams. *Ultrasound image attributes of bovine ovarian follicles and endocrine and functional correlates.* Journal of Reproduction and Fertility 112:19-29, 1998.

80. K. Pearson. *Mathematical contributions to the theory of evolution III. Regression, Heredity, and Panmixia*. Philosophical Transactions of the Royal Society of London 187: 253-318,1956.

81. R.C. Littell, G.A. Milliken, W.W. Stroup, R.D. Wolfinger, O. Schabenberger. *SAS for Mixed models,* SAS Publishing, pp. 814, 2006.

82. A.S. Penzias, A.M. Emmi, A.K. Dubey, L.C. Layman, A.H. DeCherney, and R.H. Reindollar. *Ultrasound prediction of follicle volume: is the mean diameter reflective?* Fertility and Sterility 62: 1274-1276, 1994.

83. M.K. Eissa K.Hudson, M.F. Docker, R.S. Sawers, and J.R. Newton. *Ultrasound follicle diameter measurement: an assessment of interobserver and intraobserver variation*. Fertility and Sterility 44: 751-754, 1985.

84. A. Kyei-Mensah J. Zaidi, R. Pittrof, A. Shaker, S. Campbell, and S.L. Tan. *Transvaginal three-dimensional ultrasound: accuracy of follicular volume measurement.* . Fertility and Sterility 65: 371-376, 1996.

85. C.L. Gonzalez R. Curson, and J. Parsons. *Transabdominal versus transvaginal ultrasound scanning of ovarian follicles: are they comparable?* Fertility and Sterility 50: 657-659, 1988.

86. B.M. ter Haar Romeny, B. Titulaer, S. Kalitzin, G. Scheffer, F. Broekmans, and E. te Velde. *Computer assisted human follicle analysis for fertility prospects with 3D ultrasound*. Lecture Notes Computer Science 1613: 56-69, 1999.

87. A. Amer, M.E. Hammadeh, M. Kolkailah, and A. Ghandour. *Three-dimensional versus two-dimensional ultrasound measurement of follicular volume: are they comparable?* Archives of Gynecology and Obstetrics 268: 155-157, 2003.

88. M. Brunner, A. Obruca, P. Bauer, and W. Feichtinger. *Clinical application of volume estimation based on three-dimensional ultrasonogrpahy*. Ultrasound in Obstetrics and Gynecology 6: 358-361, 1995.

89. D. Jurkovic. *Three-dimensional ultrasound in gynecology: a critical evaluation*. Ultasound in Obstetrics and Gynecology 19: 109-117, 2002.

(Last accessed April 15, 2008)

Apendix A

More segmentation results

Below are three more segmentation results by using SRG follicle segmentation algorithm. In each result, it includes the 3D construction result of the original ovarian ultrasound images, the sequence of images of the original ovarian images, the SRG segmentation result, the manually detected follicles result, and the 3D vision of the follicles segmentation result. The first two results are typical results, and the third one is the result obtained from a noise image (poor image quality).

A.1 Two more typical results

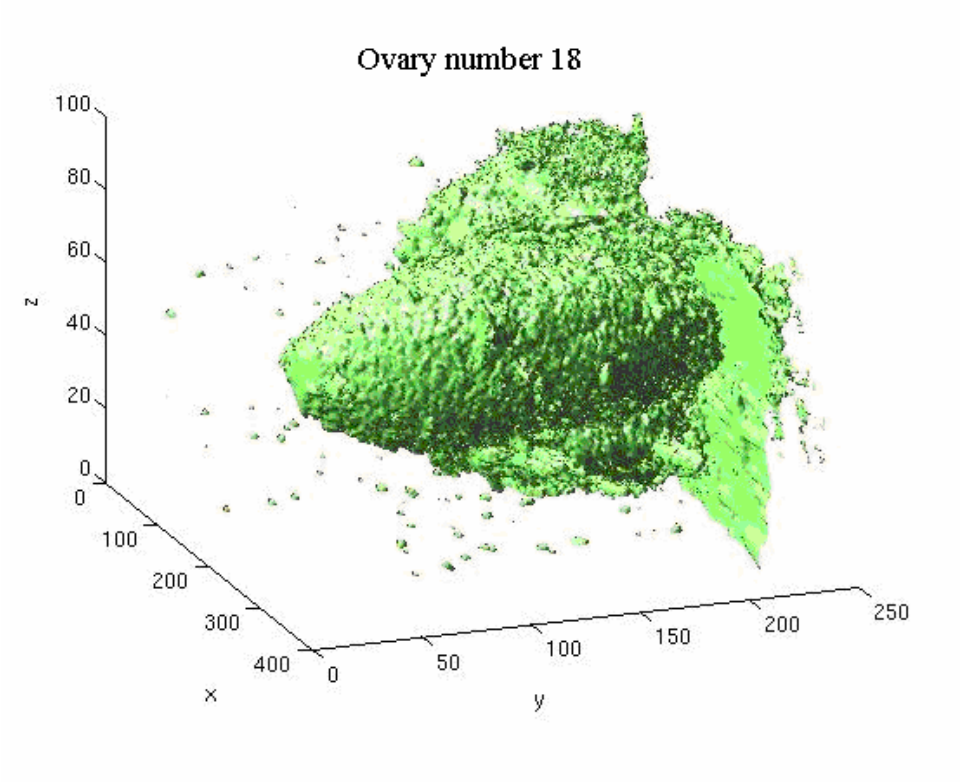

(a) 3D construction result of the cow ovary

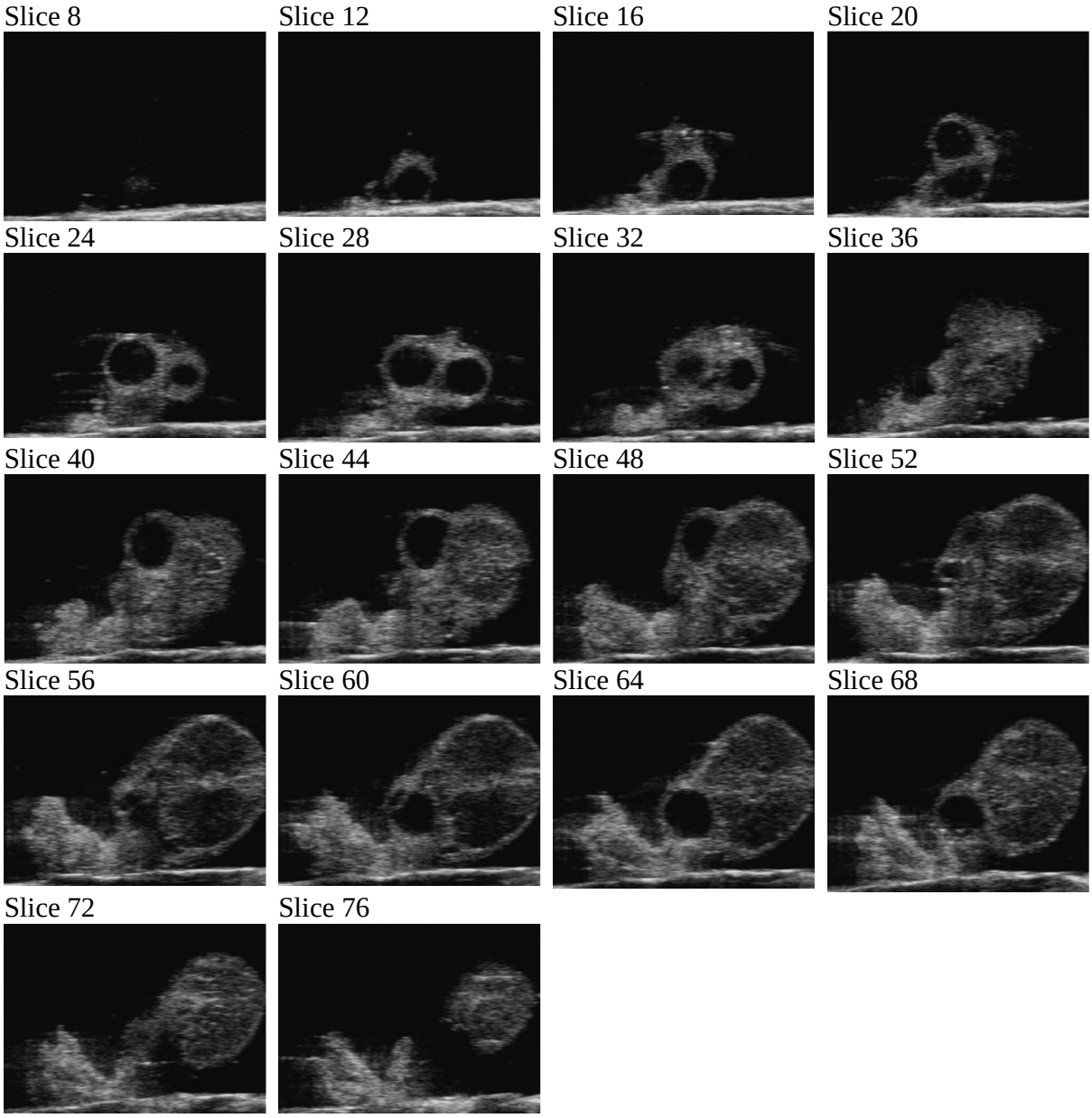

(b) The original images relative by slice number

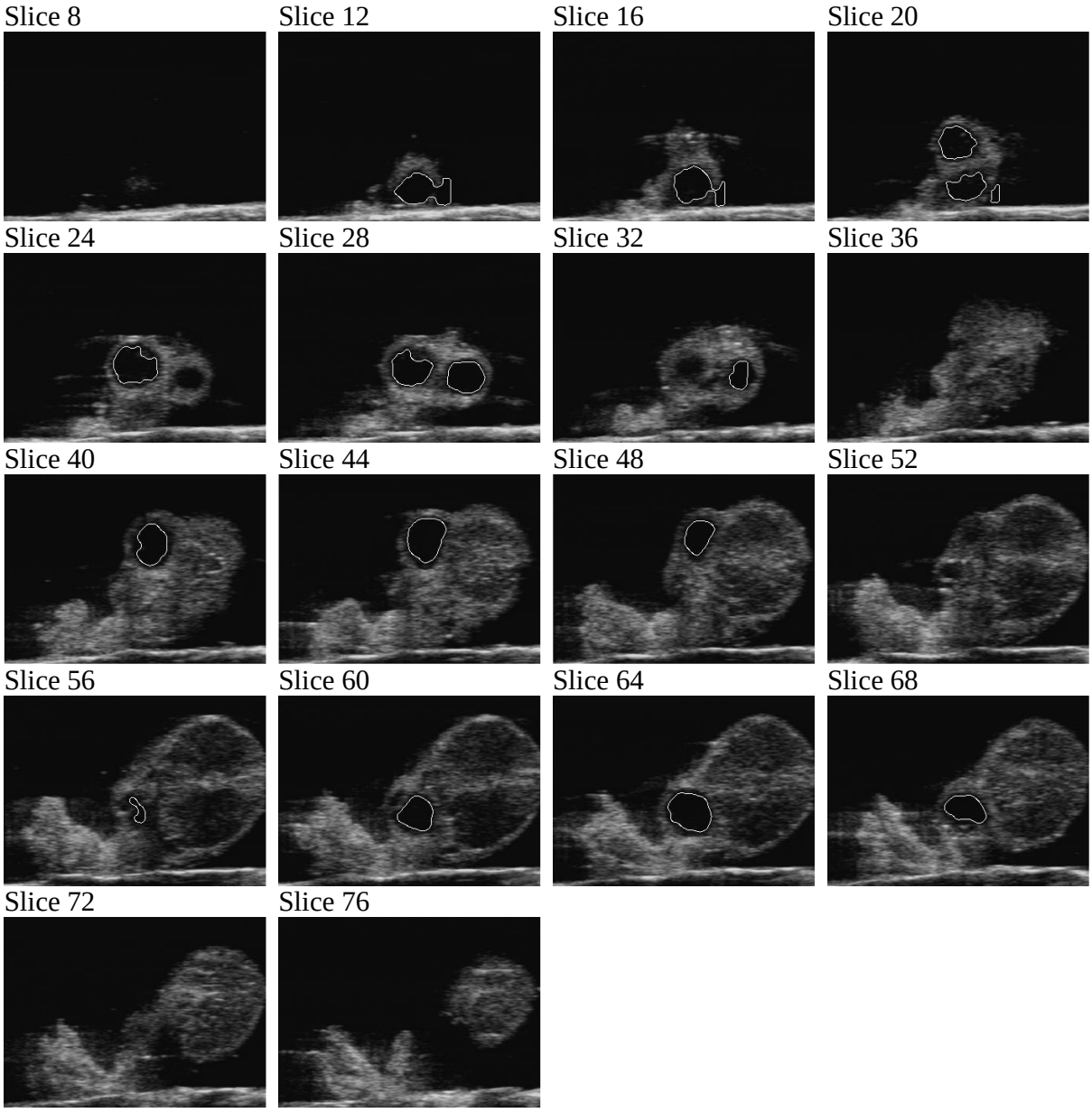

(c) The segmentation result relative by slice number

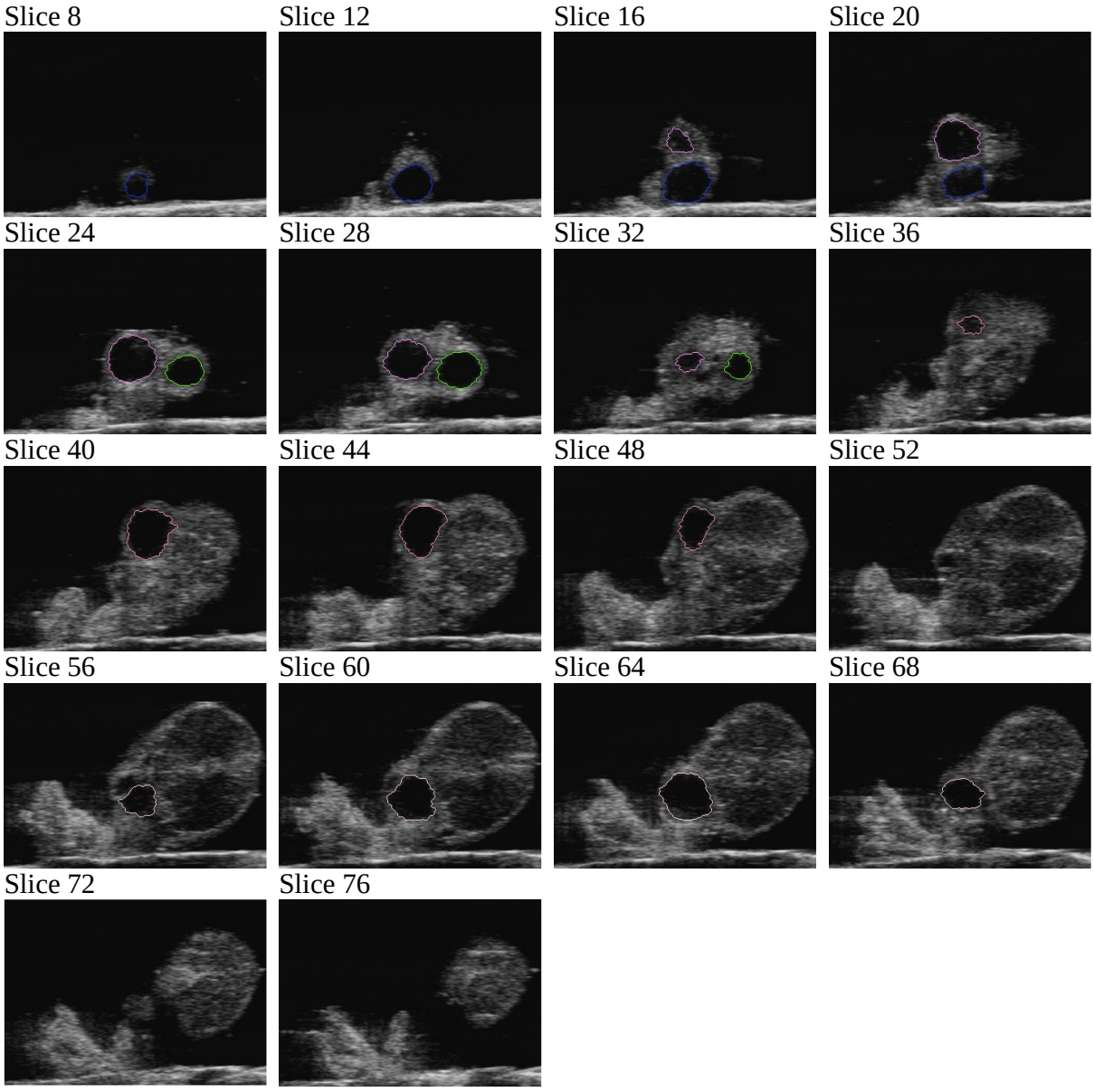

(d) The manually determined follicles by an expert

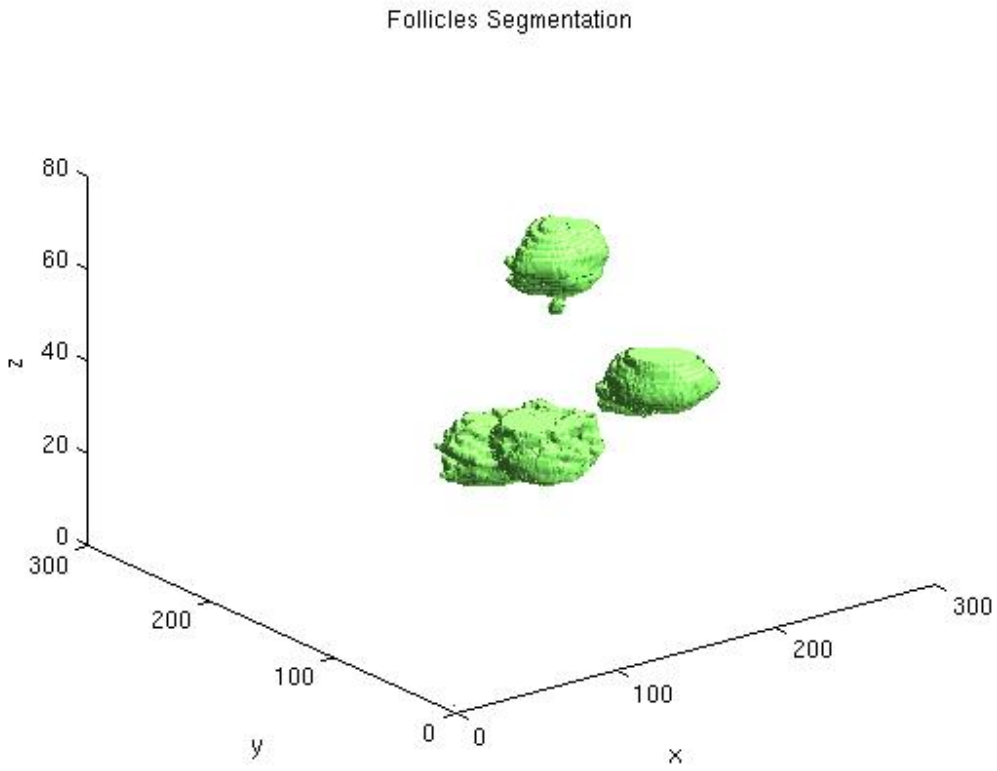

(e) The 3D vision of the follicle segmentation result

Figure A.1 The computer segmentation result of bovine ovary number 18.

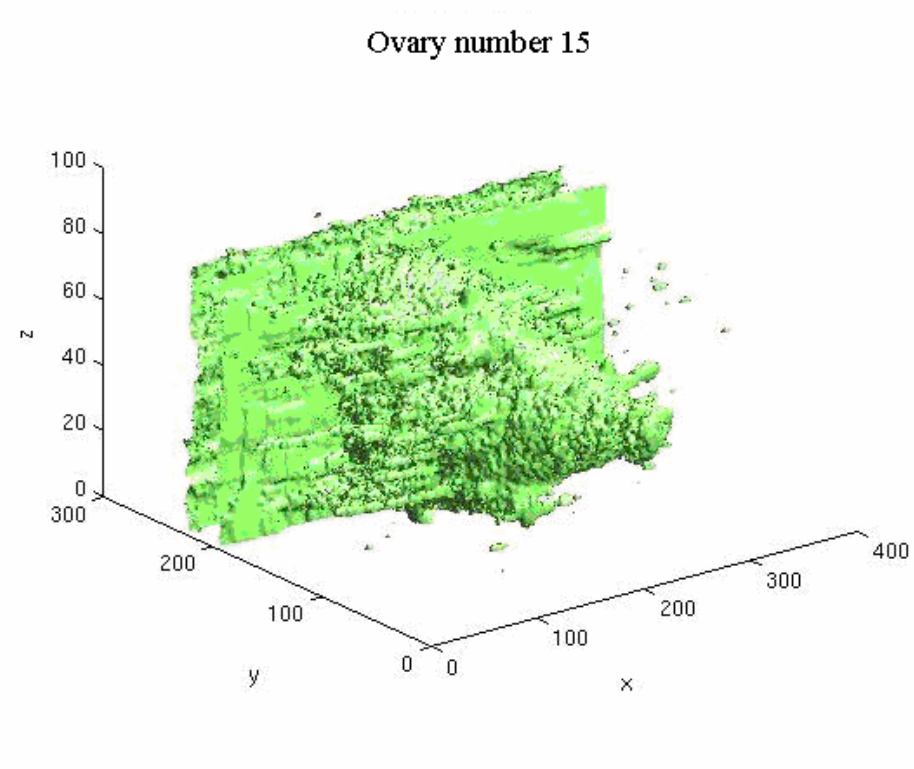

(a) 3D construction result of the cow ovary

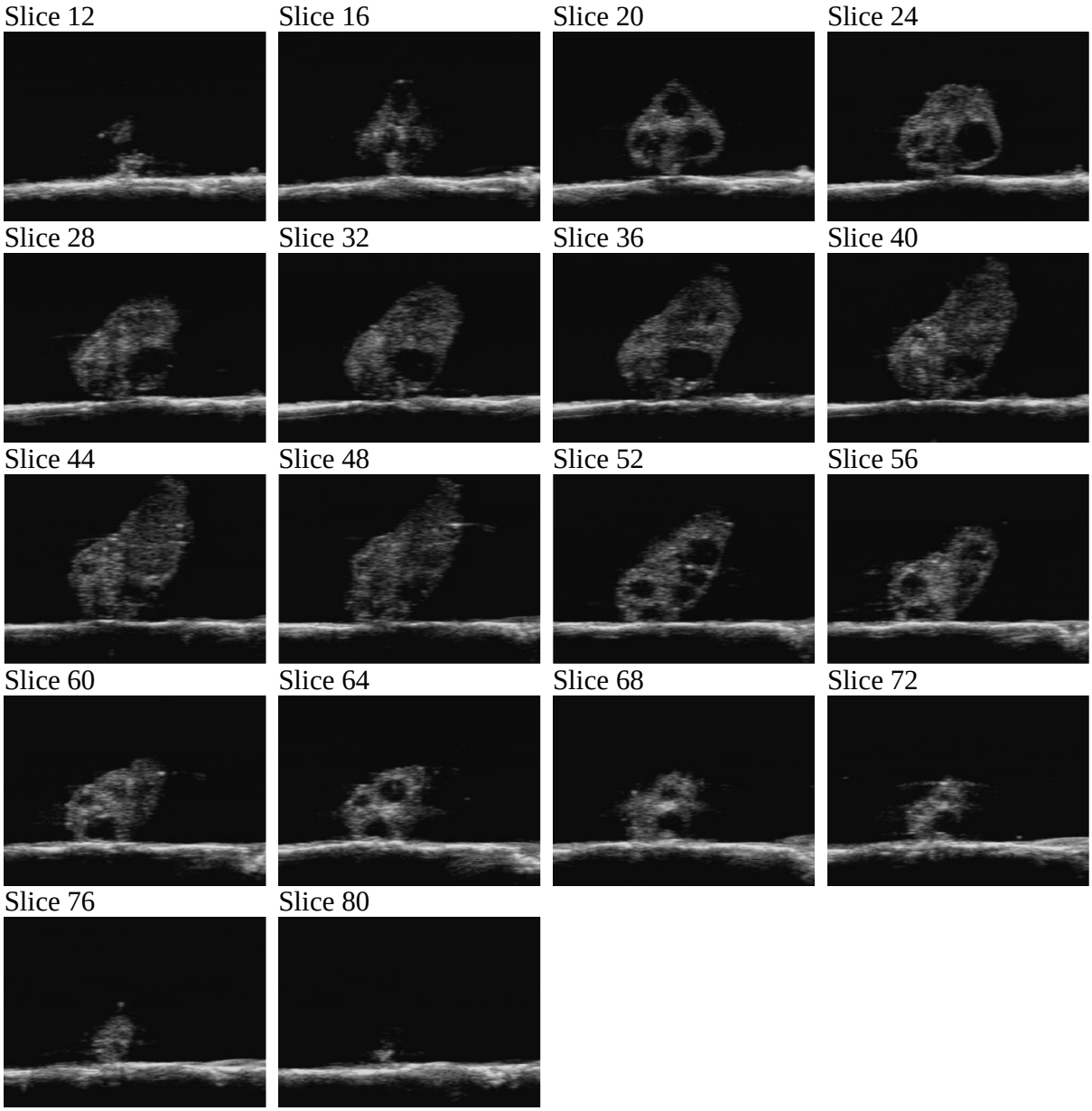

(b) The original images relative by slice number

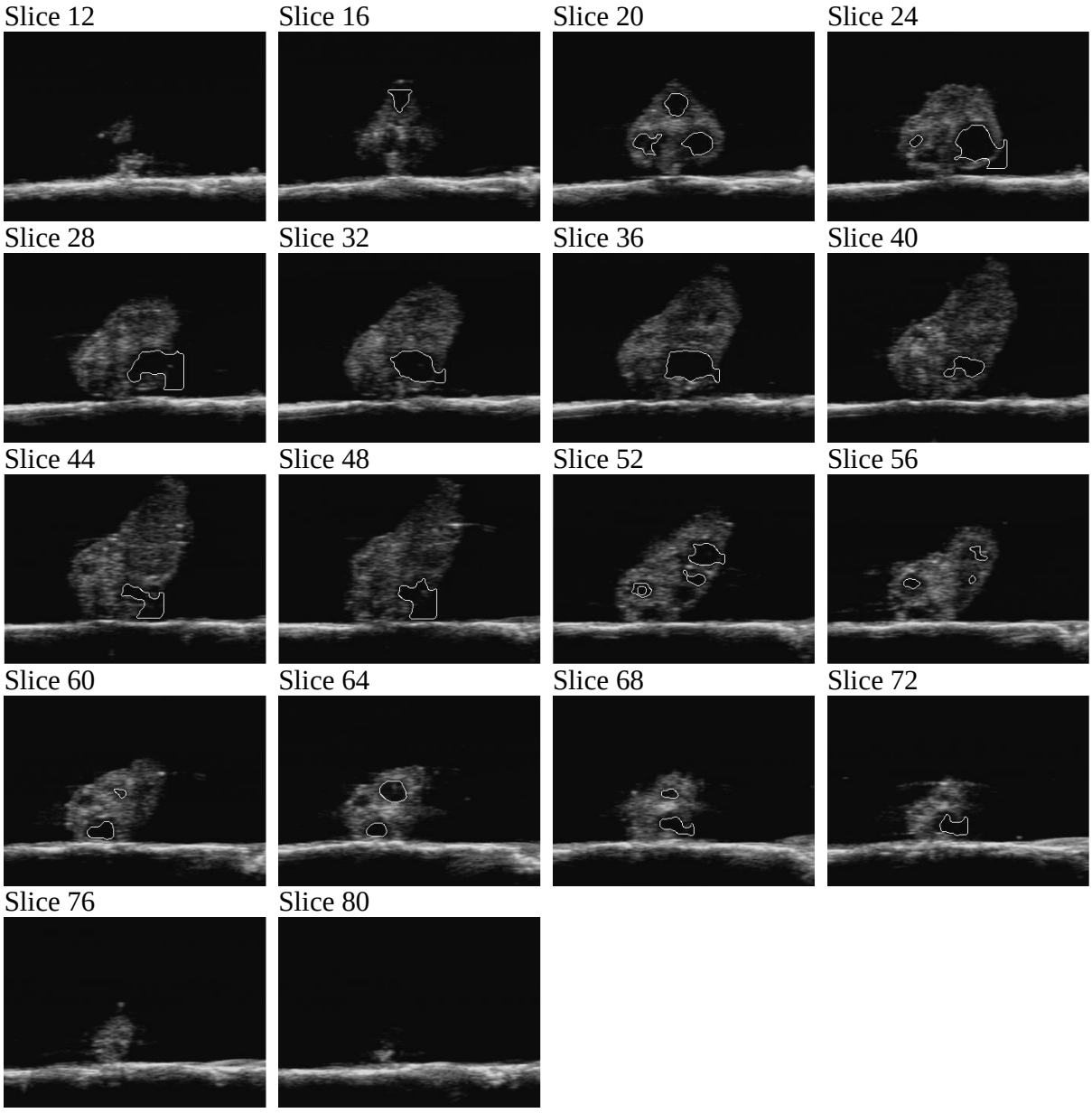

(c) The result of our algorithm relative by slice number

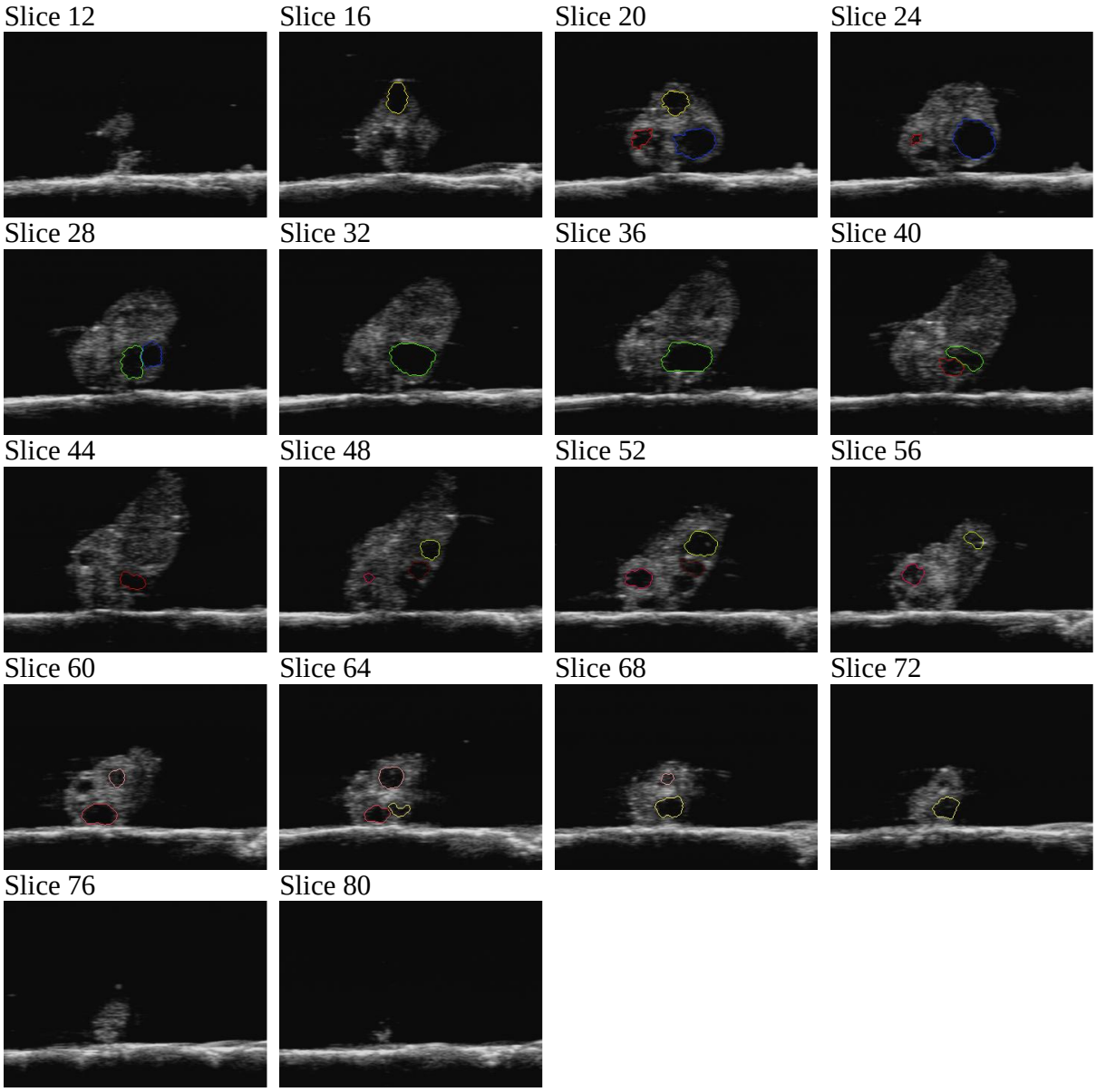

(d) The manually determined follicles by an expert

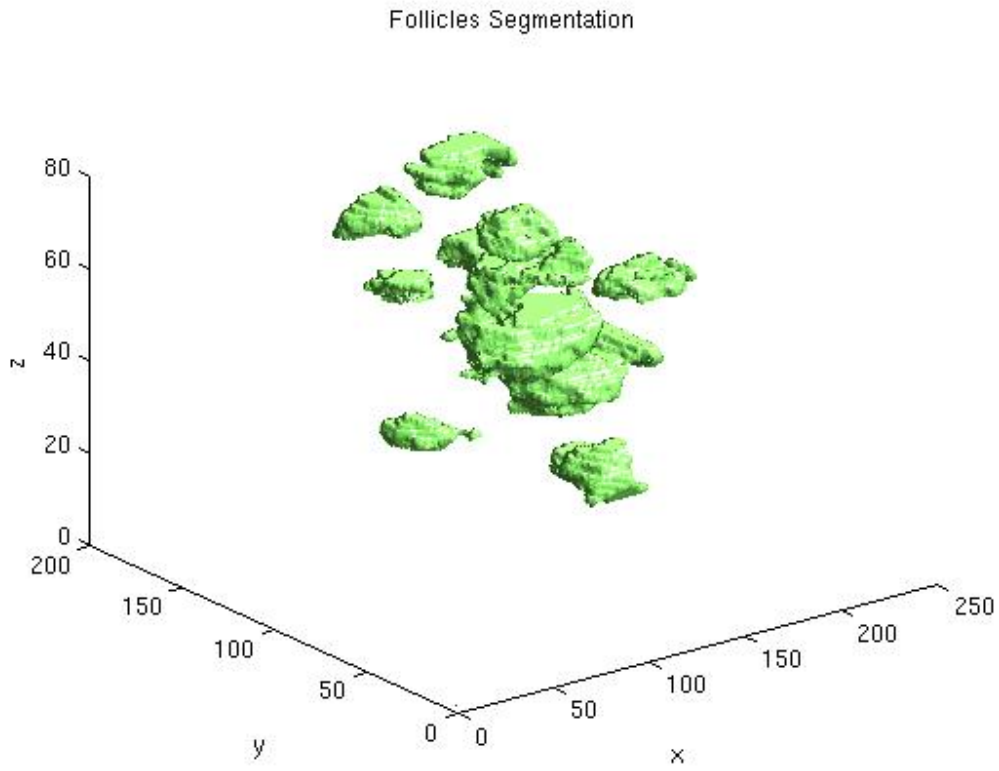

(e) The 3D vision of the follicle segmentation result

Figure A.2 The computer segmentation result of bovine ovary number 15.

A.2 Noise image

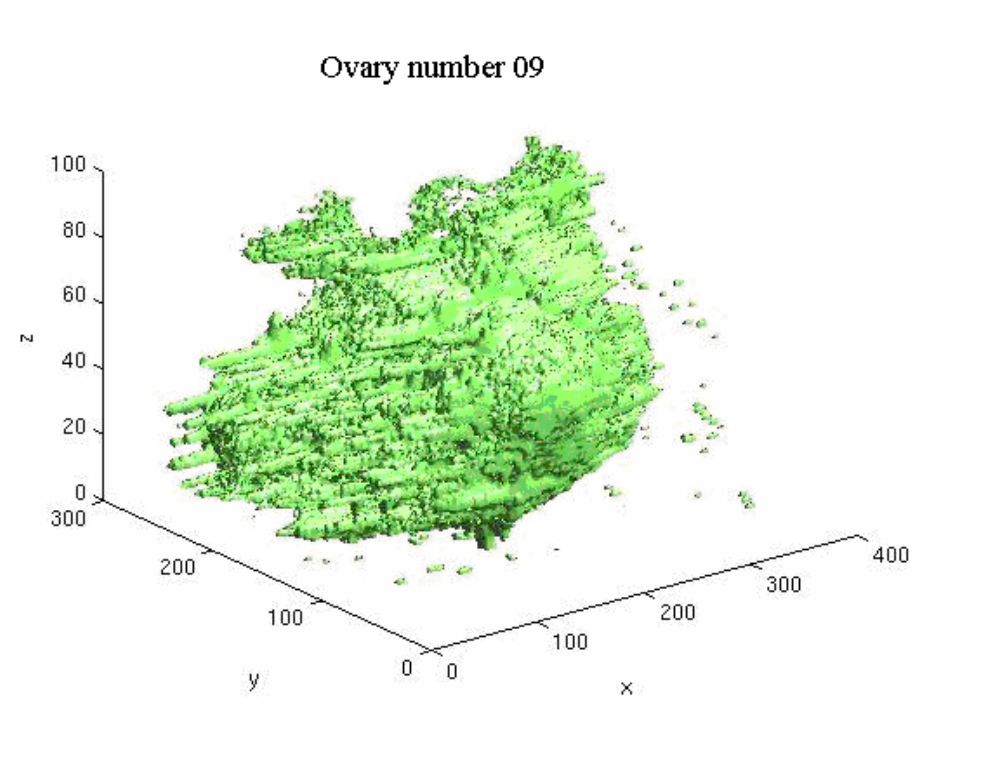

(a) The construction result of the cow ovary

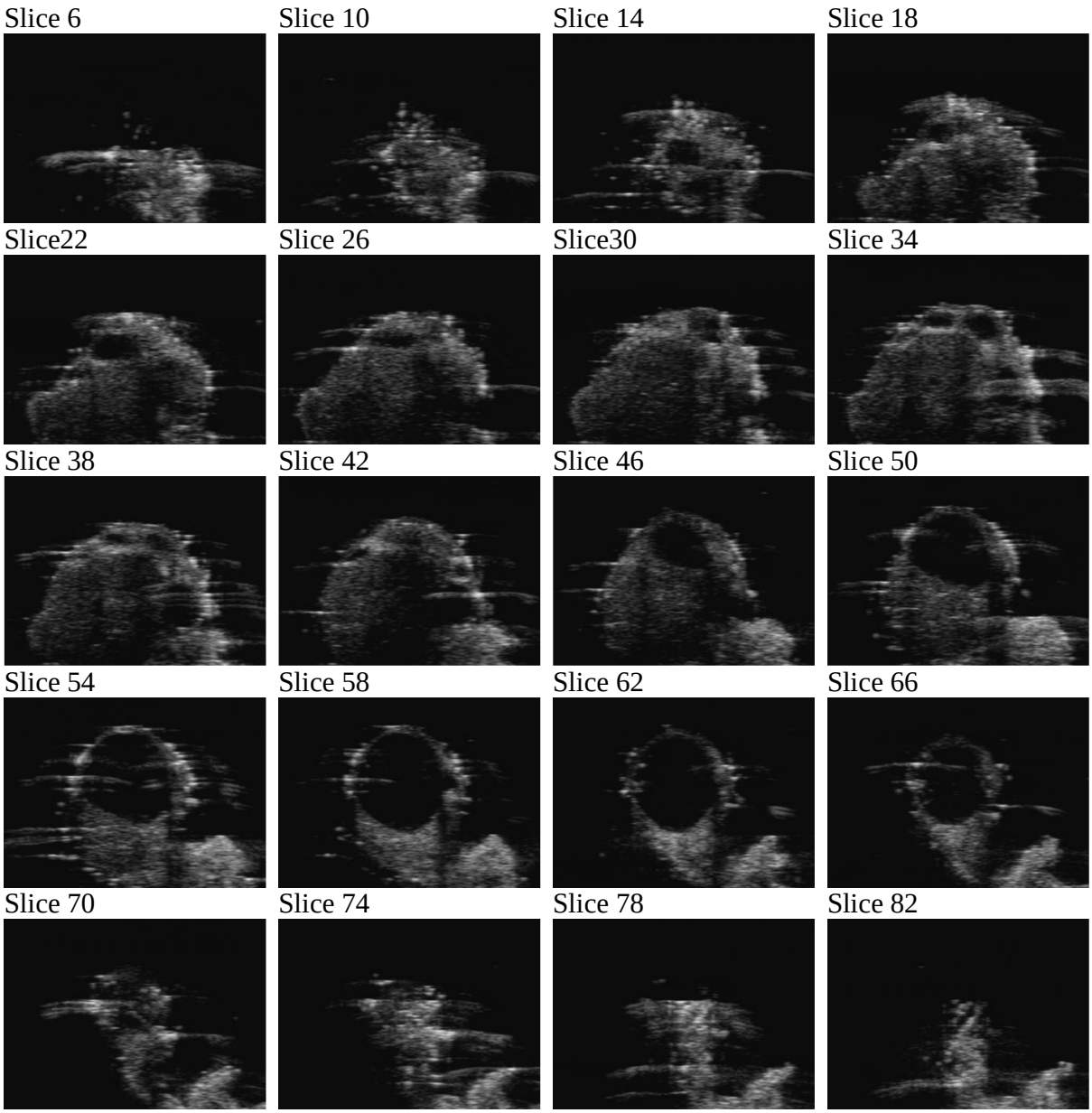

(b) The original images relative by slice number

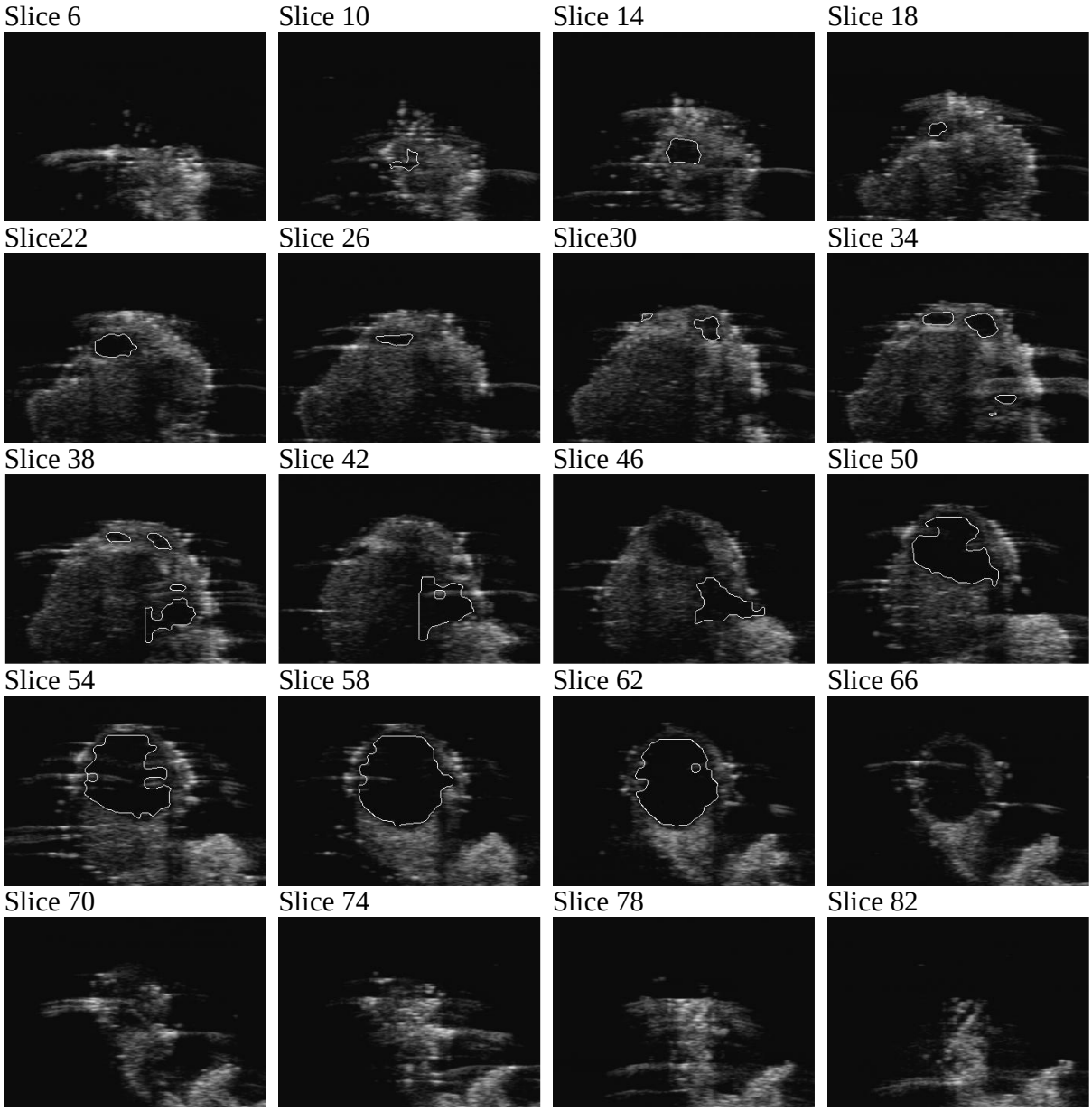

(c) The result of our algorithm relative by slice number

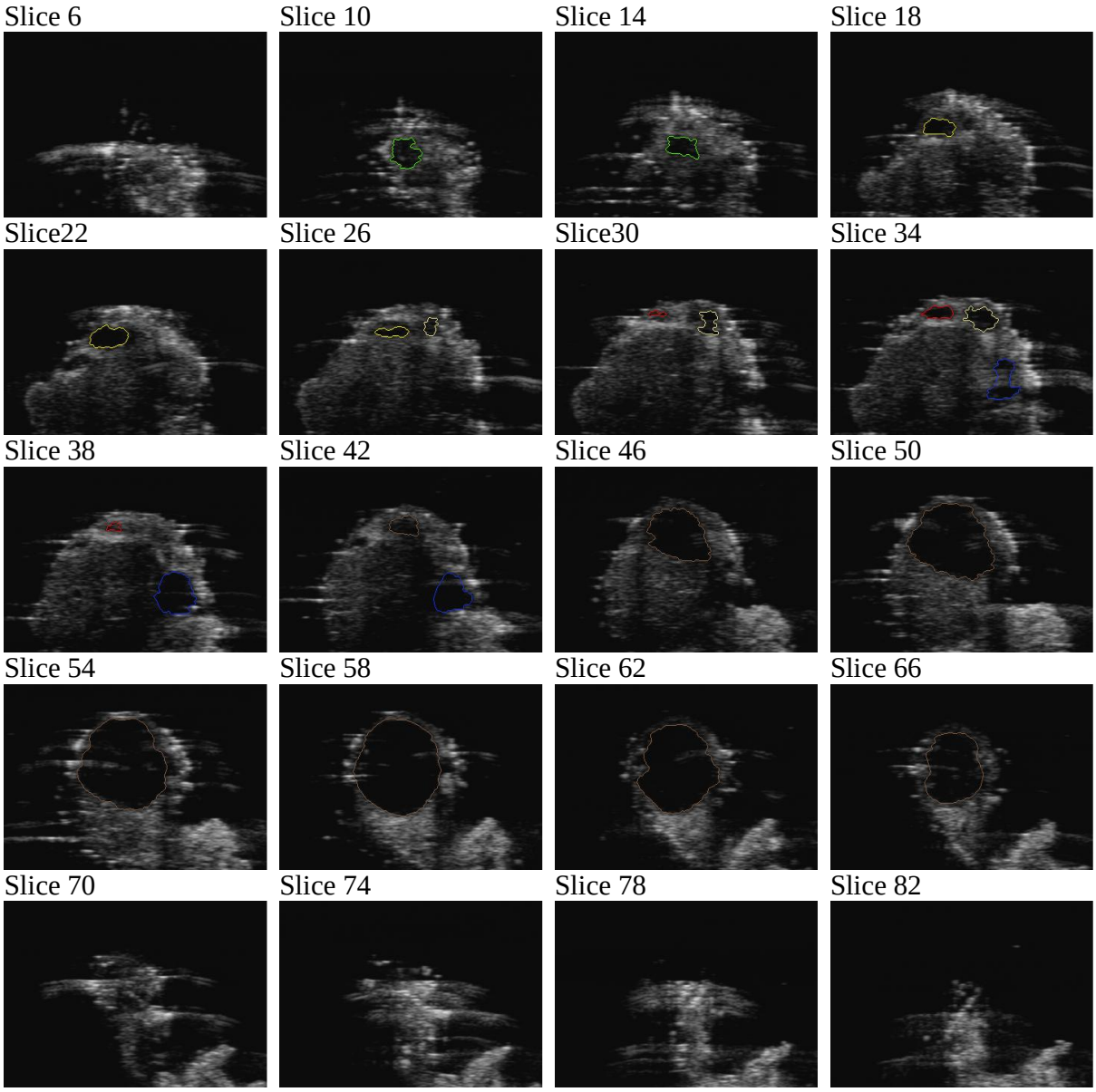

(d) The manually determined follicles by an expert

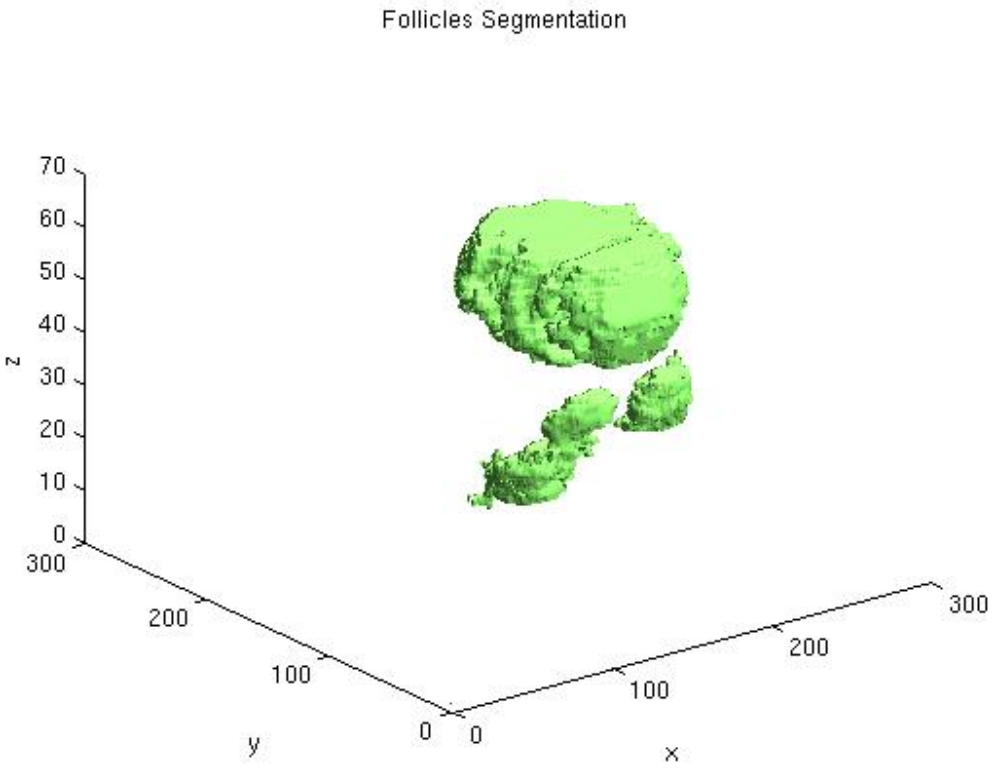

(e) The 3D vision of the follicle segmentation result

Figure A.3 The computer segmentation result of bovine ovary number 09.

Apendix B

Software Documents

Below are the codes of SRG algorithm. The contents of the software documents are as following:

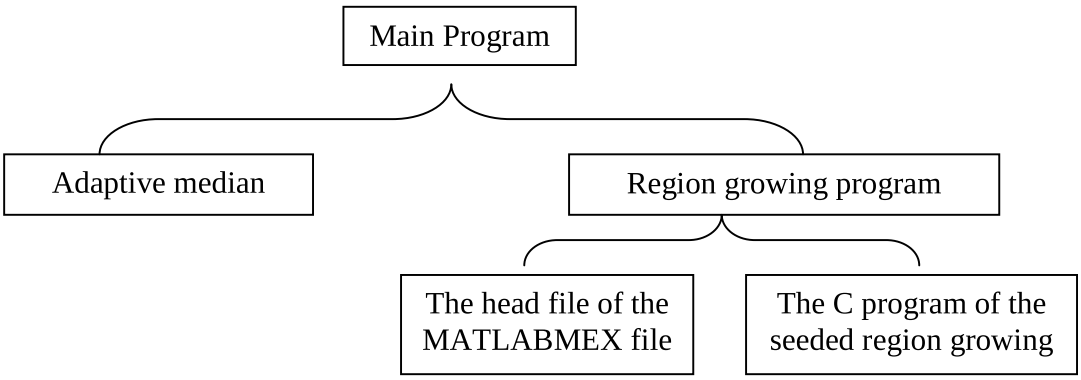

B.1 Main Program

```
clear all
close all

% This is the program that segment each follicle from a volume of a bovine ovary.

function [Lnew,Lcompare] = fsegment(Seeds)

%%%%%%%%%%%%%%%%%%%%%%%%%%%%%%%%%%%%%%%%%%%%%%%%%%%%%%%%%%%%%%%%
% The input data is an array of the index of seed points. For example, the form of      %
% input array is:  Seeds = [1751838, 1919445, 3034747, 2736132, 2465981].              %
%%%%%%%%%%%%%%%%%%%%%%%%%%%%%%%%%%%%%%%%%%%%%%%%%%%%%%%%%%%%%%%%

% Location of data files.

filebase = '/tmp_mnt/student/lvq533/Desktop/1-30-01/cow ovary 010';

% Load the images and construct the images into a volume of the bovine ovary.
```

```
startFram = 0;
endfram = 91;
for i = startFram:endfram
  if i <= 9
    filename = filebase,num2str('0'),num2str(i,'%2d'),num2str('.BMP')];
  else
    filename = [filebase,num2str(i,'%2d'),num2str('.BMP')];
  end
  temp = imread(filename);
  temp = rgb2gray(temp);
  rect =[120 120 350 245];
  temp = imcrop(temp,rect);
  j = i+1;
  image(:,:,j) = temp;
end

%Medican filter preprocessing (see subfunction of the median filter)
[m,n,o] = size(image);
Imed = adamedfilt(image);
Imed = uint8(Imed);

%Calculate the mean grey level and the standard deviation of the ovary
%volume
Mean = mean(Imed(:))*0.7;
Std = 20;

%Calculate the number of seed points.
a = size(Seeds,2);

%Region growing, setup and run the MATLAB MEX file of the 3D region
%growing(see subfunction of regiongrow.m and its MEX files)
image_mod = image(:,:,1);
mex regiongrow_vs.cpp neighborhood.cpp
Lnew = zeros(m,n,o);
Ltmp = zeros(m,n,o);
volume =[];

Lnew = regiongrow(Imed,Seeds(1),40,Mean,Std,m,n,o,image_mod,0,8,6);
if Lnew(1) == 3 || Lnew(2) == 3||Lnew(3) == 3
  Thresh = 0;
  while  Lnew(1) == 3 || Lnew(2) == 3||Lnew(3) == 3
    Thresh = Thresh+1;
    Th = 0.1*Thresh;
    Lnew = regiongrow(Imed,Seeds(1),40,Mean,Std,m,n,o,image_mod,Th,8,6);
  end
end
Lnew = imfill(Lnew,8,'holes');
```

```
%post-processing part by smoothing the segmentation result (selectable)
Lnew = smooth3(Lnew);

%continue to segment the other follicles
for i = 2:a
  Ltmp = regiongrow(Imed,Seeds(i),40,Mean,Std,m,n,o,image_mod,0,8,6);
  if Ltmp(1) == 3 || Ltmp(2) == 3||Ltmp(3) == 3
    Thresh = 0;
    while  Ltmp(1) == 3 || Ltmp(2) == 3||Ltmp(3) == 3
      Thresh = Thresh+1;
      Th = 0.1*Thresh;
      Ltmp = regiongrow(Imed,Seeds(i),40,Mean,Std,m,n,o,image_mod,
           Th,8,6);
    end
  end
    Ltmp = imfill(Ltmp,8,'holes');
    Ltmp = smooth3(Ltmp);
    Lnew = imadd(Lnew,Ltmp);
End

%3D segmentation result visilization.
figure, isosurface(Lnew,0.5), title('Follicles Segmentation')
xlabel x, ylabel y, zlabel z
view(3), camlight, lighting gouraud

%Write the result into a result fold
filebase2 = '/tmp_mnt/student/lvq533/Desktop/1-30-01/segmentation/';
for k = 1:o
   Tem = Lnew(:,:,k);
   se1 = strel('disk',6);
   Tem2 = imclose(Tem,se1);
   I = image(:,:,k);
   E = edge(Tem2,'sobel');
   Le = uint8(255.*E);
   Lcom = imadd(Le,I);
   figure,imshow(Lcom);
   filename = [filebase2,num2str(k,'%2d'),num2str('.jpg')];
   imwrite(Lcom,filename,'jpg');
   Lcompare(:,:,k) = Lcom;
End
```

B.2 Subfunctions

B.2.1 Adaptive median filter

```
function M = adamedfilt(image)

%This is a Matlab subfunction that smooth the 3D volume using adaptive
%median filter.

%Input is the 3D ovary volume.
[x,y,z] = size(image);
M = zeros(size(image));

for i = 1:z
   Tem = image(:,:,i);
   T = mean(Tem(:))*0.4;
   Tem1 = Tem;
   Tem2 = Tem;
   t1 = find(Tem1 >= T);
   Tem1(t1) = 0;

   % For the pixels greater than the threshod T, a 11*11 windows is used.
   Medt1 = medfilt2(Tem1,[11 11]);
   t2 = find(Tem2 < T);
   Tem2(t2) = 0;


   % For the pixels less than the threshod T, a 5*5 windows is used.
   Medt2 = medfilt2(Tem2, [5 5]);
   Med1 = imadd(Medt1,Medt2);

   % The median filter smoothing is proformed twice.
   Tem3 = Med1;
   Tem4 = Med1;
   t3 = find(Tem3 >= T);
   Tem3(t3) = 0;
   Medt3 = medfilt2(Tem3,[11 11]);
   t4 = find(Tem4 < T);
   Tem4(t4) = 0;
   Medt4 = medfilt2(Tem4, [5 5]);
   Med = imadd(Medt3,Medt4);
   M(:,:,i) = uint8(Med);
end
```

B.2.2 Region growing

```
function L = regiongrow(varargin)

%This is the 3D region growing based follicle segmentation program.
%
%L computes a label matrix identifying the grown region. The elements
%abeled 1 belong to the ROI of the follicle.
%L = regiongrow(A,conn) computes the growing region using the specified
%3D connectivity.
%   conn may have the following scalar values:
%
%       6     three-dimensional six-connected neighbourhood
%       18    three-dimensional 18-connected neighbourhood
%       26    three-dimensional 26-connected neighbourhood
%
%L = regiongrow(A,conn2) computes the growing region using the
%specified 2D connectivity.
%   conn2 may have the following scalar values:
%
%       4    two-dimensional 4-connected neighborhood
%       8    two-dimensional 8-connected neighborhood
%
% Input-output specs
% ================================================
% A     - full, real, numeric, logical
%       +/- Inf OK, but NaNs not allowed
%       empty OK
%
% Seed  - the index of seed point
%
% Dif   - the threshold of the difference between two adjacent pixels.
%         In this research, it is a constant number.
%
% Mean0 - the threshold of the mean grey level of ROI.
%
% Sd0   - the threshold of the standard deviation of ROI.
%
% numx, numy, numz - the size of the input image A.
%
% A2    - a two dimension matrix, same size of each slice in volume A.
%
% Thresh- the parameter of the program stop crition P.
%
% L     - full, double array, same size as A
```

```
[A,Seed,Dif0,Mean0,Sd0,numx,numy,numz,A2,Thresh,conn2,conn] =
                                                    parse_inputs(varargin{:});

L = regiongrow_vs(A,Seed,Dif0,Mean0,Sd0,numx,numy,numz,A2,Thresh,conn2,
    conn);

function [A,Seed,Dif0,Mean0,Sd0,numx,numy,numz,A2,Thresh,conn2,conn] =
                                                    parse_inputs(varargin)

iptchecknargin(11,12,nargin,mfilename);

A = varargin{1};
iptcheckinput(A,{'numeric' 'logical'}, {'real' 'nonsparse'}, ...
          mfilename, 'A', 1);
Seed = varargin{2};
Dif0 = varargin{3};
Mean0 = varargin{4};
Sd0 = varargin{5};
numx = varargin{6};
numy = varargin{7};
numz = varargin{8};
A2 = varargin{9};
Thresh = varargin{10};
conn2 = varargin{11};

if nargin < 12
   conn = conndef(ndims(A), 'maximal');
else
   conn = varargin{12};
   if isa(conn,'strel')
      conn = getnhood(conn);
   else
      iptcheckconn(conn, mfilename, 'CONN', 12);
   end
end
```

B.2.3 The head file of the Matlab MEX file

```
#include "neighborhood.h"
#include "regiongrow_vs.h"
#include "mex.h"

////////////////////////////////////////////////////////////////////////////////////////////////////////////
//
// REGIONGROW_VS MEX-file
//
// Input-output specs: see regiongrow.m
```

```
////////////////////////////////////////////////////////////////////////////////////////////////////////////////
////////////////////////////////////////////////////////////////////////////////////////////////////////////////
void check_inputs(int nlhs, mxArray *plhs[], int nrhs, const mxArray *prhs[])
{
   if (nrhs != 12)
   {
      mexErrMsgIdAndTxt("Images:regiongrow_vs:invalidNumInputs", "%s",
                        "REGIONGROW_VS needs 11 input arguments.");
   }
}

////////////////////////////////////////////////////////////////////////////////////////////////////////////////
extern "C"
void mexFunction(int nlhs, mxArray *plhs[], int nrhs, const mxArray *prhs[])
{
   void *I;
   double *L,*Seed,*Mean0,*Sd0,*Dif0,*num_x,*num_y,*num_z, *I2,
        *Thresh;
   int num_elements1;
   const int *input_size, *input_size2;
   int ndims,ndims2;
   mxClassID class_id;
   Neighborhood_T nhood, nhood2;
   NeighborhoodWalker_T walker, walker2;

   check_inputs(nlhs, plhs, nrhs, prhs);

   if (mxIsLogical(prhs[0]))
   {
      I = mxGetLogicals(prhs[0]);
   }
   else
   {
      I = mxGetData(prhs[0]);
   }
   Seed = mxGetPr(prhs[1]);
   Dif0 = mxGetPr(prhs[2]);
   Mean0 = mxGetPr(prhs[3]);
   Sd0 = mxGetPr(prhs[4]);
   num_x = mxGetPr(prhs[5]);
   num_y = mxGetPr(prhs[6]);
   num_z = mxGetPr(prhs[7]);
   num_elements1 = mxGetNumberOfElements(prhs[0]);
   class_id = mxGetClassID(prhs[0]);
   input_size = mxGetDimensions(prhs[0]);
   ndims = mxGetNumberOfDimensions(prhs[0]);
```

```
I2 = mxGetPr(prhs[8]);
input_size2 = mxGetDimensions(prhs[8]);
ndims2 = mxGetNumberOfDimensions(prhs[8]);

Thresh = mxGetPr(prhs[9]);

plhs[0] = mxCreateNumericArray(ndims, input_size, mxDOUBLE_CLASS,
        mxREAL);
L = mxGetPr(plhs[0]);

nhood = nhMakeNeighborhood(prhs[11],NH_CENTER_MIDDLE_ROUNDDOWN);
walker = nhMakeNeighborhoodWalker(nhood,input_size,ndims,
       NH_SKIP_CENTER);

nhood2 =nhMakeNeighborhood(prhs[10],
                                    NH_CENTER_MIDDLE_ROUNDDOWN);
walker2 = nhMakeNeighborhoodWalker(nhood2,input_size2,ndims2,
                                          NH_SKIP_CENTER);


switch (class_id)
{
case mxLOGICAL_CLASS:
   compute_regiongrow((mxLogical *)I,Seed,Dif0,Mean0,Sd0,
                           num_elements1,ndims,input_size,num_x,
                           num_y,num_z,walker,walker2, Thresh,L);
   break;
case mxUINT8_CLASS:
   compute_regiongrow((uint8_T *)I,Seed, Dif0,Mean0,Sd0,
                          num_elements1,ndims,input_size,num_x,
                          num_y,num_z,walker, walker2,Thresh,L);
   break;
case mxUINT16_CLASS:
   compute_regiongrow((uint16_T *)I,Seed, Dif0,Mean0,Sd0,
                          num_elements1,ndims,input_size,num_x,
                          num_y,num_z,walker, walker2,Thresh,L);
   break;
case mxUINT32_CLASS:
   compute_regiongrow((uint32_T *)I, Seed,Dif0,Mean0,Sd0,
                           num_elements1,ndims,input_size,num_x,
                           num_y,num_z,walker, walker2, Thresh,L);
   break;
case mxINT8_CLASS:
   compute_regiongrow((int8_T *)I,Seed, Dif0,Mean0,Sd0,
                          num_elements1,ndims,input_size,num_x,
                          num_y,num_z,walker, walker2, Thresh,L);
   break;
```

```
    case mxINT16_CLASS:
      compute_regiongrow((int16_T *)I,Seed, Dif0,Mean0,Sd0,
                         num_elements1,ndims,input_size,num_x,
                         num_y,num_z,walker, walker2, Thresh,L);
      break;
    case mxINT32_CLASS:
      compute_regiongrow((int32_T *)I, Seed,Dif0,Mean0,Sd0,
                         num_elements1,ndims,input_size,num_x,
                         num_y,num_z,walker, walker2,Thresh,L);
      break;
    case mxSINGLE_CLASS:
      do_nan_check((float *)I, num_elements1);
      compute_regiongrow((float *)I,Seed, Dif0,Mean0,Sd0,
                          num_elements1,ndims,input_size,num_x,
                          num_y,num_z,walker, walker2, Thresh,L);
      break;
    case mxDOUBLE_CLASS:
      do_nan_check((double *)I, num_elements1);
      compute_regiongrow((double *)I,Seed, Dif0,Mean0,Sd0,
                         num_elements1,ndims,input_size,num_x,
                         num_y,num_z,walker, walker2,Thresh,L);
      break;
    default:
      mxAssert(false, "");
      break;
    }

    nhDestroyNeighborhood(nhood);
    nhDestroyNeighborhoodWalker(walker);

    nhDestroyNeighborhood(nhood2);
    nhDestroyNeighborhoodWalker(walker2);
}
```

B.2.4 The C program of the Matlab MEX file

```
#ifndef _REGIONGROW_VS_H
#define _REGIONGROW_VS_H

#define INIT 0
#define FICTITIOUS -1

#include "mex.h"
#include "neighborhood.h"
#include "queue.h"
#include "math.h"
```

```
////////////////////////////////////////////////////////////////////////////////////////////////////////////////////////
//
////////////////////////////////////////////////////////////////////////////////////////////////////////////////////////
template<typename _T>
inline void do_nan_check(_T *F,int num_elements)
{
   for (int p = 0; p < num_elements; p++)
   {
      if (mxIsNaN(F[p]))
      {
         mexErrMsgIdAndTxt("Images:regiongrow_vs:expectedNonNaN",
                           "%s",
                           "Input image may not contain NaNs.");
      }
   }
}
////////////////////////////////////////////////////////////////////////////////////////////////////////////////////////
//                                                                                                                    //
// Algorithm: see Chapter 2 3D Follicle Segmentation of Ultrasound Volume of                                          //
//                                    Bovine ovary                                                                    //
//                                                                                                                    //
////////////////////////////////////////////////////////////////////////////////////////////////////////////////////////
template<typename _T>
void compute_regiongrow(_T *I, double *Seed,double *Dif0,double *Mean0,
                        double *Sd0,int N,int ndims,
                        const int *input_size,double *num_x,
                        double *num_y,double *num_z,
                        NeighborhoodWalker_T walker,
                        NeighborhoodWalker_T walker2,double *Thresh,
                        double *L)
{
   Queue<int32_t> SeedQueue;
   double        Volume;
   double        Label = (double) 1, mean, meanold, standard,
                 standardold;
   int           non_compact,k,p,q,dxstop=0,dystop=0,dzstop=0;
   _T            D1,D2;
   int           Dif,Mn,Sd,num_of_growing;
   int           xs,ys,zs,zp,xp,yp,rp,xv,yv,zv,rv,rz,b,c,rq,
                 A,r,circlesnumber,u,w,o;
   double        xz,yz,zz,xq,yq,zq,zqmin,zqmax,yqmin,yqmax,
                 xqmin,xqmax,xqmean,yqmean,zqmean,ind1,ind2,
                 ind3,tempx,tempy,tempz,slicearea,z,v,distance,
                 distancemax,VolumeSphere,zaxis,yaxis,xaxis,axismax,
                 dx,dy,dz,distance2,distancemax2,VolumeSphere2,
                 Comp,Length,Length2;
   // If the input array is empty, there's nothing to do here.
```

```
   if (N == 0)
   {
      return;
   }

  // Initialize output array.
   for (k = 0; k <N; k++)
   {
      L[k] = INIT;
   }


  // Initialize the seed points queue.
    SeedQueue.initialize(32);

 // Get the boundary pixels of the region need to be grew.
    Volume = 1;
    SeedQueue.put(FICTITIOUS);

    L[(int)Seed[0]] = Label;
    mean = I[(int)Seed[0]];
    standard = 0;
    SeedQueue.put((int)Seed[0]);


//Change index value to subindex,like ind2sub in Matlab
    slicearea = (num_x[0])*(num_y[0]);

    zs = (int)Seed[0]/(int)slicearea+1;
    ys = ((int)Seed[0]%(int)slicearea)/((int)num_x[0])+1;
    xs = ((int)Seed[0]%(int)slicearea)%((int)num_x[0]);

//Use to find the minimum axis of each direction
    zqmin = zs;
    zqmax = zs;
    yqmin = ys;
    yqmax = ys;
    xqmin = xs;
    xqmax = xs;

    zqmean = zs;
    yqmean = ys;
    xqmean = xs;
//initionalize the number of pixels who pass the homogeneous test but //doesn't pass the
compactness test

    non_compact = 0;
```

```
   distancemax = 1;

   A = 0;

// Region growing

////////////////////////////////////////////////////////////////////////////////////////////////////////////////////////
//The code following is the region growing process
////////////////////////////////////////////////////////////////////////////////////////////////////////////////////////
while (true)
 {
  p = SeedQueue.get();
  if (p == FICTITIOUS)
   {
     if (SeedQueue.getSequenceLength() <= Length*Thresh[0])
        {
          SeedQueue.freeSequence();
          break;
        }
        else if (SeedQueue.getSequenceLength() == non_compact)
        {
          SeedQueue.freeSequence();
          break;
        }
        else
        {
          A++;
          non_compact = 0;
          SeedQueue.put(FICTITIOUS);
          circlesnumber = 0;
          while(true)
          {
            p = SeedQueue.get();
            if (p == FICTITIOUS)
            {
              circlesnumber++;
              VolumeSphere2 = 4/3*3.1415926*(distancemax2-1)
                          *(distancemax2-1)*(distancemax2-1)/6;
              Comp = Volume/VolumeSphere;
              if ((circlesnumber > 6) || (Comp > 2.15)
                 ||(SeedQueue.getSequenceLength() == 0))
              {
                SeedQueue.freeSequence();
                Length2 = 0;
                break;
              }
                Length2 = 0;
```

```
        SeedQueue.put(FICTITIOUS);
        p = SeedQueue.get();
    }

    zp = (int)p/(int)slicearea+1;
    u = p - (int)slicearea*(zp-1);

    nhSetWalkerLocation(walker2, u);
    while (nhGetNextInboundsNeighbor(walker2, &r, NULL))
    {
      w = r +(int)slicearea*(zp-1);
      meanold = mean;
      standardold = standard;
      mean = (Volume*meanold + I[w])/(Volume+1);
      standard = standard+(I[w]-mean)*(I[w]-mean)
               +Volume*(mean-meanold)*(mean-meanold);

      D1 = I[w];
      D2 = I[p];
      Dif = abs((int)D1 - (int)D2);
      Mn = abs((int)I[w] - (int)meanold);
      Sd = abs((int)standard - (int)standardold);
      if ((L[w] != Label) && ((double)Dif < Dif0[0]) &&
        ((double)Mn < Mean0[0]) &&
        ((double)Sd < Sd0[0]))
       {
         distance2 = sqrt((zq-zs)*(zq-zs)+(yq-ys)
                  *(yq-ys)+(xq-xs)*(xq-xs));
         if (distance2 > distancemax2)
         {
           distancemax2 = distance2;
         }
         L[w] = Label;
         SeedQueue.put(w);
         Volume++;
         Length2++;
       }
    }
}

SeedQueue.initialize(32);

for (k = 0; k <N; k++)
{
  if(L[k] == Label)
  {
    nhSetWalkerLocation(walker, k);
```

```
        while (nhGetNextInboundsNeighbor(walker, &q, NULL))
        {
          if(L[q] != Label)
          {
            SeedQueue.put(k);
            break;
          }
        }
      }
    }
    Length = SeedQueue.getSequenceLength();
    SeedQueue.put(FICTITIOUS);
    p = SeedQueue.get();
  }
}

zp = (int)p/(int)slicearea+1;
yp = ((int)p%(int)slicearea)/((int)num_x[0])+1;
xp = ((int)p%(int)slicearea)%((int)num_x[0]);

nhSetWalkerLocation(walker, p);
while (nhGetNextInboundsNeighbor(walker, &q, NULL))
{
  zq = (int)q/(int)slicearea+1;
  yq = ((int)q%(int)slicearea)/((int)num_x[0])+1;
  xq = ((int)q%(int)slicearea)%((int)num_x[0]);

  //Only when the centroid point of growing region did not move
  //too far away from the seed point the growing can continue.

  if ((dxstop==0 && dystop==0 && dzstop==0)
    ||( dxstop==1 && xq==xp && dystop==0 && dzstop==0)
    ||(dystop==1 && yq==yp && dxstop==0 && dzstop==0)
    ||(dzstop==1 && zq==zp && dxstop==0 && dystop==0)
    ||(dxstop==1 && dystop==1 && xp==xq && yp==yq)
    ||(dxstop==1 && dzstop==1 && xp==xq && zp==zq)
    ||(dystop==1 && dzstop==1 && yp==yq && zp==zq))
  {
    //Calculate the new mean value and mean standard
    meanold = mean;
    standardold = standard;
    mean = (Volume*meanold + I[q])/(Volume+1);
    standard = standard+(I[q]-mean)*(I[q]-mean)
            +Volume*(mean-meanold)*(mean-meanold);
    D1 = I[q];
    D2 = I[p];
    Dif = abs((int)D1 - (int)D2);
```

```
Mn = abs((int)I[q] - (int)meanold);
Sd = abs((int)standard - (int)standardold);

if ((L[q] != Label) && ((double)Dif < Dif0[0])
  && ((double)Mn < Mean0[0]) && ((double)Sd < Sd0[0]))
{

  //Calculate the offset of the maximum axis of grown
  //region in different direction x,y,z
  dxstop = 0;
  dystop = 0;
  dzstop = 0;

  if (zq < zqmin)
  {
    zqmin = zq;
  }
  if (zq > zqmax)
  {
    zqmax = zq;
  }
  if (yq < yqmin)
  {
    yqmin = yq;
  }
  if (yq > yqmax)
  {
    yqmax = yq;
  }

  if (xq < xqmin)
  {
    xqmin = xq;
  }
  if (xq > xqmax)
  {
    xqmax = xq;
  }
  zaxis = zqmax - zqmin;
  yaxis = yqmax - yqmin;
  xaxis = xqmax - xqmin;

  zqmean = zaxis/2 + zqmin;
  yqmean = yaxis/2 + yqmin;
  xqmean = xaxis/2 + xqmin;
  //Calculate the offset between new centroid point and
  //seed point
```

```
dz = abs((int)zqmean - (int)zs);
dy = abs((int)yqmean - (int)ys);
dx = abs((int)xqmean - (int)xs);

//If the offset is too big, then the whole region
//growing program stop q
if(dx >= 10)
{
  dxstop = 1;
}
if(dy >= 10)
{
  dystop = 1;
}
if(dz >= 5)
{
  dzstop = 1;
}

//Calculate the maximum distance between the boundary
//pixel and seed point
distance = sqrt((zq-zs)*(zq-zs)+(yq-ys)*(yq-ys)
        +(xq-xs)*(xq-xs));
if (distance > distancemax)
{
  distancemax = distance;
}

//Calculate the volume of the ball which the radius
//equal to the maximum distance between the boundary
//pixel and seed point
VolumeSphere = 4/3*3.1415926*(distancemax-1)
            *(distancemax-1)*(distancemax-1)*0.15;

//Compactness test(compare the real volume with the
//calculate global volume)
if (Volume <= 3000)
{
  if(Volume/VolumeSphere < 1.8)
{
  L[q] = Label;
  SeedQueue.put(q);
  Volume++;
}
else
{
    SeedQueue.put(p);
```

```
                non_compact++;
              }
          }
          else
          {
             if(Volume/VolumeSphere < 1.3)
             {
               L[q] = Label;
               SeedQueue.put(q);
               Volume++;
             }
             else
             {
               SeedQueue.put(p);
               non_compact++;
             }
           }
        }
        else
        {
           mean = meanold;
           standard = standardold;
        }
     }
  }
}

//Use to check whether leaking happened or not, if the centroid point //move awary too
much from the seed point, that means leak happened.
L[0] = dxstop+2;
L[1] = dystop+2;
L[2] = dzstop+2;

mxAssert(SeedQueue.getSequenceLength() == 0, "");
}
#endif //_REGIONGROW_VS_H
```

***Note: For running the program, all of the software programs should be put in the same directory. Moreover, some related Matlab build in functions need to be put in the same directory. The functions as following: neighborhood.h, neighborhood.cpp, iptutil.h, iptutil_cpp.h, queue.h, sequencemex.h.**